LOCAL OPTOELECTRONIC PROPERTIES OF

ZINC-PORPHYRIN/GOLD MOLECULAR INTERFACES

Xi Chen

A DISSERTATION

in

Materials Science and Engineering

Presented to the Faculties of the University of Pennsylvania

in

Partial Fulfillment of the Requirements for the

Degree of Doctor of Philosophy

2014

Supervisor of Dissertation

_____

Dr. Dawn A. Bonnell,
Henry Robinson Towne Professor of Materials Science and Engineering
Vice Provost of Research

Graduate Group Chairperson

_____

Dr. Shu Yang, Professor of Materials Science and Engineering and Chemical and Biomolecular Engineering

Dissertation Committee

Dr. Cherie Kagan, Professor of Electrical and Systems Engineering, Materials Science and Engineering, and Chemistry
Dr. Bohdana Discher, Research Assistant Professor of Biochemistry and Biophysics
Dr. Russell J. Composto, Professor of Materials Science and Engineering, Bioengineering and Chemical and Biomolecular Engineering.

LOCAL OPTOELECTRONIC PROPERTIES OF

ZINC-PORPHYRIN/GOLD MOLECULAR INTERFACES

ACKNOWLEDGMENT

With all the rest pieces of puzzle put together, the acknowledgment seems to be the last one for this dissertation. Throughout my 6 year journey toward a PhD degree, I had the honor to work with and be supported by quite a few people, to whom I would like to express my gratitude before I present you my research.

First I would like to thank my PhD advisor, Dr. Dawn Bonnell, whom I had the privilege to learn from. With her guidance I was able to overcome all hurdles in my research and grew from a rookie to an experienced researcher, and with the freedom she gave me, I was able to explore alternative paths for my career and found my passion. I feel so lucky to have such a great academic advisor and a great life mentor.

I'm also grateful for my dissertation committee members, Dr. Composto, Dr. Discher and Dr. Kagan. I really appreciate all the discussion regarding my project, especially the questions during my thesis proposal, which made me thoroughly think about my research and lead to my achievement in the end.

I'd like to thank all the current and former Bonnell Group members with whom I had the greatest honor working with. I really appreciate the effort Sanjini, Dave, Kendra, Matt put in training me on different scanning probe instruments which are the fundamental research tools for me, and I definitely enjoyed working with Stephen writing the review and the book chapter on the cutting edge field of scanning impedance microscopy. I also want to thank John for helping me with my qualification exam, as well as Carlos for the insightful suggestions on my research. I want to especially thank Erie for spending a lot of time pushing me through the final experiment measurements and

helping me revising my thesis with great insight and patience. And also I'd like to thank Jiechang and Jiaxin, for their support and discussion, and also for making the office a great place to be in everyday.

I'd like to thank all my collaborations, who provided me samples, research tools and so many great ideas for my research to carry on. I really appreciate the financial support from NBIC NSEC DMR08-32802, without which none of this would have been done. It was really a pleasure working as a teaching assistant with, or attending the classes of a lot of Penn faculties and I'm thankful that I learned so much from them. And to the Penn staffs that have helped me directly or indirectly, especially Pat, Vicky and Irene who made my PhD life so much easier, I'm truly grateful.

During the 6 years of my PhD life at Penn I met so many friends, without whom I could never had so much fun or survive so much frustration. I'd like to thank my fellow MSE PhD students for helpful discussion as well as moral support, my Penn Men's Volleyball Club teammates for helping me to keep a fit body and a young heart, my Penn Bridge teammates for keeping me relaxed while still have a sharp mind, and my consulting case practice partners for helping me to find my ideal job. I'd also like to thank Xinyi Deng, Yibo Zhao, Yue Ning, Tianshi Ji, Xiang Hao, Weiyu Zhang, Lingyan Zhao, and many others for helping me with all kinds of things in life, and keeping my PhD life colorful.

I want to specially thank my family: my dad, mom and grandma. I really appreciate my dad and mom for raising me to be who I am today. They paid so much attention to my education and my well-being, and they gave me the freedom to make my own life choice ever since I was thirteen. And I'm really grateful that my grandma kept

taking care of my life throughout my elementary and junior high school, preparing me every meal. I still remember every moment how they enjoyed my slightest achievements and encouraged me to keep going forward with all my effort, and every moment how they sympathize with my failures and stood by me, trying to pull me up from the ground. I cannot emphasize enough how much I love them.

Lastly I'd love to thank my beautiful fiancée, who right now is sound asleep on the couch. For the past two years she stood by my side, guided me and supported me. As a fellow PhD student in science, she comprehended every piece of joy or frustration of mine to share my laughter and tears, and she understood most part of my research to provide lots of insights and discussion to inspire me. She always led the way by telling me the right things to do, and whenever I do so, life turns for the better, hence the graduation and the job offer. I feel so lucky to have her around yet I don't know how to express my gratefulness. But I can say for sure that, I want to hold her hands for always, and to take care of her, and spend the rest of my life with her.

And now the puzzle is finished.

ABSTRACT

LOCAL OPTOELECTRONIC PROPERTIES OF

ZINC-PORPHYRIN/GOLD MOLECULAR INTERFACES

Xi Chen

Dr. Dawn A. Bonnell

This research consists in designing a series of experiments to determine the molecular orbital energy levels of zinc-porphyrin molecule when vertically attached to Au(111) substrate. To study the zinc-porphyrine molecular orbitals we use visible light of different wavelengths. Thiolated zinc-porphyrin oligomer molecules link to Au(111) surface, embedded within an 1-octanethiol self-assembled monolayer. Current-Voltage characterization technique allow us to determine the electronic orbital structures of different zinc-porphyrin oligomer single molecules via scanning tunneling microscope. Coupling lasers of different wavelengths and the tunneling junction, illumination effect on the molecular orbital energy levels of zinc-porphyrin molecules is investigated. The results indicate that the experimental zinc-porphyrin orbital energy levels are qualitatively consistent with previous calculations and experiments of similar porphyrin molecules. With illumination at given wavelengths, HOMO-LUMO gaps decreases for zinc-porphyrin molecules, and under dark condition the dimer zinc-porphyrin molecule

shows a larger HOMO-LUMO gap than the monomer counterpart. We propose a charged molecule model to explain the light illumination effect, and we attribute the larger HOMO-LUMO gap in dimer molecule to a mixing of face-to-face bundling and tilting of the molecules.

TABLE OF CONTENTS

LIST OF TABLES

LIST OF FIGURES

CHAPTER 1 Introduction

The past several decades witnessed the swift development of silicon-based micro- and nano-scale electronics. Taking advantages of the improvement in the "top-down" nanofabrication techniques [1], the size of metal-oxide-semiconductor field effect transistor (MOSFET) [2], the individual building block of the device chips, is getting smaller rapidly, resulting in the exponential growth in the processing power and speed, as described by Moore's law [3]. However, the downsizing of silicon-based devices cannot continue forever, as the physics of materials and fabrication techniques reach their limits: electrons leak from one device to another; silicon cannot be doped uniformly at these scales; and photolithography process limits the device size due to diffraction. To further scale down other ideas emerged, such as adoption of high-k oxides [4] and development of novel device structures such as FinFETs [5].

Scientists also looked beyond traditional semiconductor materials. Organic molecules can behave like electronic device components when attached to electrodes, as Aviram and Ratner proposed in their idea of a molecular rectifier in 1974 [6], and the invention and development of the scanning tunneling microscope provided a powerful tool to experimentally study the electron transport properties of single molecules. Research in molecular electronics intensified ever since [7], with devices such as molecular diodes [8-10], molecular transistors [11-16], and molecular switches and memory [17-22].

Molecular electronics offers advantages such as smaller size, self-assembly, dynamical stereochemistry, and high tailorability through composition and geometry

[23]. Among different organic molecules, porphyrin molecules exist extensively in natural biological systems and manifest rich electronic and optical properties, and thus have been extensively studied. Previous work done on porphyrin molecule and its derivatives have moved the goal of molecular electronic devices closer to realization. With self-assembly, porphyrin networks on substrates can be constructed, structurally creating molecular electronic circuitry. Certain knowledge of electronic properties of porphyrin molecules has been achieved, revealing the electronic structures and transport mechanisms theoretically and experimentally. Light interaction with molecular conduction junction [24-27], and also, micro-scale nanoparticle based devices [28-31]exploiting both the electronic and photonic properties of porphyrin molecules have been investigated, fabricated and characterized, further pointing to the possibilities of molecular optoelectronic devices realization. However to accomplish understanding and improving organic optoelectronic devices, we still need to understand the interaction of single porphyrin molecular electronic structure with light of different wavelengths, within a device configuration.

The goal of this research is to use zinc-porphyrin as a model probe system to experimentally determine the molecular orbital energy levels of zinc-porphyrin molecules, as well as to understand the illumination effect on the modulation of porphyrin electronic structures. We want to explore, investigate, and address the following questions: What is the single porphyrin molecule electronic structure when chemisorbed on the substrate in a vertical configuration? How will the energy of the HOMO or LUMO levels change when porphyrin molecules absorb photons? What is the effect of the number of oligomers in the porphyrin wire on the molecular electronic

states? We carefully design a set of experiments to answer the above questions, exploring the optoelectronic properties of zinc-porphyrin single molecules under a device configuration using photo-assisted scanning tunneling microscope.

The research goal presents us several challenges to be met. First regards the sample preparation. In order to measure the properties of the porphyrin molecules in a device configuration, we need to ensure that the porphyrin molecular wire is perpendicular to the substrate. Second and third challenges lie in the experimental setup of photo-assisted scanning tunneling microscopy. The laser needs to be properly aligned to illuminate the zinc-porphyrin molecules under the scanning tip, and to ensure the optimization of the illumination. Furthermore, we want to achieve a stable tunneling junction under light illumination, so all scanning tunneling spectra can be acquired under a stable condition to reveal correct information about the molecule.

Through carefully designed experiments we are able to meet the challenges mentioned above. The first challenge is met by using 1-octanethiol molecule self-assembled monolayers as hosting matrix, of which the zinc-porphyrin molecules are inserted in the defect areas. The second challenge is met by adjusting the laser spot position to maximize the zero voltage offset of the I-V spectra taken from an n-doped GaAs(100) sample. The third challenge is met by monitoring the Z piezo position of the scanning tunneling microscope to ensure a new thermal equilibrium state is reached after changing the illumination conditions.

This dissertation is organized in the following manner. Chapter 2 serves as an introduction on porphyrin molecules, which covers the basics of the porphyrin molecule, and summarizes the current state of research. Section 2.1 describes the structure of the

most simple porphine molecules, as well as metalloporphyrins. Section 2.2 discusses optical spectroscopic properties of porphyrin molecules and how it is explained by M. Gouterman's four-orbital model. Section 2.3 covers previous theoretical and experimental research on electronic properties of porphyrin molecules.

Chapter 3 describes the experimental methods and procedures adopted in this research, and addresses challenges. Section 3.1 describes the preparation of mixed monolayer samples, where zinc-porphyrin molecules align perpendicular to the substrate with the assist of the 1-octanethiol self-assembled monolayer hosting matrix. Section 3.2 describes the experimental setup and operation of photo-assisted scanning tunneling microscopy, including tuning the laser toward the tip-sample junction and relaxation of laser-induced heating.

Chapter 4 presents all the results obtained using the experimental methods described in Chapter 3. Section 4.1 describes the optical absorption spectroscopy results on the PZn_n molecules in solution, which provide some insights on the molecular orbital energy levels. Section 4.2 demonstrates the topography information of the mixed monolayer sample, confirming the insertion of PZn_n molecules. Section 4.3 presents the scanning tunneling spectroscopy data under different illumination conditions, of different organic molecules: 1-octanethiol in Section 4.3.1, PZn_1 molecule in Section 4.3.2, and PZn_2 molecule in Section 4.3.3.

Chapter 5 discusses the results associated with different molecules under different experimental conditions. Section 5.1 describes capacitive and resistive models used to obtain the molecular orbital energy levels from differentiated scanning tunneling spectroscopy measurements. Sections 5.2 and 5.3 describe the illumination effects on

PZn_1 and PZn_2 molecule electronic structures, especially HOMO-LUMO gaps, respectively. Section 5.4 covers the macrocycle coupling effect on molecular orbital energy levels of the zinc-porphyrin molecules in this research.

Chapter 6 summarizes the major conclusions of this research, and proposes some possible future research directions, such as to improve the experiments, to theoretically calculate the electronic structures of the zinc-porphyrin molecules when vertically attached, to further study the light interaction with the zinc-porphyrin molecules, and to fabricate zinc-porphyrin based optoelectronic devices.

Let us start with our research in the field of organic optoelectronic where we address fundamental aspects of the interaction of Zn-porphyrin molecules and visible light. The relevance of porphyrin encompasses several fields in science, from biological systems to chemical and physical properties that is the focus of the present work. Such broad scientific output is motivating and encouraging to contribute fundamentals aspects of porphyrin-light interaction to several branches of the scientific community. Next chapter addresses the necessary introduction to porphyrin molecules.

CHAPTER 2 Structure and Properties of Porphyrin Molecule

Research on molecular electronics has intensified since Aviram and Ratner's theoretical proposal of a molecular rectifier in 1974 [6], and now has grown into a prosperous interdisciplinary field. With the high tunability of electronic properties via control of the chemical structures and the highly-dense integration possibility via self-assembly, organic molecules present great potential toward the realization of the next generation of electronic devices. Among all classes of organic molecules, natural photo-activated proteins, with porphyrin macrocycles as active cores, manifest rich electronic and photonic properties and thus have raised the possibility of optoelectronic device applications. This chapter serves as an introduction on porphyrin molecules. Section 2.1 describes the structure of porphyrin molecule, while section 2.2 and 2.3 discusses previous research done on the optical spectroscopy and electronic properties of porphyrin molecules respectively.

2.1 Structure of Porphyrin

Porphyrin molecules comprise a family of organic compounds that exist extensively in natural biological systems. The simplest porphyrin molecule is porphine, which is structurally tetrapyrroles, as shown in Figure 2.1. The porphine is a planar macrocycle formed by four pyrrole molecules interconnected via methine bridging units. The carbon atoms are labeled depending on their positions; a) α positions, next to nitrogen, b) β positions, opposite to nitrogen in the pyrroles, and c) meso-carbons, in the bridging methine.

The alternating double bonds in the porphine macrocycle provide the delocalized π electrons. The porphine macrocycle has a total of 22 π electrons; however, only 18 of

them are delocalized (bold bond in Figure 2.1 left), making the macrocycle a highly conjugated system. Two double bonds located on the two diagonal pyrrole rings respectively are excluded from the conjugated system and, therefore, can be easily reduced, forming chlorin, or bacteriochlorin (Figure 2.2), depending on which double bond is reduced.

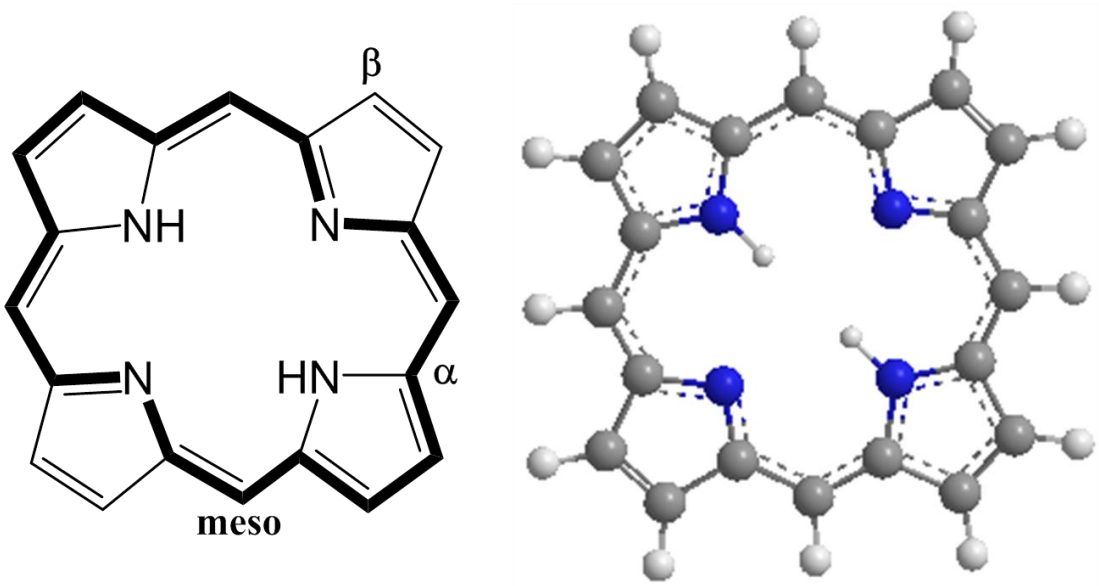

Figure 2.1 Simplest porphyrin: Porphine. Left: Molecular structure. Bonds in bold line represent the π electron circuit. Right: 3D structure. Blue: Nitrogen; Dark gray: Carbon; Light Gray: Hydrogen. Dash line shows the π electron circuit.

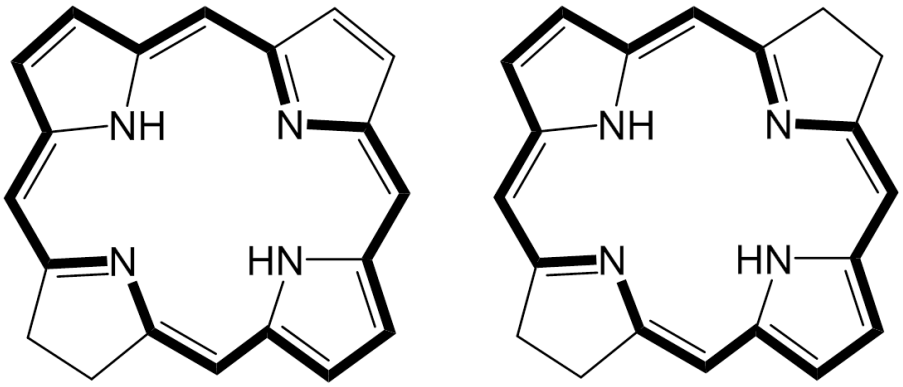

Figure 2.2 Chlorin (Left) and Bacteriochlorin (Right) structures.

The size of the porphyrin macrocycle makes it easy to accommodate different metal ions, such as Zn, Fe, Co, Ni, etc. in the center, producing metalloporphyrins [32]. The two diagonal nitrogen atoms deprotonate and bind to the metal ion forming a dianionic ligand (Figure 2.3). Due to the size of the incorporated metal, the molecule might not remain planar, but can be distorted. Although the color from the porphyrin mainly comes from electron transition from the π* to π porphyrin ring orbitals, the bound metal's d orbitals do interact with π orbitals, affecting their energies; therefore, causing color differences [33].

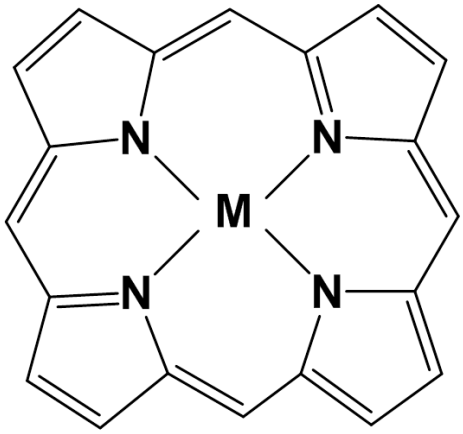

Figure 2.3 Structure of metalloporphryin cycle. M is the incorporated metal atom.

Metalloporphyrins not only give multiple colors to the compound, but also serve as active components in compounds or protein complexes, which play crucial roles in biological processes [34]. Depending on the metal ions bound to the porphyrin macrocycles, the functions vary from diatomic gas transfer (heme in hemoglobin), to light harvesting and energy conversion (Mg-chlorin in chlorophyll), to electron transfer (heme in cytochrome c).

Chlorin plays the crucial role in photosynthesis, converting solar energy into chemical energy. Such capability of light harvesting, electron and energy transfer motivate researchers to study the optical and electronic properties of porphyrin macrocycles.

2.2 Optical Spectroscopy Properties of Porphyrin

Multiple efforts were taken to study optical properties of porphyrin. Since porphyrins often exhibit intense absorption bands within the wavelength range of visible light, which is the basis of the characteristic colors, UV-Visible absorption spectroscopy is, therefore, one of the most prevalent experiments on porphyrin. Figure 2.4 shows typical tetraphenylporphyrin (H_2TPP) and zinc-tetraphenylporphyrin (ZnTPP) UV-visible absorption spectra [35].

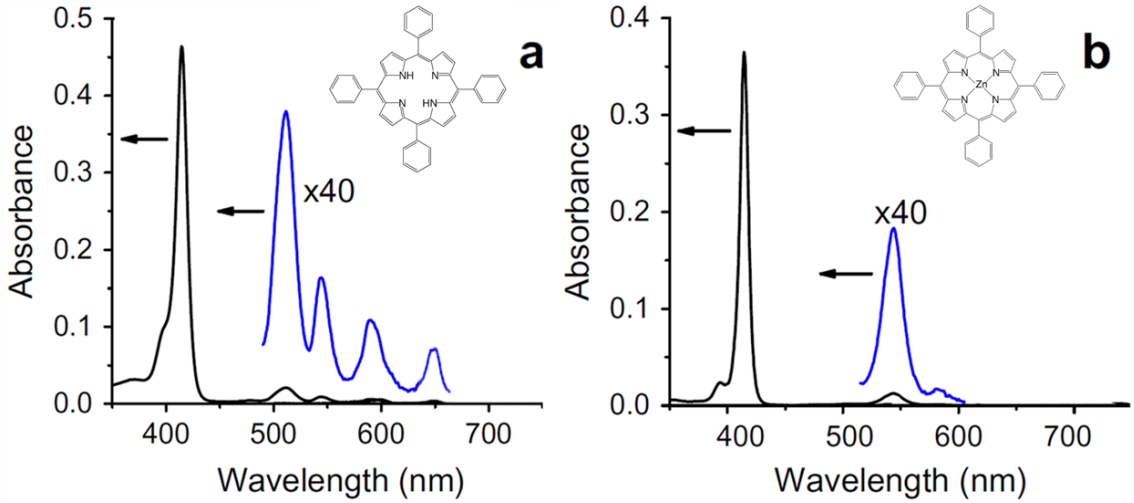

Figure 2.4 Steady state absorption spectra in hexane at 300 K of (a) H_2TPP (b) ZnTPP. Adapted from Ref. [35].

Generally, two distinct regions present in the UV-visible absorption spectrum of porphyrin, similar to Figure 2.4. The first involving an intense peak around 400nm is referred as B band or Soret band, and involves a strong electronic transition from the

ground state, S0, to the second excited state, S2. The second region with weak peaks in a range around 550nm are referred to as Q bands, and involve weak electronic transitions from the ground state, S0, to the first excited state, S1. As shown in Figure 2.4, Q bands can present between two and four weak peaks with different intensities. The number and intensity of the Q bands are affected by the metalation and substitution groups on the macrocycle.

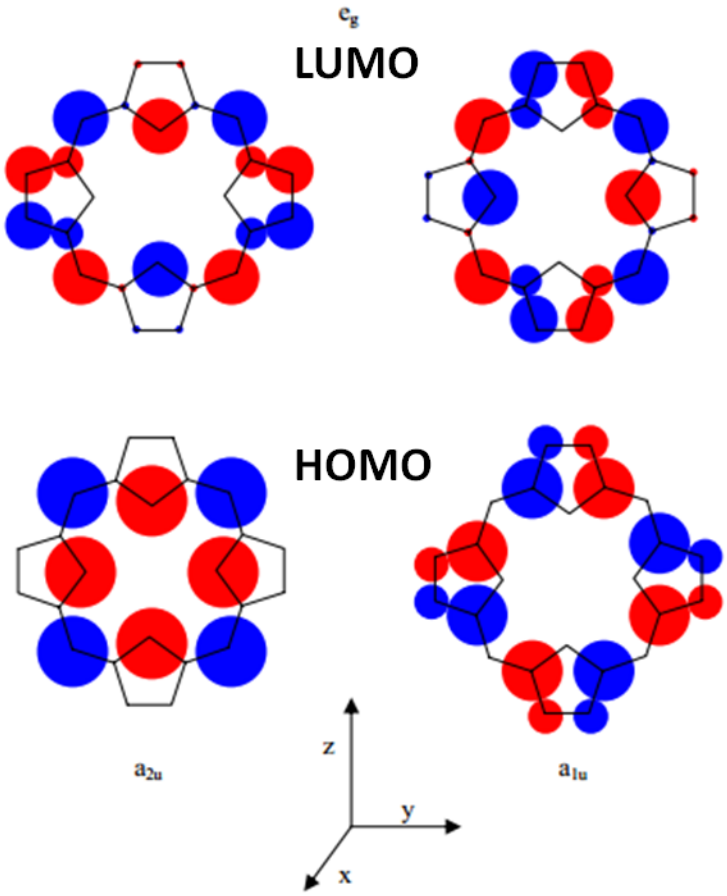

Figure 2.5 Gouterman four-orbital model, explaining the optical absorption spectra of simple porphryin molecules. Adapted from Ref. [36]

To explain Q and B band positions and multiplicities of porphyrin optical absorption spectra, M. Gouterman proposed a four-orbital model in the 1960s [37] . The

theory states that the absorption bands involve transitions between two highest occupied molecular orbitals (HOMO) and two lowest unoccupied molecular orbitals (LUMO), and the metal centers, as well as the substituents on the macrocycle, affect the energies of those orbitals. Figure 2.5 describes the HOMO and LUMO levels for porphyrin without a metal center. Further details in the porphyrin energy levels indicate that the LUMOs (b_1, b_2) are degenerate while the HOMOs (c_1, c_2) consist of two non-degenerate orbitals, owing to the molecular vibrations within the porphyrin macrocycle, see Figure 2.6.

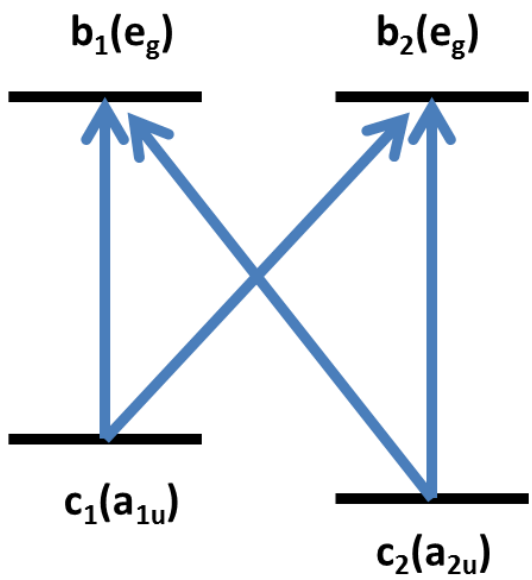

Figure 2.6 Electron transitions from ground state to excited states of porphyrin molecules, described by Gouterman four-orbital model.

A mathematical technique called configuration interaction (CI) can find the best molecular orbital wave functions (more stable) for the ground and excited states. CI describes the interaction of different electronic states (configuration), by mixing bonding and antibonding wave functions with same symmetry. The mixing of wave functions gives rise to energy splitting of two excited states, one corresponding to the Soret or B band, the other associated with the Q bands. The singlet states from transitions of c_1 to b_1

and c_2 to b_2 have similar symmetry, while singlet states from c_2 to b_1 and c_1 to b_2 transitions have similar symmetry. Therefore, by mixing wave functions with similar symmetries, CI generates a new set of more stable wave functions, which represent the excited states. All singlet states have similar energy, and consequently constructive interference corresponds to one strong B band, while the destructive interference yields two transitions with different intensities, corresponding to weak Q bands. Metalloporphyrin macrocycles are structurally equivalent in y and z directions and therefore have higher symmetry compared to free base porphyrin (Figure 2.1, 2.3), thus resulting in the two peaks of Q bands (Figure 2.4b). For free base porphyrin, the y and z components each have two Q bands, resulting in a total of four peaks (Figure 2.4a).

At this stage we see how porphyrin molecule interacts with UV and visible lights. With optical spectroscopy of the porphyrin molecule, the preliminary electronic structure information is revealed. More powerful theoretical and experimental tools have been used to examine the electronic properties of porphyrin macrocycles, and are reviewed in the next section.

2.3 Electronic Properties of Porphyrin

Applications in molecular electronic devices dictate that porphyrin molecules need to be attached to solid surfaces and to operate in ambient environments. The properties of porphyrin molecules, as well as the porphyrin-substrate interface, in ambient conditions need to be understood. J. Otsuki describes achieving molecular electronics with porphyrin (Figure 2.7) in his review [38]. Considerable progress has been made on the structure side, including designed order self-assembled porphyrin monolayers on highly ordered pyrolytic graphite (HOPG) and metal substrates. For the

much more challenging step of constructing non-periodic surface assemblies, which is essential toward the realization of molecular electronic circuits, no practical approaches have been demonstrated via the bottom-up approach to date. When it comes to the perspective of function in molecular electronics, research hasn't reached beyond the initial stage, and is still focused on the investigation of electronic properties of porphyrin-related molecules.

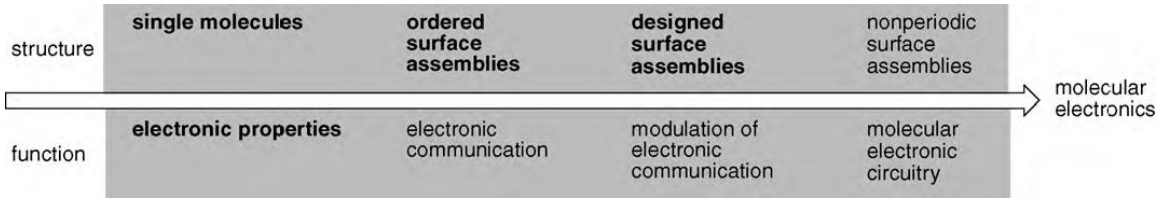

Figure 2.7 Map toward realization of molecular electronics in porphyrin. Achievements have been made in the area in bold font, while topics in plain letter are future challenges. Adapted from Ref. [38]

Toward understanding functional aspect, there are a number of investigations of the porphyrin molecular electronic properties theoretically via density functional theory (DFT) [39-42] and symmetry adapted cluster – configuration interaction (SAC-CI) [43], and also experimentally via scanning tunneling microscopy/spectroscopy (STM/STS) [44-56] and STM breakjunctions [57-62].

As previously stated in Section 2.2, the Gouterman four-orbital theory explains the optical spectroscopy of porphyrin molecule well in terms of peak intensities and multiplicities. Although it reveals important information, the theory only covers four orbitals that are close to the HOMO/LUMO levels, and does not describe the whole molecular orbital structure of porphyrin.

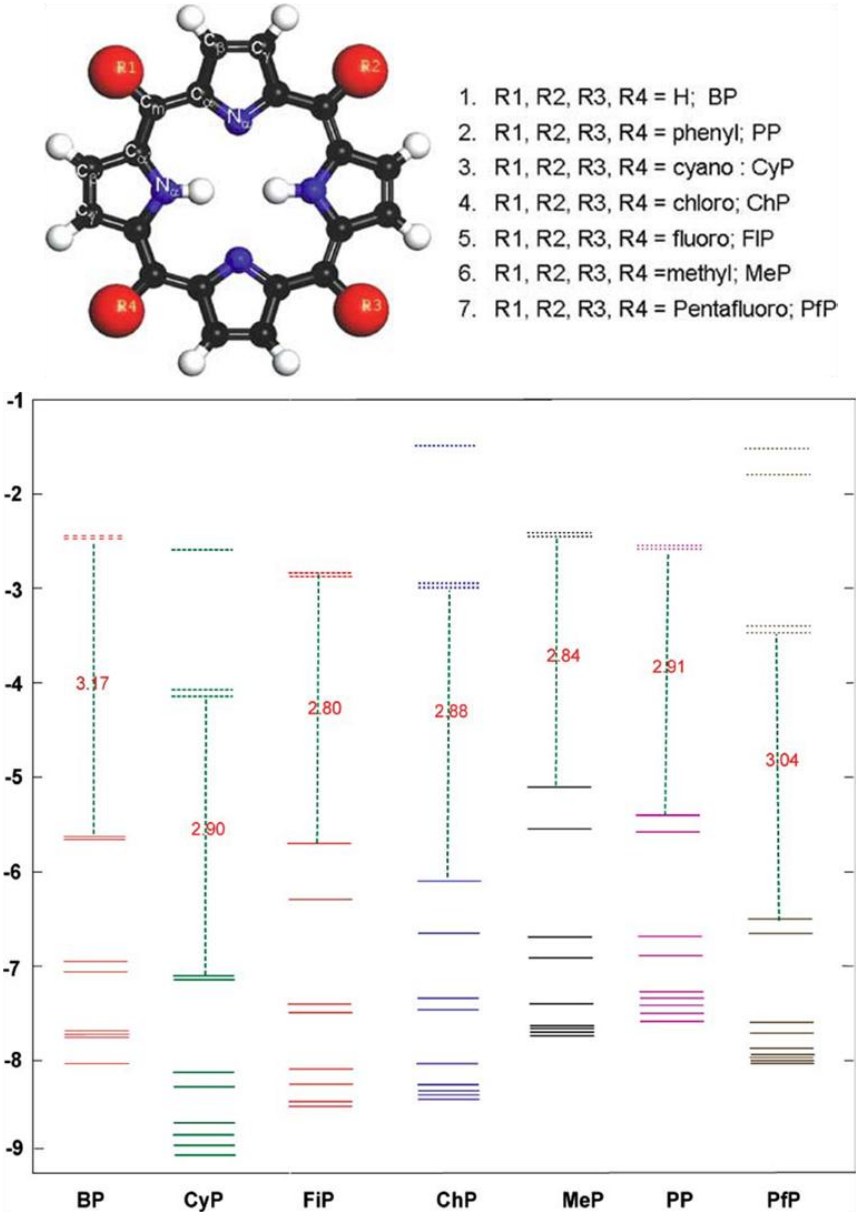

Figure 2.8 Structure (Top) and molecular orbital energy level diagram for the free base porphyrin and porphyrins with different meso-substituents. Solid lines represent HOMOs while dotted lines represent LUMOs. Adapted from Ref. [39]

DFT calculations have been carried out on different porphyrin molecules in an attempt to determine the full molecular orbital structure. N. Venkataramanan et al. [39] used DFT and time-dependent DFT to study the electronic structure of different symmetries of meso-substituted porphyrin molecules, and constructed a frontier molecular orbital energy level diagram (Figure 2.8). It shows that the degeneracy of

HOMO and HOMO-1 orbitals varies with different meso-substituents. HOMO and LUMO levels are lower for electron-withdrawing (CyP, ChP, FlP) meso-substituent groups, while higher for electron-donating (MeP, PP) meso-substituent groups. Simulated absorption spectra were also constructed, showing that porphyrins with meso-substituted electron donating groups exhibit redshift in Q bands, while an increase of peak intensity in B band is associated with electron withdrawing group substituents.

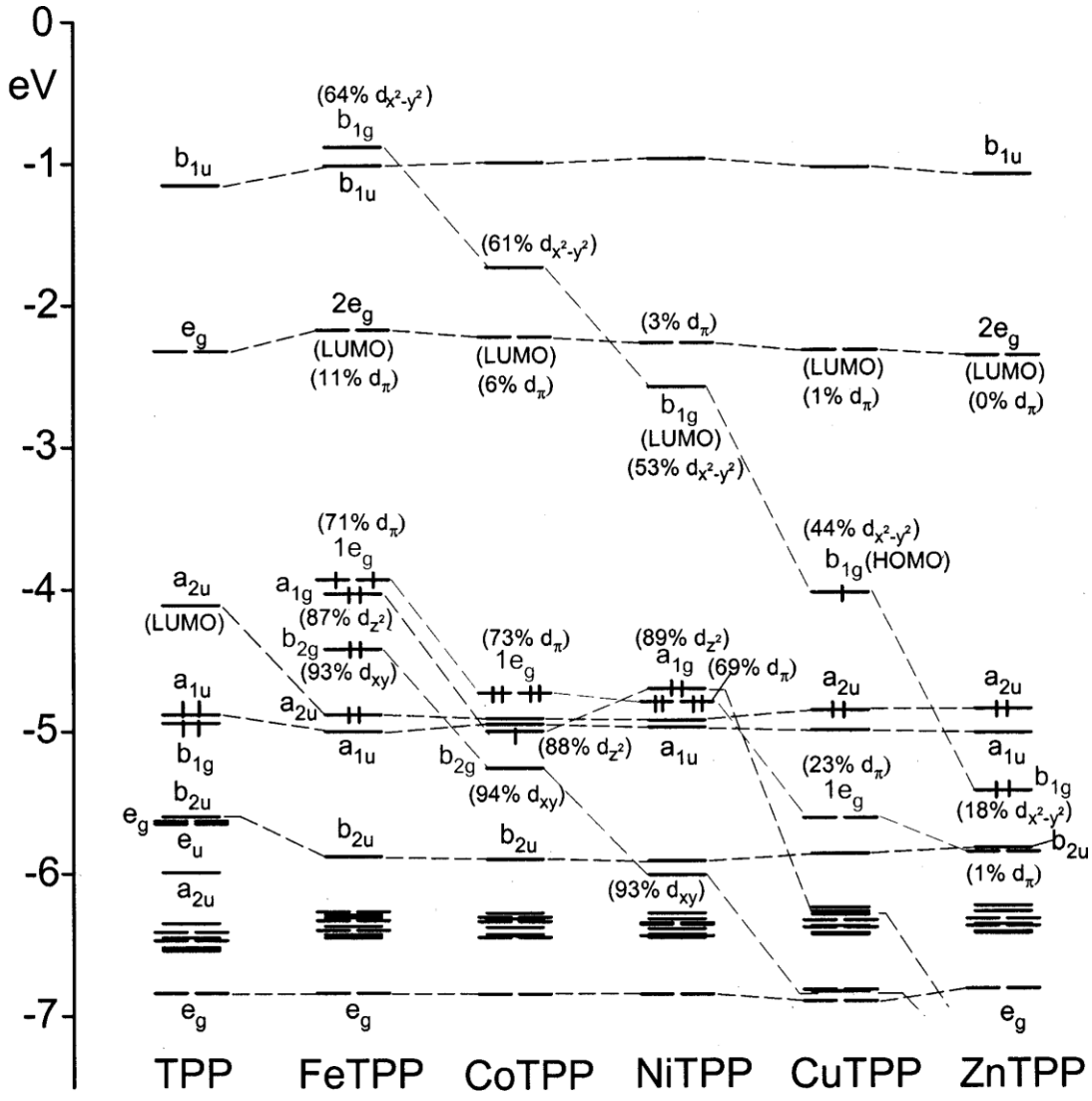

Figure 2.9 Molecular orbital energy levels for TPP and MTPPs. Moving from Fe to Zn across the periodic table, the energies of the metal d-orbitals become lower. Adapted from Ref. [40]

M. -S. Liao and S. Scheinera performed systematic DFT calculations [40], determining not only molecular orbital structures, but also binding energies, ionization potentials, and electron affinities of a porphyrin molecule with different metalations, charges, axial ligands and peripheral substitutions. Results show that (Figure 2.9), molecular orbitals of porphyrin molecules vary with d orbitals of the incorporated metal ion. For Fe, Co, Ni, and Cu, the HOMOs are metal 3d-like, while for Zn the 3d-orbitals are lower than the porphyrin π orbitals in energy.

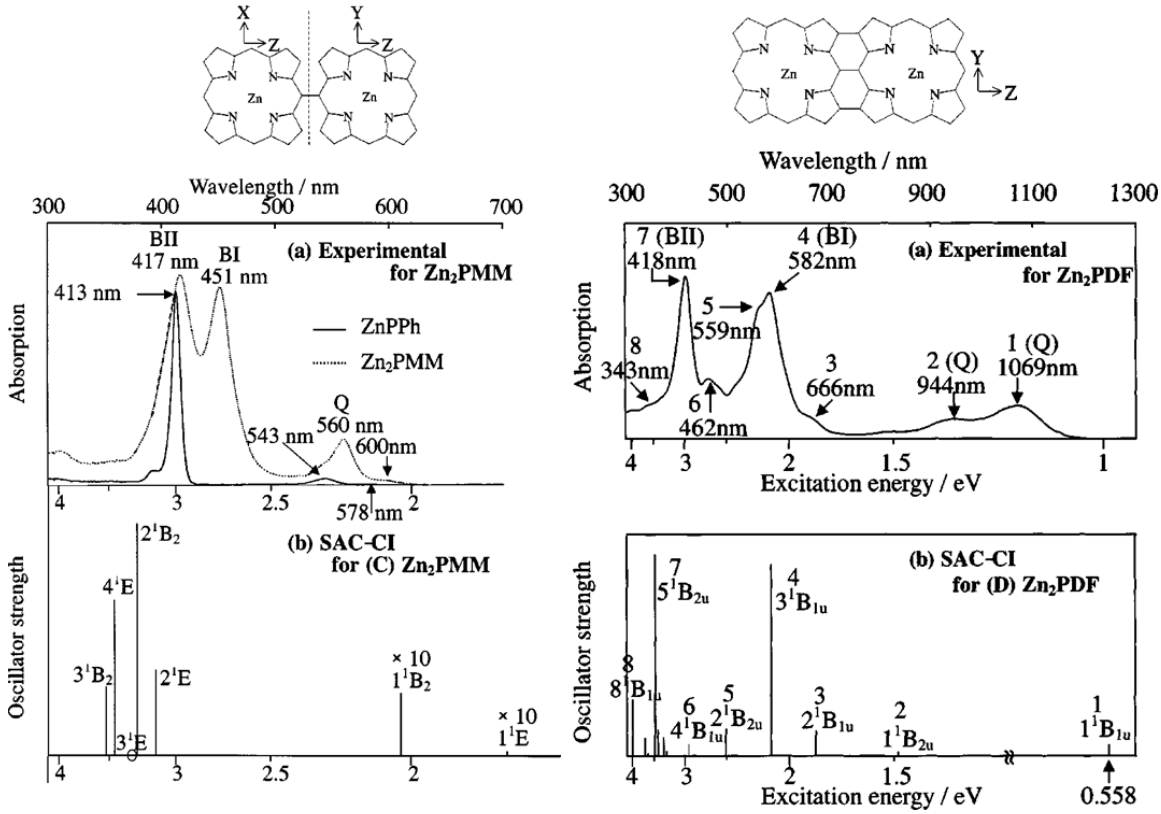

Figure 2.10 Structure, experimental spectrum and theoretical spectrum of zinc porphyrin meso-meso linked dimer Zn_2PMM (left) and zinc porphyrin doubly fused dimer Zn_2PDF (right). Adapted from Ref. [43]

T. Miyahara et al [43] studied ground and excited states of zinc porphyrin monomers, meso-meso linked (Zn_2PMM), and doubly fused (Zn_2PDF) zinc porphyrin dimers with SAC/SAC-CI method. Electronic orbital level diagrams of all three

molecules were constructed, and such information was further used to study the molecular excited state energies and optical spectra. For Zn_2PMM, the dimerization further splits the HOMO and HOMO-1, as well as LUMOs, resulting in the split of the Soret band (Figure 2.10 left). For Zn_2PDF, molecular orbital levels became more complicated since the coupling of two macrocycles brought in more delocalized π electrons, resulting much smaller HOMO-LUMO energy gap, and a further split of the Soret band (Figure 2.10 right).

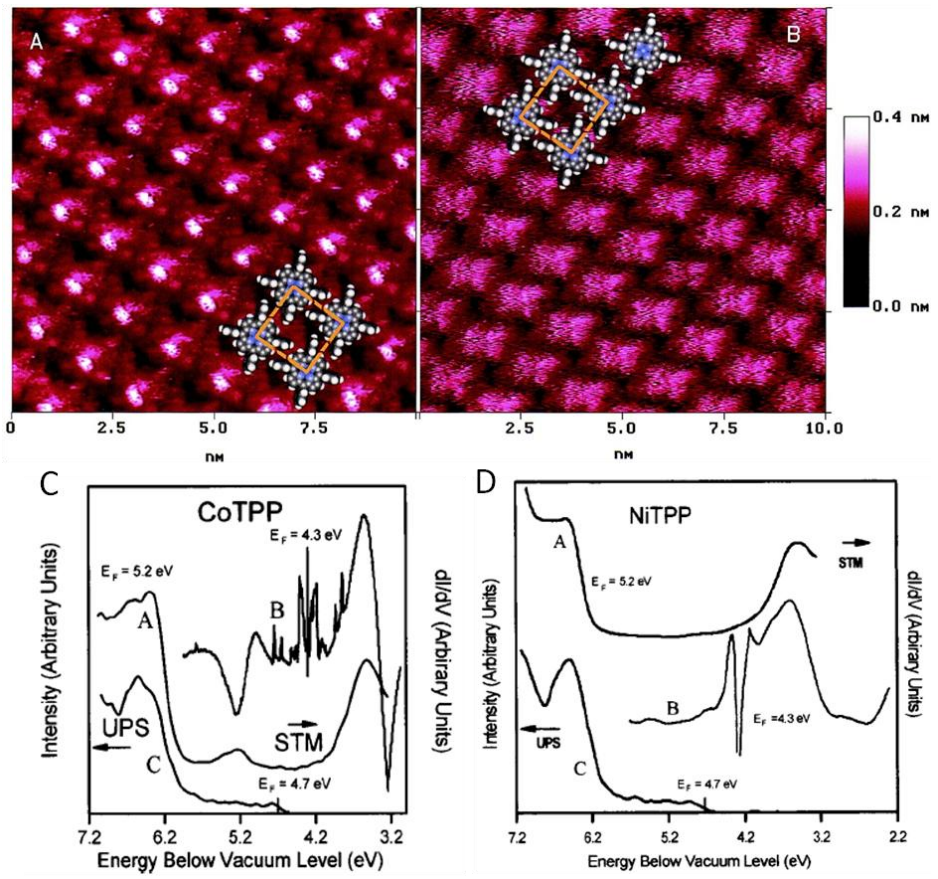

Figure 2.11 STM topography image of (a) CoTPP and (b) NiTPP on Au(111). Combined results of UPS (curve C), STS (curve A), and Normal tunneling intensity vs. voltage (curve B) of (c) CoTPP and (d) NiTPP. Curvepositions on the x-axis are adjusted for differences in device work function. Adapted from Ref. [44, 45]

In addition to theoretical calculations, a variety of experiments have been carried out to probe the electronic structures of porphyrin molecules. L. Scudiero et al. [44, 45] conducted a series of experiments performing STM and STS on Ni and Co tetraphenylporphyrin (NiTPP and CoTPP) self-assembled monolayers on Au(111) surface. STS indicates π HOMO and π* LUMO for NiTPP and CoTPP lie at about -1.2eV and 1.7eV with respect to the Fermi level of the Pt/Ir tip, as shown in Figure 2.11. In CoTPP STS a small peak at -0.1eV was also observed, and is attributed to half-filled d_z^2 orbital on the Co atom. Such a peak was not present in STS spectra of NiTPP since d_z^2 orbital of Ni atom is filled. Similar results have been published on Ni octaethylporphyrin as well [46].

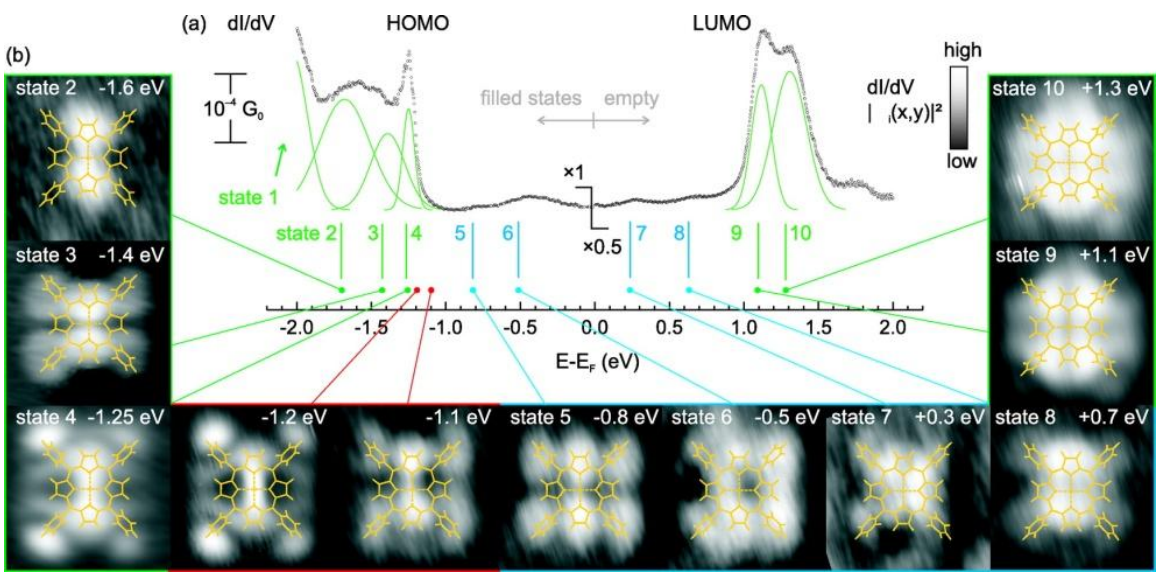

Figure 2.12 STS spectrum and conductance maps of different energies of single $AuTPP^+$ cations on Au(111). Multiple Gaussian peaks are fitted to data and assigned to different states. Adapted from Ref. [49]

S. Müllegger et al. [48, 49] did low temperature STS studies on AuTPP single molecules on the Au(111) surface. The research investigated the HOMO-LUMO structure both theoretically and experimentally, and produced electronic state maps under

constant current conditions, showing spatially resolved density of states within a single porphyrin macrocycle (Figure 2.12). The STS spectra exhibit a significant deviation of HOMO-LUMO gap energy from DFT calculated value in gas phase, pointing to molecule-substrate interaction. The STS dI/dV spectra was further deconvoluted into multiple Gaussian peaks with each peak associated with different molecular orbitals and Au(111) surface or interface states. DFT calculations were also conducted, investigating the interaction of the porphyrin and Au(111) surface. It was concluded that Au(III) d states mix to HOMO and LUMO of the porphyrin molecule. Furthermore, the contribution of Au d orbitals can be tuned.

A particular interesting study was performed by Y. Majima et al [50] on Tribenzosubporphine via STM/STS. Tribenzosubporphine is a triangular shaped molecule with 14 delocalized π electrons, which makes it aromatic. Reacted with a self-assembled monolayer of 1-heptanethiol molecules on Au(111) surface, the subporphine molecule was anchored to the substrate and electronically decoupled from the gold surface (Figure 2.13a). STS measurements were performed with tungsten tip both on the subporphine molecule and bare SAMs (Figure 2.13c). A capacitor in series model was used to evaluate the HOMO-LUMO energy gap, with the SAM as one insulating capacitance layer, and the tip-molecule vacuum distance as the other. The HOMO-LUMO gap was evaluated as 2.5eV. Negative differential resistance (NDR) was observed when the subporphine adsorbed onto the STM tip (Figure 2.13d). Such NDR phenomena result from resonant tunneling through the frontier molecular orbitals of the tribenzosubporphine and its cation adsorbed on the tip.

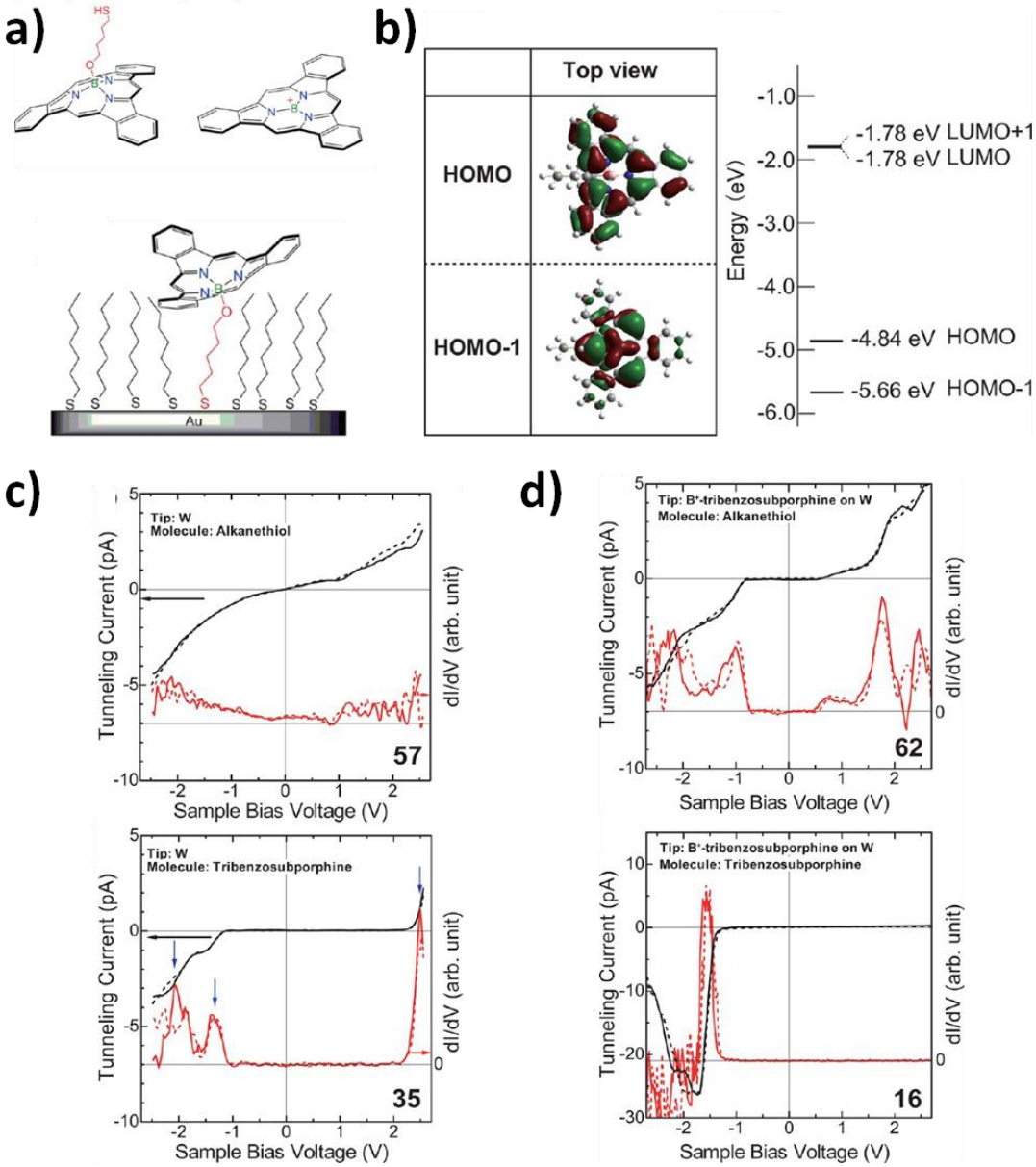

Figure 2.13 (a) Molecular structure of Tribenzosubporphine and schematic of its attachment to the self-assembled monolayer. (b) DFT calculated molecular orbitals and their energy levels. (c) STS measurements (I-V and dI/dV -V) on 1-heptanethiol (top) and tribenzosubporphine (bottom) with bare W tip. (d) STS measurements (I-V and dI/dV -V) on 1-heptanethiol (top) and tribenzosubporphine (bottom) with the subporphine cation anchored to the tip. Notice the NDR happens with the subporphine cation attached to the tip when scanning over the subporphine. Adapted from Ref. [50]

Other studies attempted to examine perpendicular configuration of the porphyrin at the substrate [51, 52]. To achieve the perpendicular geometry, alkanethiol self-

assembled monolayers act as a matrix and support for thiolated porphyrin macrocycles. Current voltage spectra were collected to demonstrate the difference of transport between porphyrin molecule and the alkanethiol supporting matrix; however, there were no attempts to show detailed electronic state structures.

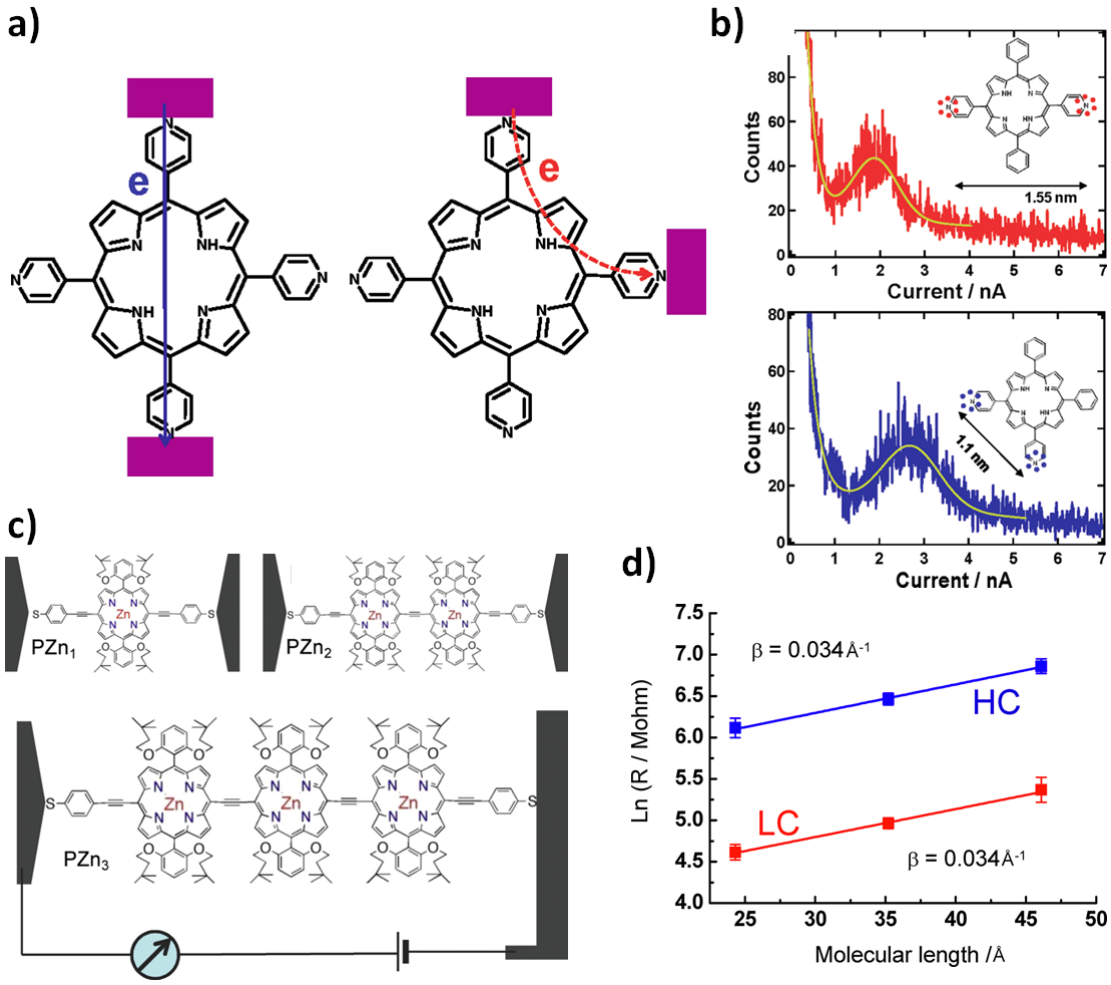

Figure 2.14 (a) Charge transport pathways through a single tetrapyridylporphyrin (TPyP) molecule in an STM break junction. Left: the longer "para" position, Right: the shorter "ortho" position. (b) Current histogram of Top: para-DPyP, Bottom: ortho-DPyP fitted by a gaussian plus exponential function as a guide to the eye (yellow curve). Inset: molecular structure. (c) Schematic of STM break junction-based single molecule conductance measurements for dithiol terminated PZn_n compounds. (d) Resistance vs length of the molecule. The red and blue lines correspond to high conductance (HC) and low conductance (LC) data. The β values are calculated based on $R = R_0\exp(\beta L)$. Adapted from Ref. [58, 59]

STM breakjunctions were adopted to study the charge transport within single porphyrin or porphyrin oligomer molecular wires. Z. Li et al. [58] performed STM breakjunction study of porphyrin with four pyridyl meso-substituents (TPyP) and similar structures (ortho-DPyP and para-DPyP). By comparing current histograms of all three molecules, it was found that the charge transport pathway was dominated by the farther anchoring groups in “para” position, rather than the shorter path between the neighboring groups in “ortho” positions (Figure 2.14a, b). The same group also conducted research on dithiolated porphyrin oligomer molecular wires [59]. Each wire exhibits dual molecular conductance, while molecular resistance across the break junction increases linearly with respect to the molecular wire length in each conductance regime. These properties are described with the incoherent hopping transport mechanism (Figure 2.14c, d). In the low conductance regime, charge carriers transport through fully stretched molecules, while in the high conductance regime, charge carriers transport through the molecules bound now at an angle to the electrode surface normal.

With fundamental electronic properties of porphyrin molecule being probed optically and electronically, few experimental efforts were made to understand the effect of the interaction with light on porphyrin electronic structures. To achieve that goal, experiments were conducted, with the procedures described in the next Chapter.

CHAPTER 3 Experimental methods and Procedures

The work on the porphyrin molecule and its derivatives brings the goal of molecular electronic devices closer to realization. To exploit porphyrin electronic and photonic properties to make optoelectronic devices, we need to understand the interaction of porphyrin electronic structure with light within a device configuration. Section 3.1 includes the preparation of the mixed monolayer sample where the porphyrin achieves the device configuration, and section 3.2 describes the setup and operation of scanning probe microscopy/spectroscopy with light illumination at tip-sample junction.

3.1 Mixed Monolayer Preparation

To explore porphyrin based optoelectronic devices, we need to understand the interaction of the porphyrin electronic structure with light. The sample needs to be prepared with the porphyrin molecules in a device configuration with the longitudinal axis of the porphyrin molecule perpendicular to the substrate. To achieve the configuration a mixed monolayer of alkanethiol and zinc-porphyrin molecules were prepared. First, α-thiol terminated meso-to-meso ethyne bridged (porphinato)zinc(II) supermolecules (PZn_n molecule) were synthesized as previously reported [28-30, 63-66], as shown in Figure 3.1. Such molecules are fully conjugated, have large absorption cross-sections and demonstrate near barrier-less charge transport properties [64-66].

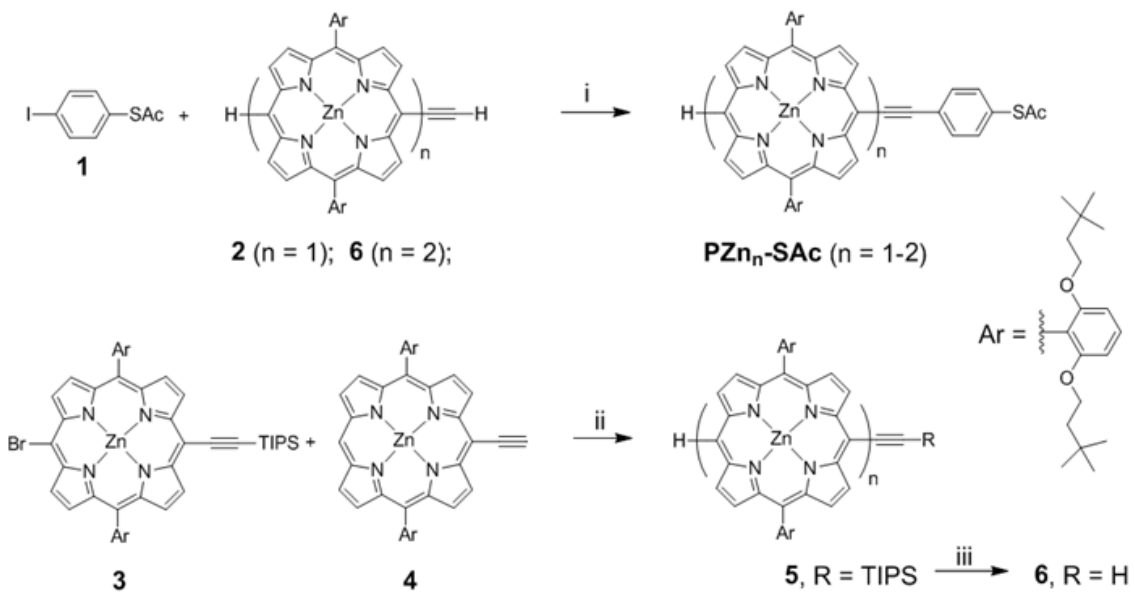

Figure 3.1 Synthesis of a-Acetythio-Terminated (Porphinato)Zn(II) Arrays. (i) $Pd(PPh_3)_4$, THF/DIEA, 35-40°C; (ii) Pd_2dba_3, P(*o*-tol)$_3$, THF/Et_3N, 60°C; (iii) TBAF, THF, 0°C; Adapted from Ref. [63]

3.1.1 Alkanethiol Self-Assembled Monolayer

Self-assembled monolayers (SAMs) are ordered molecular monolayers formed spontaneously through chemisorption of the head group of a surfactant molecule onto the substrate. Of all molecular thin films, one of the most studied are the self-assembled monolayers of alkanethiol molecules on Au(111) surface [67, 68].

Alkanethiol is a hydrocarbon chain of variable length with a sulfur head group, as show in in Figure 3.2. Once adsorbed on Au(111) surface, the molecule loses a hydrogen atom and binds to the substrate through the sulfur head group, forming a thiolate (Au-S) bond [69]. Driven by the high affinity of the thiolate bond, as well as hydrophobic intermolecular interactions between hydrocarbon chains, alkanethiol molecules form closed packed structures on Au(111) surfaces [68]. Due to the simplicity and flexibility of the preparation procedure, the stability of the monolayer, and the tunability of surface

properties, alkanethiol SAMs were often adopted to build more complex nanoscale structures [70].

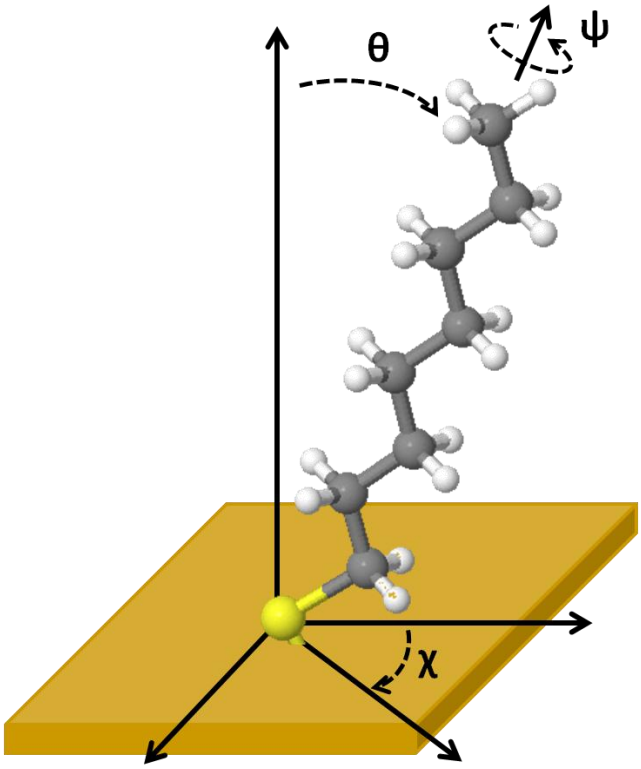

Figure 3.2 Schematic of a 1-octanethiol molecule bound to substrate via thiol group. Yellow: sulfur atom; Gray: carbon atoms; White: hydrogen atoms. Here θ refers to the tilt angle of the molecular axis from surface normal of the substrate; χ describes the angle of precession and ψ is the twist angle which defines the angle of rotation around the hydrocarbon chain axis.

Previous studies [71-73] showed that the alkanethiol molecules tilt ~30° from the surface normal, forming a (√3×√3)R30° hexagonal closed-packed overlayer with unit cell spacing of 4.97 Å. The overlayer structure was confirmed via low energy helium diffraction [71], atomic force microscopy [74] and scanning tunneling microscopy [75] studies. A superstructure of c(4×2) also presented in STM studies, showing larger apparent height than (√3×√3)R30° structure [75, 76]. The origin of the c(4×2) superstructure has been discussed in the context of hypotheses such as; a) different

molecular tilt angles θ [77], b) different twist angles ψ of hydrocarbon chain [78], and c) unsymmetrical location of the sulfur headgroups [79]. However, the underlying principle for the formation of the c(4×2) superlattice is still under discussion. Defect sites such as vacancies of the adsorbate or grain boundaries usually exist and can be observed from STM images, and are crucial for the next step of the mixed monolayer preparation.

In our experiment we choose 1-octanethiol (Alfa Aesar, 98%) as the molecule to form SAMs structure. Au(111) thin films on mica (purchased from Agilent Technologies) were first cut to fit in the STM sample holder, then flame annealed with hydrogen for 30 seconds to achieve an atomically flat Au(111) surface. About 0.05 ml (one drop) of 1-octanethiol was dropped on the bottom of the micro reaction vessel, where the Au(111) samples were inserted. The reaction vessel was capped and incubated in oven at about 75°C for 15 minutes. Longer time will reduce the density of defects of SAMs, which is disadvantageous for the subsequent steps. The preparation of SAMs is finished by a rinse and dry step with 2-propanol and ultra high purity nitrogen. After this procedure the 1-octanethiol SAMs were ready for the insertion of the PZn_n molecule (Figure 3.3).

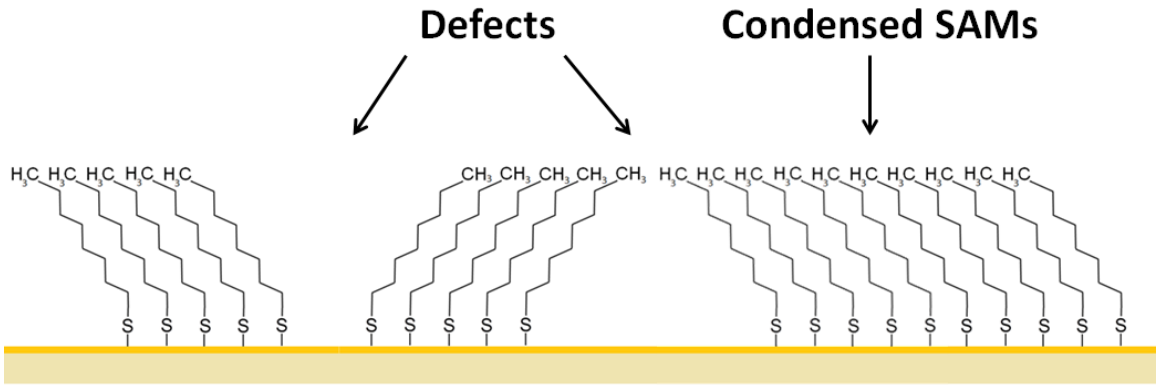

Figure 3.3 Schematic of 1-octanethiol SAMs on substrate. Condensed phase forms while defects such as vacancies and grain boundaries exist.

3.1.2 Zinc-Porphyrin Molecule Insertion

In order to measure the electronic properties of isolated single porphyrin molecules while attached to an electrode, the molecules need to be separated on the substrate with the long axis of the molecules aligned perpendicular to the substrate. To ensure the vertical alignment as well as individual molecule separation, 1-octanethiol SAMs were used as host matrix.

The adsorption process of the alkanethiol SAMs is highly dynamic; the alkanethiol molecules on the surface exchange with thiol molecules in the solution [80]. Multiple types of defects are found in SAMs, such as molecular vacancies, gold surface step edges and monolayer grain boundaries. In the vicinity of those defect sites, molecular exchange is expected to be more active, since at those sites adsorbed alkanethiol molecules are more accessible to the solvent [70]. As a result the defects can be utilized to achieve selective chemisorption of a second adsorbate molecule. The above mentioned methods have been previously adopted and demonstrated with different molecules such as: a) phenylene ethynylene [81], b) 11-mercaptoundecanoic acid [82], and c) other porphyrin molecules [51, 52]. We refer to “insertion” as the process of attaching the PZn_n molecules in the SAMs-substrate ensemble.

As shown schematically in Figure 3.4, thiolated PZn_n (only n=1 shown in figure) molecules were chemisorbed on the Au(111) surface via the Au-S bond, within or in the vicinity of defects of the 1-octanethiol SAMs.

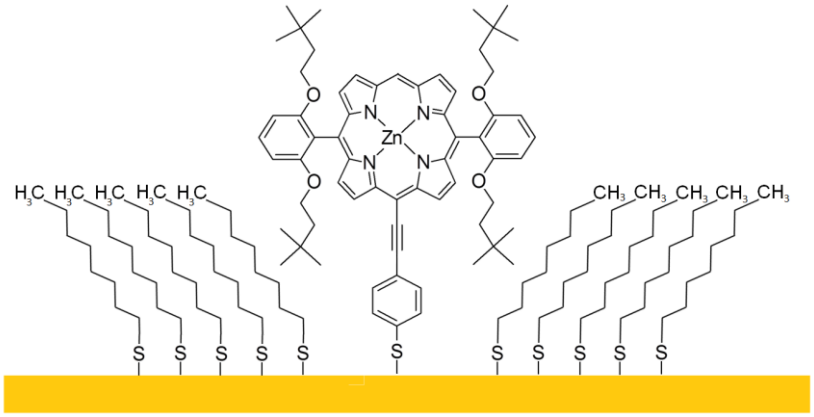

Figure 3.4 Schematic of mixed monolayer of PZn_1 molecules and 1-octanethiol molecules on substrate.

To achieve the insertion, approximately 1µM concentration solution of S-acetyl-protected PZn_n molecules was prepared in distilled THF, and then 6-10µL NH_4OH solution (28 to 30 w/w %, Certified ACS Plus, Fisher Chemical) per 1mL of THF was added, exposing the thiol functional group. The freshly prepared 1-octanethiol SAMs on gold film was then immersed into PZn_n solution for a specified time between 1 hour and 48 hours. A list of experimental parameters used in order to optimize the PZn_n chemisorption, is shown in Tables 3.1 and 3.2. Then the sample was removed from the solution and repeatedly rinsed with distilled THF and dried with flowing nitrogen (3 times). All procedures involving PZn_n molecules were accomplished in a glove box purged with ultra high purity nitrogen.

Table 3.1 Parameters used in attempt to achieve PZn_1 molecules insertion into 1-octanethiol matrix.

NH_4OH solution/THF	4µL/mL	6µL/mL	8µL/mL	10µL/mL
NH_4OH/THF / Time	1.03g/L	1.55g/L	2.07g/L	2.58g/L
1hr	No PZn_1	No PZn_1	Low Density	PZn_1 stable occasionally
2hrs	No PZn_1	No PZn_1	PZn_1 not stable	N/A
3hrs	No PZn_1	Low Density	PZn_1 not stable	N/A
24hrs	Low Density	Low Density	PZn_1 stable occasionally	PZn_1 stable
48hrs	Low Density	Low Density	PZn_1 stable	N/A

Table 3.2 Parameters used in attempt to achieve PZn_2 molecules insertion into 1-octanethiol matrix.

NH_4OH solution/THF	4μL/mL	6μL/mL	8μL/mL	10μL/mL
NH_4OH/THF / Time	1.03g/L	1.55g/L	2.07g/L	2.58g/L
1hr	No PZn_2	N/A	N/A	N/A
2hrs	N/A	No PZn_2	N/A	N/A
24hrs	Low Density	Low Density	PZn_2 stable	No PZn_2
48hrs	Low Density	PZn_2 stable	PZn_2 stable	N/A

3.2 Scanning Tunneling Microscopy/Spectroscopy

Scanning tunneling microscopy/spectroscopy (STM/STS) is a powerful tool in studying 3D information about sample surface structure at atomic or molecular levels. Since the original development by Gerd Binnig and Heinrich Rohrer [83], the application of STM has expanded to include topography images at atomic resolution [84], electronic structure information [85], atom and molecule manipulation [86], lithography [87].

STM operates with precise control of tip-sample junction distance at the sub-nanometer scale. Figure 3.5 shows a typical STM setup. Under the applied voltage, the electrons tunnel through the tip-sample gap, forming a current flow. The current scales exponentially with the tip-sample distance, and thus can be monitored and used as the feedback mechanism for maintaining the constant tip-sample gap. With a biased tip raster

scanning across the surface under a setpoint of tunneling current, surface topographical information can be investigated at the atomic level.

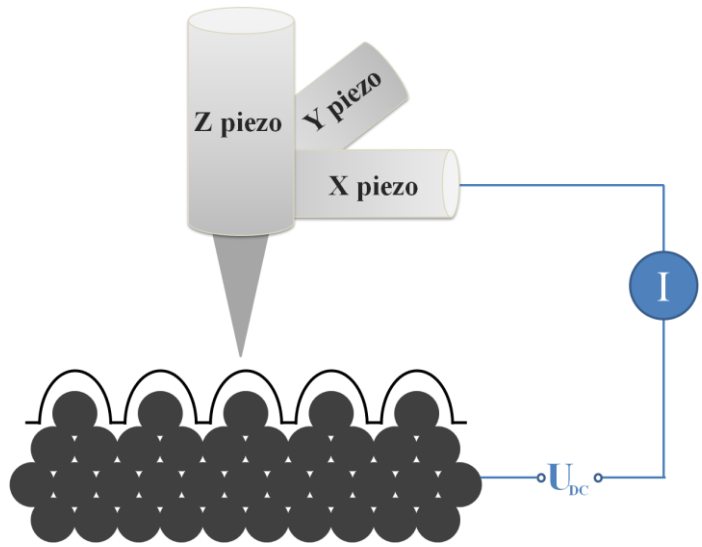

Figure 3.5 Schematic drawing of Scanning Tunneling Microscopy/Spectroscopy setup. Spheres in the sample represent atoms. Topographical information can be acquired as illustrated by the solid line with bumps.

At locations of interest, while the tip-sample distance fixed, measurement of the current is taken as a function of voltage, yielding information on the local electronic structure. Such measurements are referred to as scanning tunneling spectroscopy (STS). The measured tunneling current contains the information of local density of states (LDOS) of the sample ρ_S and tip ρ_T, according to the equation 3.1 [88],

$$I \propto \int_0^{eV} d\varepsilon\, \rho_S(E_F - eV + \varepsilon)\, \rho_T(E_F + \varepsilon) \tag{3.1}$$

where E_F is Fermi energy of the tip and V is the applied bias across the tip-sample junction. With the approximation of a constant tip DOS, the IV curve is essentially probing the LDOS of the location of interest. The derivative dI/dV can be directly related to LDOS as described in equation 3.2.

$$\frac{dI}{dV} \propto \rho_S(E_F - eV + \varepsilon) \tag{3.2}$$

In our experiment, by varying the applied voltage, the Fermi energy level of the tip with respect to the sample changes, thus different electronic orbitals of the PZn_n single molecule can be probed. As illustrated in Figure 3.6, when the sample is under positive bias, the E_F of the tip will be lower than that of the substrate and could be in the same energy level as the PZn_n HOMO, so electrons can transport through resonant tunneling from the PZn_n HOMO into the STM tip. When the tip is under negative bias, the E_F of the tip will be higher than the substrate and, consequently, could match the energy level of PZn_n LUMO, injecting electrons into the PZn_n molecule. This enables us to examine the electronic structure of the ground state, as well as the excited state of PZn_n single molecule.

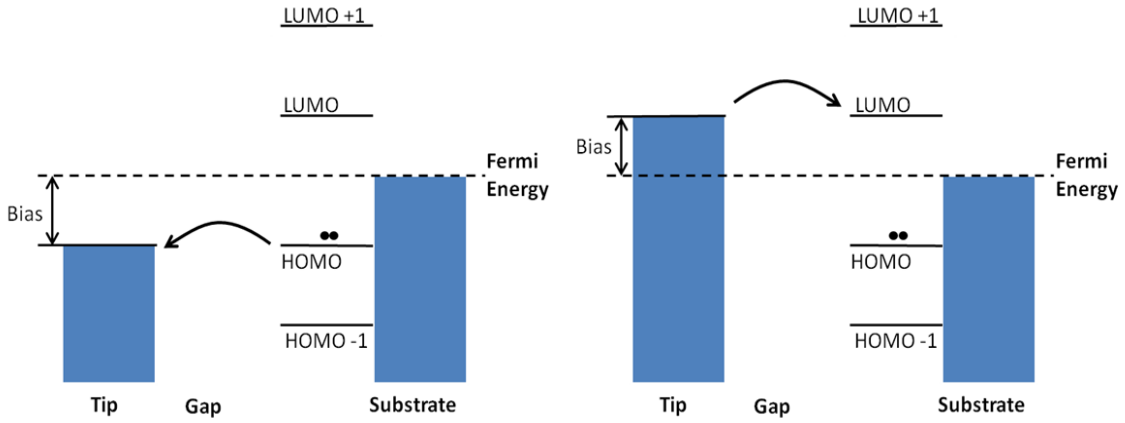

Figure 3.6 Illustration of how STS probes electron orbital alignment. Left: negative sample bias. Right: positive sample bias.

In our experiments all STM/STS measurements were acquired under high vacuum (HV) conditions and room temperature. Pt/Ir (80/20) tips were mechanically prepared with a wire cutter (Tronex Technology Inc.). Mixed monolayer sample were prepared as mentioned in Chapter 3.1, and then loaded in the custom made sample holder (Figure 3.7) so the sample bias would be directly applied to the Au(111) surface. After the sample and tip were loaded, the vacuum chamber was pumped down with a mechanical pump then a

turbo pump to a typical pressure of about 10^{-5} Torr. At this pressure molecular resolution images can be achieved using an Omicron UHV STM 1 system operated by an RHK SPM1000 control system. Typical imaging conditions of the current setpoint and sample bias voltage were 300pA, +2.5V.

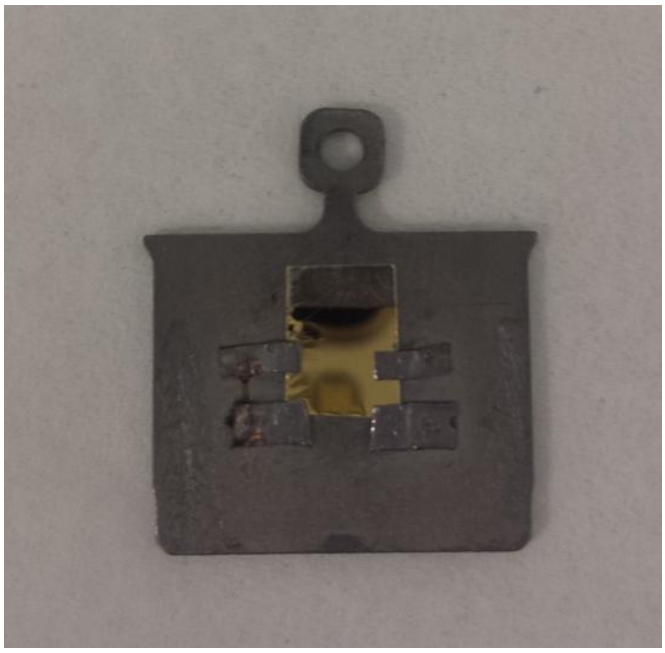

Figure 3.7 Image of STM sample holder. Since gold film was deposited on the insulating mica, to ensure contact with Au(111) film, four pieces of Ta strips were spot welded on a Omicron STM Ta sample substrate to hold the sample in place.

To aqcuire spectroscopy data on the molecule of interest, a series of STM scans were conducted. A topographical image was first scanned to ensure the successful formation of the alkanethiol SAMs, and to locate isolated PZn_n molecules. The possible thermal drift was then quantified by comparing subsequent scan of the same area, which could be as large as 5nm/frame, depending on scanning speed. A third scan was done, during which IV spectra were collected over a voltage range of -2.5V to 2.5V at the defined locations, with the feedback loop temporarily turned off, maintaining a fixed tip-sample gap distance during the voltage ramp. Current data collected over the molecule of

interest (alkanethiol or PZn_n) of each defined region (Figure 3.8) were then averaged respectively, eliminating the occasional spikes caused by instrumentation. The derivative of IV curves was then calculated (Nanotec WSxM 5.0 and OriginPro 8.0) and plotted to show the information of local density of states. Such STM/STS experiments were performed under both dark and different illumination conditions, on different PZn_n molecules.

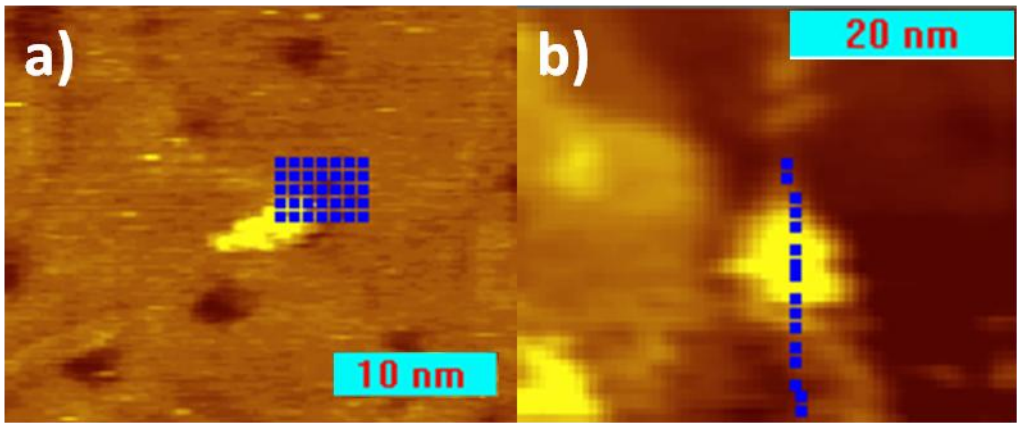

Figure 3.8 STM Images of different PZn_1 single molecules embedded in SAM matrix. IV spectra were collected at the blue spots in (a) defined region; (b) defined line. Spectra from the blue spots on top of PZn_1 molecule were averaged to give the electronic states information of PZn_1 molecule, while spectra from the blue spots on top of 1-octanethiol were averaged and used as reference.

3.2.1 Photo-assisted Scanning Tunneling Microscopy/Spectroscopy

STM is able to provide atomic level spatial resolution, yet when it comes to acquiring information of different chemical species STM has a limit. While optical spectroscopy can access detailed electronic states to the vibrational chemical bond level, it hardly provides localized information. To gain high spatial resolution and detailed information of the electronic structure simultaneously, a combination of STM and optical excitation was proposed and described as “photo-assisted STM”.

In general there are three fundamental methods of photo-assisted STM [89]: (a) STM/STS measurement before and after light irradiation; (b) STM/STS measurement with and without light irradiation; (c) STM/STS measurement with irradiation of light with different parameters (such as wavelengths).

In 2002 Grafström reviewed [90] the progress in the field since the first photoassisted STM measurement in 1987 [91], covering the research done on light-induced effects in STM including thermal effects, nonlinear effects, surface photovoltage on semiconductors, surface plasmon effects and others. The majority of the photoassisted STM measurements were conducted on semiconductors, investigating surface photo-voltages and surface density of states.

A decade has passed since, yet not many photoasisted STM studies have been carried out on organic molecules [25, 92-97]. As summarized in Chapter 2, the porphyrin molecule, as one of potential optoelectronic device candidates, was the target of STM research, yet with the exception of the Ho group [98], photoassisted STM research on porphyrin has not been reported. Ho's experiments coupled laser to the STM junction, achieving high spatial resolution at atomic scale within single Mg porphyrin molecule on oxidized NiAl(110) surfaces. With the double barrier junction the single porphyrin molecule can be charged and discharged at certain threshold voltage, and such threshold voltage varies with the energy of the coupling light, providing information on the energy level of a higher LUMO+1, which was 1.55eV above the LUMO experimentally, consistent with the 1.6eV from DFT calculations. However in Ho's experiments the porphyrin macrocycle lied parallel to the substrate, so that the properties were not investigated under a device configuration.

In our experiments diode lasers of wavelengths of interest were mounted outside the vacuum chamber with an x-y-z translational mini-stage, and adjusted to an angle so incident light was brought to tip-sample junction through a viewport, as shown in Figure 3.9. STM tip was brought to vicinity of the sample surface, and then laser was turned on and tuned to tip-sample junction, and kept on for the final tip approach and data acquisition. The data under dark and different illumination condition were then compared. The specifications of the laser used in the experiments are listed in table 3.3.

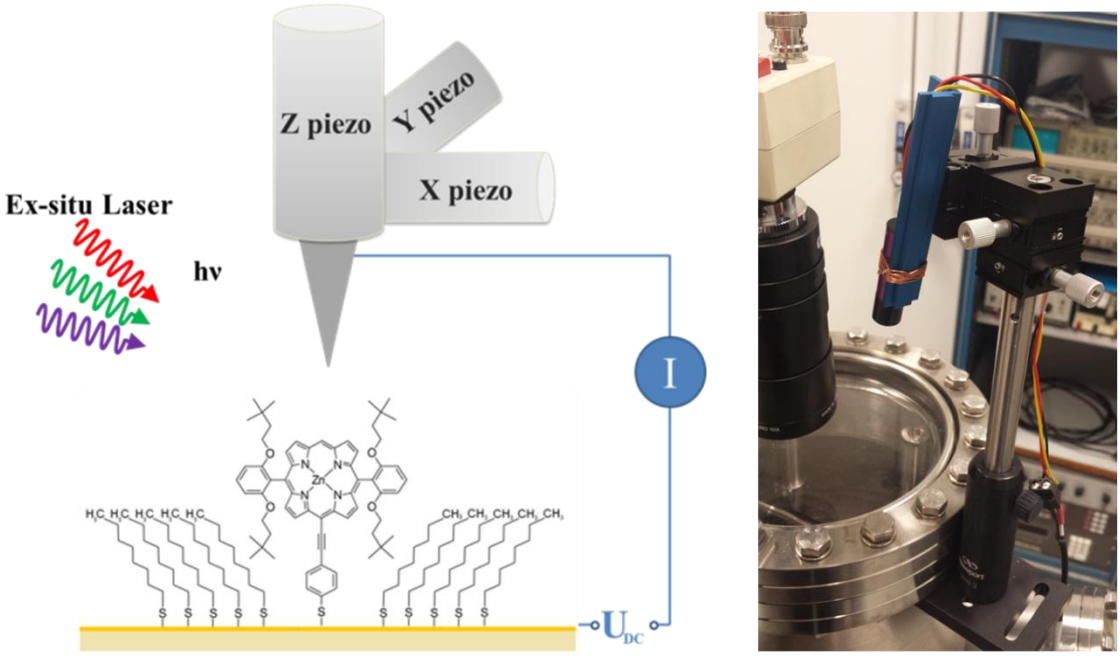

Figure 3.9 Schematic drawing and photo of STM/STS setup

Table 3.3 Specifications of continuous wave diode Lasers used in the STS measurements.

Laser Color	Wavelengths (nm)	Power (mW)	Photon Energy (eV)
Blue	405	5	3.06
Green	533	3	2.33
Red	655	5	1.89

To combine the STM with light illumination, several issues need to be addressed including laser tuning and achieving a stable tunneling gap under illumination.

3.2.2 Tuning the Laser toward the Tip-Sample Junction

The first challenge is tuning the laser to properly illuminate the sample surface below the tip, and optimize the angle of irradiation, as well as the position of light spot to maximize the effect of the light. Possible shadowing effect by the STM tip might influence the illumination of the molecule. Also the laser beam has an intensity profile with a width larger than the tunneling gap distance, so ability to adjust the alignment of the laser beam is required to make sure the local area probed by STM is illuminated under the beam intensity maximum.

Using an x-y-z translational mini-stage attached directly on the STM chamber, we were able to tune the position and angle of laser irradiation with high precision, as shown in Figure 3.9. A 405 nm 20mW laser was first tuned toward the tip-sample junction coarsely with observation by eye, and then finely adjusted with position monitored via a CCD camera. The wavelength of the laser was chosen because it overlaps with the optical

absorption B-band (peaked around 440nm) of PZn_n molecule, and we expect to see light induced effect in STS. To optimize the laser alignment, IV spectra were repeatedly collected on an n-doped GaAs (100) sample under illumination, and laser spot position is adjusted until current offset at zero voltage can be maximized.

To ensure that the spectra changes are a direct effect of light absorption (instead of heating of the tip or sample or other possible effects), control studies with an n-doped GaAs (100) sample, as well as a bare Au (111) thin film on mica were compared. During the experiment, IV spectra were collected on both samples first without optical illumination. Then with laser directed at the tip-sample junction, after the system reached to equilibrium, IV spectra were collected again under the same scanning conditions. It can be seen (Figure 3.10), for the Au(111) surface, the IV spectra were almost straight lines and showed no change upon illumination. The IV curves did have slight offsets about 1pA at zero voltage (Figure 3.10 inset), the value of which also did not vary with changing of the illumination condition, and can be attributed to instrumentation capacitance coupling. This was as expected since the incident photon energy (3.1eV) is much smaller than the work function of gold (5.1eV) so the photoelectric effect was not present. However, for the n-doped GaAs(100) sample (Figure 3.11), with laser illumination at the tip-sample junction, the zero voltage offset changed from ~2pA to ~7pA, more than 3 times larger than seen in dark IV spectra (Figure 3.11 inset). Similar effects can be seen with other lasers used in the experiments. Photons with energy larger than a typical 1.4eV direct bandgap of GaAs can be absorbed, resulting in carrier generation in the semiconductor surface. Thus, even at zero bias, more carriers were generated in the GaAs and tunnel through the tip-sample gap to cause an increase in

current. With the above control study, the illumination was optimized and the current voltage spectra change can be attributed to the introduction of laser at the tip-sample junction as a direct effect of illumination.

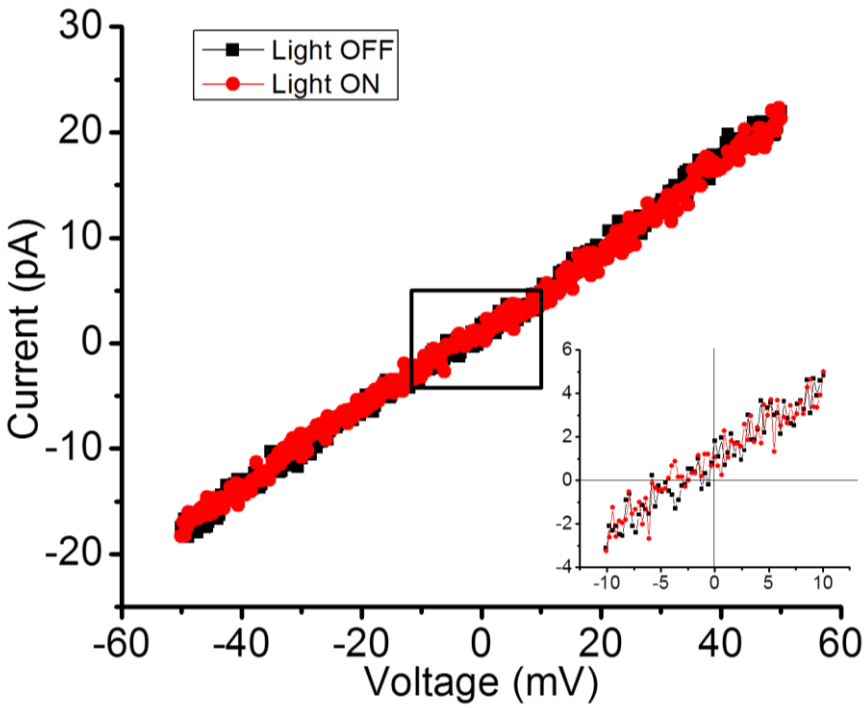

Figure 3.10 IV spectra of bare Au(111) sample with and without Laser illumination (405nm, 20mW). Tunneling setpoint is 0.5V, 500pA. Inset: Zoomed in detail of rectangle area.

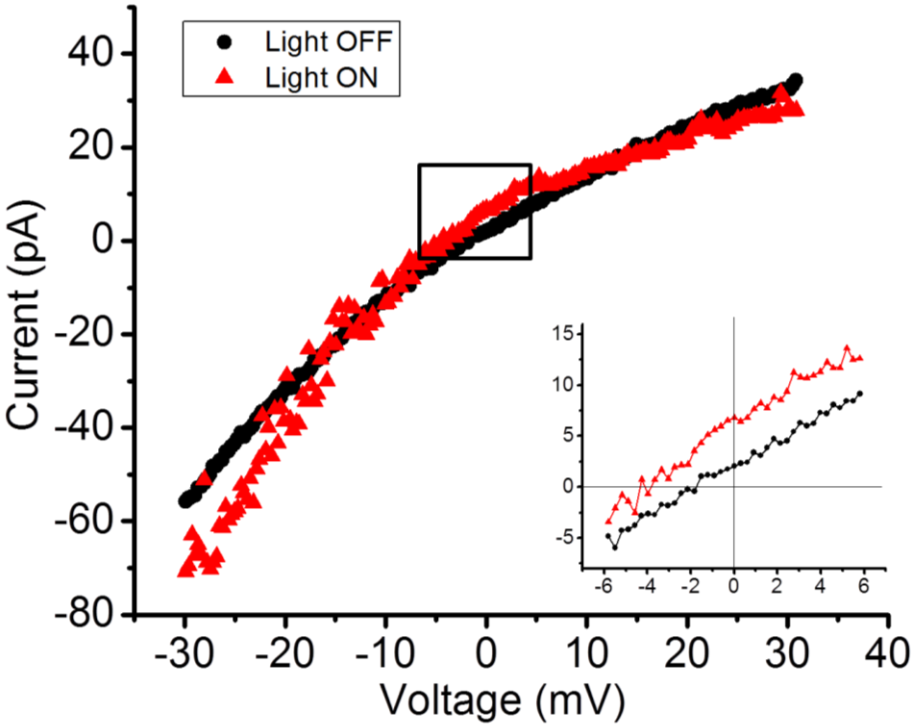

Figure 3.11 IV spectra of n-doped GaAs(100) sample with and without Laser illumination (405nm, 20mW). Tunneling setpoint is 0.5V, 500pA. Inset: Zoomed in detail of rectangle area.

3.2.3 Relaxation of Laser-induced Heating

A second challenge is achieving a stable tunneling gap under light illumination. The illumination of the tip-sample junction will unavoidably generate heat, thus inducing temperature variation at local area. The tip, sample and possibly components of the STM head may heat and expand. Meanwhile, the system adjusts to maintain the tunneling setpoint. The feedback loop will be responsible for the control and, therefore, the Z piezo position constantly changes, until the system reaches to a new thermal equilibrium state.

To exclude the interference of thermal expansion, the spectra collection should be done after equilibrium is achieved. The relaxation time of system was therefore measured by monitoring the Z piezo position using the oscilloscope function within the STM controller, with the n-doped GaAs(100) sample. As shown in Figure 3.12, under a

tunneling setpoint of 0.5V, 500pA, the Z piezo position was tuned to zero, and the system was in equilibrium. The laser was then turned on at t=60s. This induced an immediate gap distance hike of ~50nm (Note this is the value of Z piezo position calibrated to the applied voltage on Z piezo, not necessarily the exact value of the gap distance.), which can be attributed to the increase of carrier density thus the current, causing the feedback loop to respond by increasing the distance to reach the original tunneling setpoint. With time, a slow but steady decrease in the Z piezo position can be seen, as the system adjusts to the environment. At about 10 minutes later, the piezo position reaches a steady value, indicating equilibrium had been achieved.

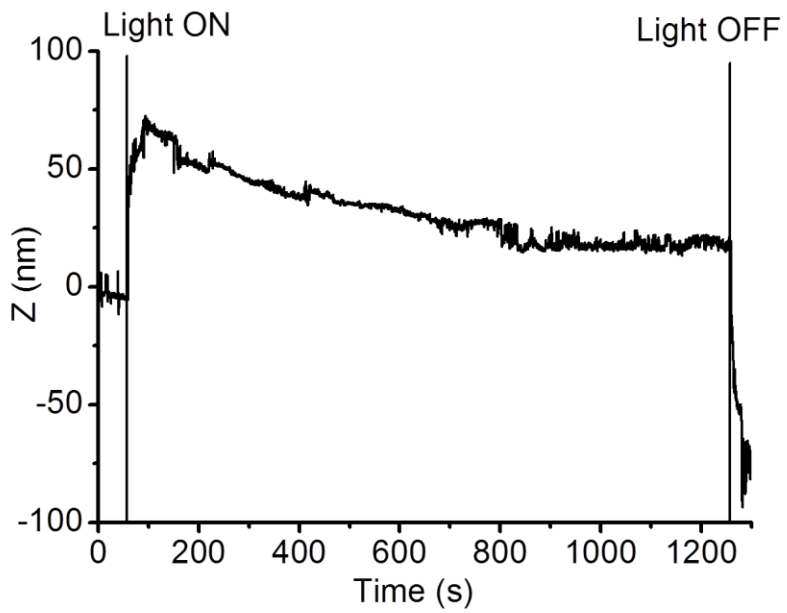

Figure 3.12 Z-Piezo position with respect to time. Measurement was done on n-doped GaAs(100) sample with feedback on, controlling the tunneling setpoint to be 0.5V, 500pA. Laser illumination started at t=60s and turned off at t=1260s.

Since the final fine approach usually took more than 10 minutes and most of the time it was conducted with the laser illumination already on the junction, it was concluded that equilibrium would be achieved once the tip is engaged tunneling to the

sample surface. This was confirmed experimentally by the lack of large scale Z-piezo position variation. For the rare times that laser was turned on after tip engagement, the data acquisition generally took place after a wait time of 10 minutes.

With the mixed monolayer sample prepared and photo-assisted STM/STS setup ready, data of topography, electronic structures were collected and analyzed, and discussed in the following chapters.

CHAPTER 4 Optoelectronic Properties of PZn_n Molecules

The primary goal of this research is to determine the molecular electronic structure of different zinc-porphyrin oligomers under different illumination conditions. In order to probe the porphyrin optoelectronic properties we perform the following procedure systematically: a) determine the single porphyrin molecular electronic structure when chemisorbed on the substrate in a vertical configuration; b) understand the effect of the number of oligomers in the porphyrin wire on the molecular electronic states; c) understand the change of the molecular orbital energy levels when porphyrin molecules absorb photons of different energy. Using the experimental methods described in Chapter 3 we proceed to show the results obtained in the following sections; section 4.1 describes the UV-vis optical spectroscopy on the PZn_n molecules in solution, section 4.2 demonstrates the topography information of the mixed monolayer sample, and section 4.3 presents the scanning tunneling spectroscopy data of 1-octanethiol and PZn_n molecules, with light of different wavelengths illuminating the tip-sample junction.

4.1 Optical Spectroscopy

The UV-vis absorption spectra of the zinc-porphyrin molecules are shown in Figure 4.1. Apart from the difference in the meso-position substitute groups, the absorption spectra are similar to those of other zinc-porphyrin molecules, presenting an intense B band around blue light wavelength, and two weak Q band peaks around the red light wavelength [28, 29, 35, 64, 65, 99, 100].

PZn_1 molecules manifest a large sharp absorption peak at 440 nm (B band) with a broaden shoulder extending to 400 nm, and two small absorption peaks centered at ~580 nm and ~650 nm (Q bands). With an extra macrocycle linked at meso- position, PZn_2

molecules show a broad B band absorption peak at ~400-520 nm and redshifted Q bands: with the weaker Q band stayed at ~580 nm, the relatively stronger Q band shifted to ~750nm. Similar broadening of the B band and redshifting of the Q bands associated with the dimer molecules were presented in multiple references and discussed extensively [64, 99]. As more macrocycles couple via the ethynyl bridge, which keep the molecule planar, the charges are more delocalized and the HOMO-LUMO gap decreases, resulting in the differences of the UV-Vis spectra between monomer and dimer zinc-porphyrin molecules. Differences between monomer and dimer are explored optoelectronically in next sections and discussed further in subsequent chapters.

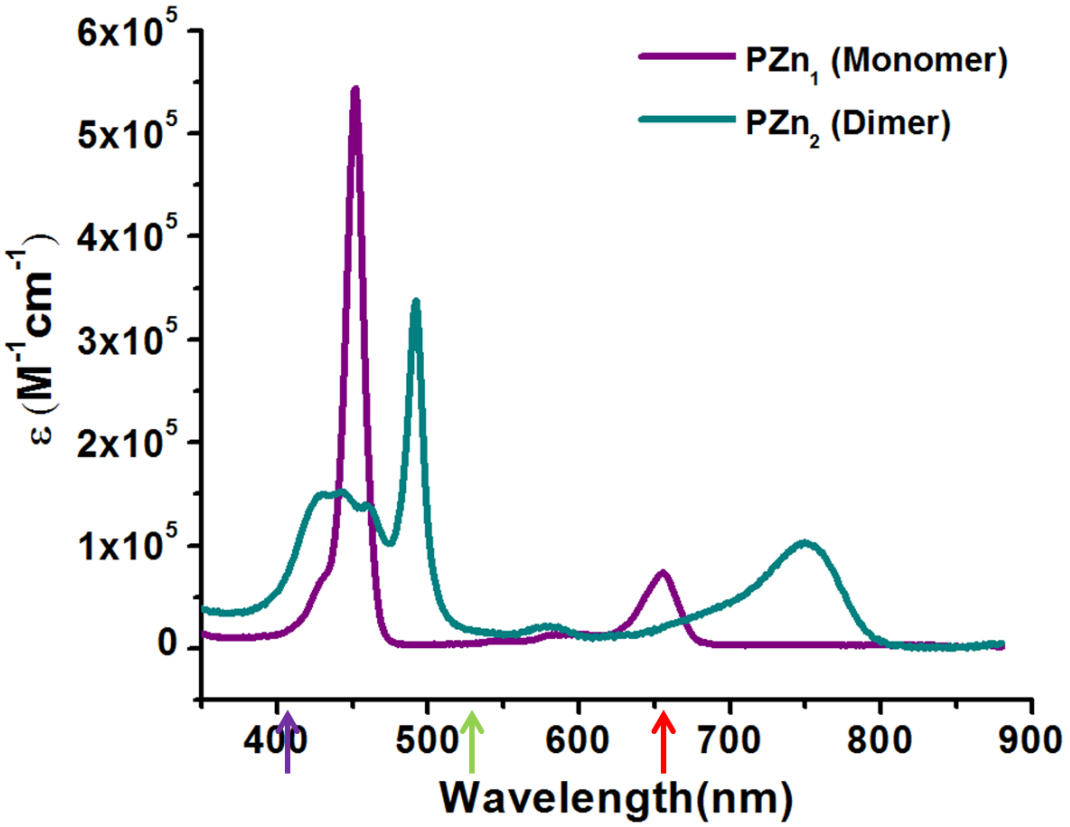

Figure 4.1 Optical absorption spectra of PZn_1 (purple) and PZn_2 (cyan) molecules in THF solution. Arrows of different colors indicate the wavelengths of illumination used in the research.

4.2 Topography Information

STM was used to investigate the structure of mixed monolayers of 1-octanethiol SAMs and inserted PZn_n molecules. Before I-V spectroscopy was performed, topography information was acquired to confirm the formation of the SAM and the insertion of the zinc-porphyrin.

4.2.1 1-octanethiol Self Assembled Monolayer

Figure 4.2 shows that topographic image of 1-octanethiol SAMs. 1-octanethiol molecules form large scale monolayers, as shown in Figure 4.2a, with boundaries along three major directions intersecting each other at 120 degrees. Defects, which are regions devoid of SAMs, appear as dark contrast in the images since the Au surface is lower than the top of the molecular layer. Cross section measurements confirm that defect area is typically 0.3 to 0.4 nm deep below the SAM surface (Figure 4.2c). Molecular resolution of the SAM is shown in Figure 4.2b, in which the image was filtered with a 2D Fast Fourier Transform, excluding the zero frequency information. The 2D surface structure agrees with previous research as described in section 3.1.1 [71-76].

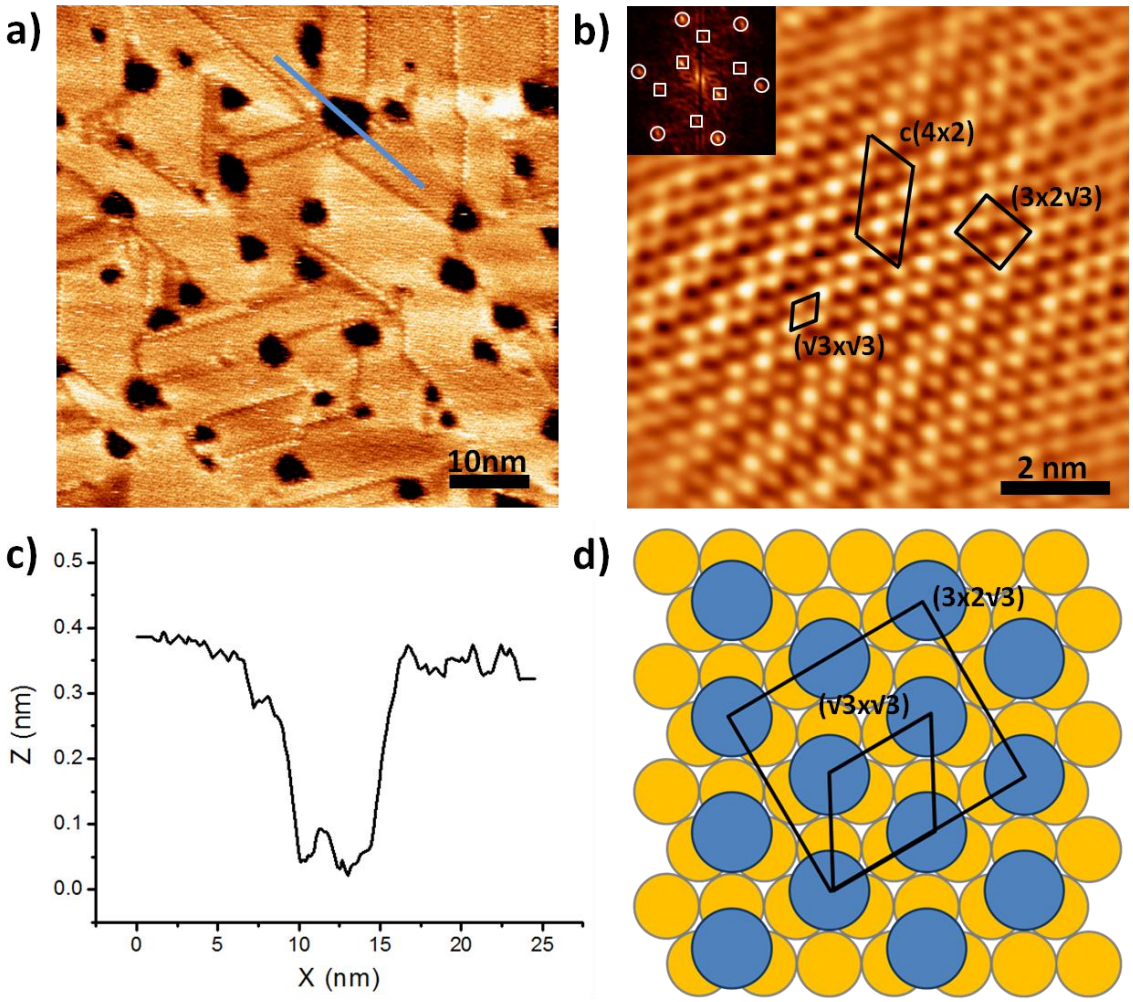

Figure 4.2 (a) Topography image of 1-octanethiol self-assembled monolayer in large scale. Full Z scale: 1.3 nm. Scanning condition is 1.0V, 100pA. (b) Molecular resolution image of 1-octanethiol SAM. Z scale: 0.1 nm Inset: Fourier transformation of the topography image. Circles represent (√3×√3) structures while squares represent (3×2√3) (or c(4×2)) superlattice. Scanning condition is 1.0V, 100pA. (c) Cross section of the defect area indicated by line in (a). (d) Schematic of surface molecular arrangement showing surface superlattice structure (√3×√3) and (3×2√3).Yellow: Au atoms; Blue: 1-octanethiol molecules.

The 1-octanethiol SAMs on Au(111) surface exhibits a highly ordered close-packed structure of (√3×√3)R30° with molecular spacing of ~0.5 nm. Some of the molecules appears brighter than others, exhibiting a (3×2√3) surface superlattice (commonly known as c(4×2) superlattice) typically observed in 1-octanethiol SAMs [75, 76, 101]. The structure is also evident in the fourier transform of the STM contrast (Figure 4.2b inset), where the bright spots in circles on the hexagonal position represents (√3×√3) structure, while the spots in squares represents (3×2√3). Such surface superstructure is schematically described in Figure 4.2d.

4.2.2 PZn_1 Molecule

PZn_1 molecules are found next to or in the defects of the 1-octanethiol matrix, and appear higher than the 1-octanethiol SAM layer as a bright spot (Figure 4.3a). The apparent lateral size of PZn_1 molecules is found to vary from 2nm to about 5nm. While the physical width of the PZn_1 molecule is 1.75nm (Figure 4.4a) [102], the larger apparent size is indicative of the aggregation of several PZn_1 single molecules. Note that the PZn_1 molecule appears as a round spot in the image. This can be attributed to the non-planar conformation of the molecule: the phenyl groups on each side are perpendicular to the porphine macrocycle so the single molecule appears larger from “top view” (Figure 4.4b) [102].

The apparent height difference of the PZn_1 molecule and the 1-octanethiol SAM layer is about 0.6-0.7 nm, as measured in cross sectional profile of the PZn_1 molecule in Figure 4.3b. The theoretical value of the height difference is 0.4 nm (Calculated via data given in [63, 103]), showing a discrepancy with the experimental value. Note that the

topographic image also contains electronic information that is convoluted with the height information.

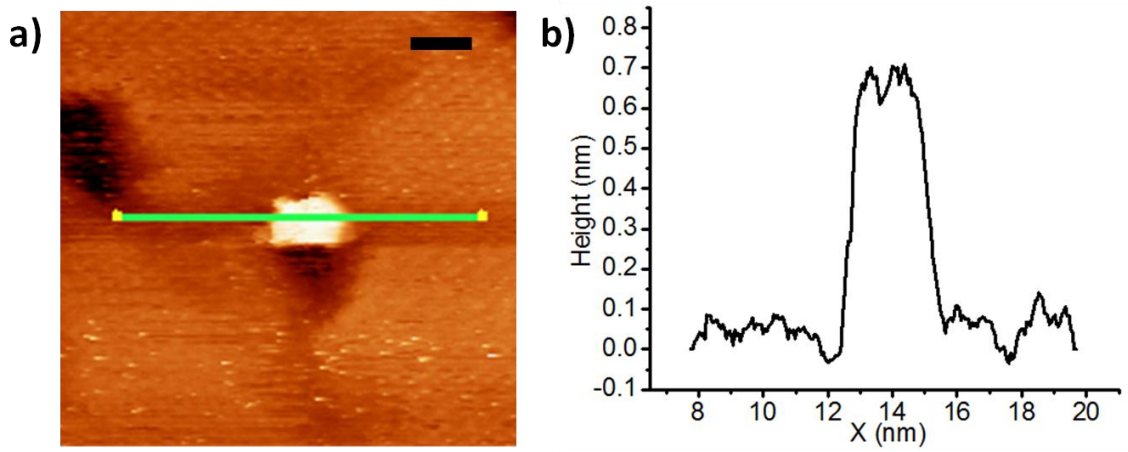

Figure 4.3 (a) 1-octanethiol SAM matrix with PZn_1 single molecule inserted in its defect. Z scale: 1.1 nm. (b) Height difference profile of a PZn_1 single molecule over the 1-octanethiol SAM. Scanning condition is 2.5V, 300pA. Scale bar: 2nm.

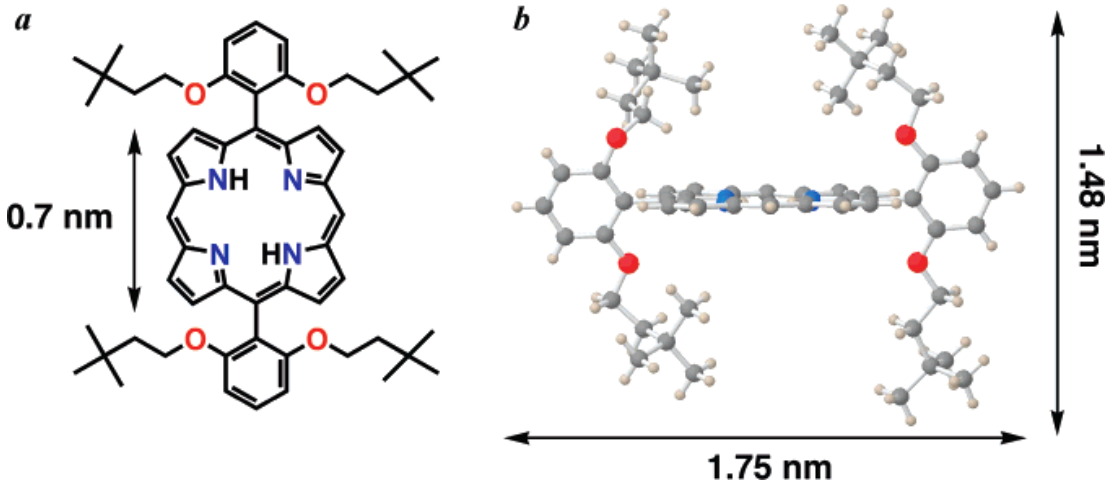

Figure 4.4 Porphyrin molecule similar to PZn_1 molecule used in this research (excluding the α-acetythiol substituent and incorporated Zn atom) (a) chemical structure; (b) crystal structure with key molecular dimensions. Adapted from Ref. [102]

4.2.3 PZn_2 Molecule

The topography image of a PZn_2 molecule in 1-octanethiol SAM is shown in Figure 4.5a. As is the case for the PZn_1 molecules, PZn_2 molecules are found next to or in the defects of the 1-octanethiol matrix. The lateral size of the PZn_2 molecule appears similar to that of the PZn_1 molecule. The apparent lateral size similarity is expected due to same anchoring mechanism as that of the PZn_1. The vertical geometry of PZn_2 is ensured by the ethynyl bonding between the two macrocycles, thus keeping the molecule straight. Consequently PZn_2 and PZn_1 single molecules should appear the same lateral size from "top view". From the profile of the PZn_2 molecule shown in Figure 4.5b, the lateral size is ~4 nm.

PZn_2 appears higher than PZn_1 in the topographic image. The apparent height difference of the PZn_2 molecule and the 1-octanethiol SAM is about 1.2 nm as seen in cross sectional profile in Figure 4.5b, 0.5 nm higher than the 0.7 nm difference of PZn_1 molecule (Figure 4.2c). The higher profile for the dimer molecule is consistent with a geometrically taller PZn_2 molecule, which contains one more PZn macrocycle than the PZn_1. The theoretical value of the length difference between the PZn_1 and PZn_2 molecules is 1.1 nm [63]. Again, the discrepancy here is certainly due to a contribution of electronic information in the STM measurement.

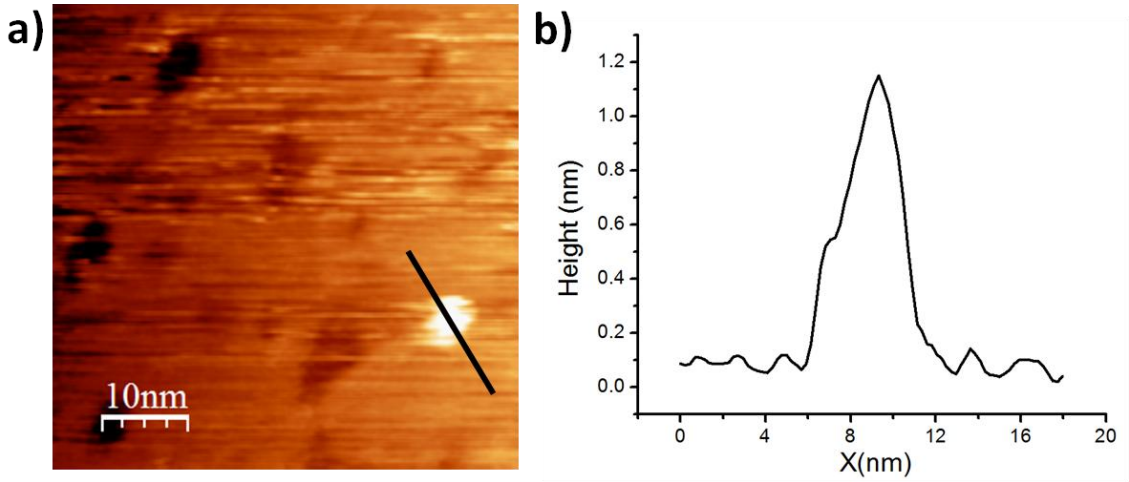

Figure 4.5 (a) 1-octanethiol SAM matrix with PZn_2 molecules. Z scale: 1.6 nm. (b) Height difference profile across the line in (a) of an aggregation of PZn_2 molecules over the 1-octanethiol SAM. Scanning condition is 2.5V, 300pA.

Topography measurements with STM confirmed the formation of 1-octanethiol SAMs and the insertion of PZn_n molecules. With PZn_n molecules in a device configuration, scanning tunneling spectroscopy was performed to gain detailed information of molecular orbital structures.

4.3 Scanning Tunneling Spectroscopy

After the first scan to locate the molecules of interest, scanning tunneling spectroscopy experiments were performed under both dark and illuminated conditions at laser wavelengths of blue (405 nm), green (533 nm), and red (655 nm) on 1-octanethiol and PZn_n molecules. I-V curves and dI/dV spectra were acquired and analyzed to reveal the molecular orbital energy levels.

4.3.1 1-octanethiol Self Assembled Monolayer

The 1-octanethiol molecule was studied as a control, since the alkanethiol molecular electronic structure is well known [104-107]. Figure 4.6 shows a specific case where I-V spectra were collected in a rectangle region containing only 1-octanethiol

molecules. The I-V curve manifests characteristics previously reported [104, 105], showing tunneling behavior through a non-rectangular smooth barrier, which can be described via the Simmons model [104, 108]. Therefore, observation of such I-V curves indicates that the measurement is showing true characteristics of 1-octanethiol molecule. Such observation can be used as an indication of a stable tip-sample tunneling junction, which usually results from a well prepared tip. I-V curves of the 1-octanethiols sometimes differ from the one shown in Figure 4.6b. Variations may include the asymmetry around zero voltage, sudden increase of current curve slope at certain voltage, current jumps, and zero current. These variations are indicative of a contaminated tip, hence discarded, and a new tip would be installed. While the latter two variations were easy to distinguish, we impose some quantitative criteria for the former two variations: 1) According to the scanning set point of 2.5V, 300pA, when the voltage is -2.5 V, due to the symmetry of the I-V curve, the current should be within (-300 ± 100) pA; 2) The current cannot change more than 150 pA within any 0.5V range. If either criterion is violated, the tip is replaced with a new one. An example of the I-V curve showing a bad tip is in Figure 4.7, where both criteria were violated: the current at -2.5V is -450pA, and current increased by ~200pA from -2.5V to -2.0V.

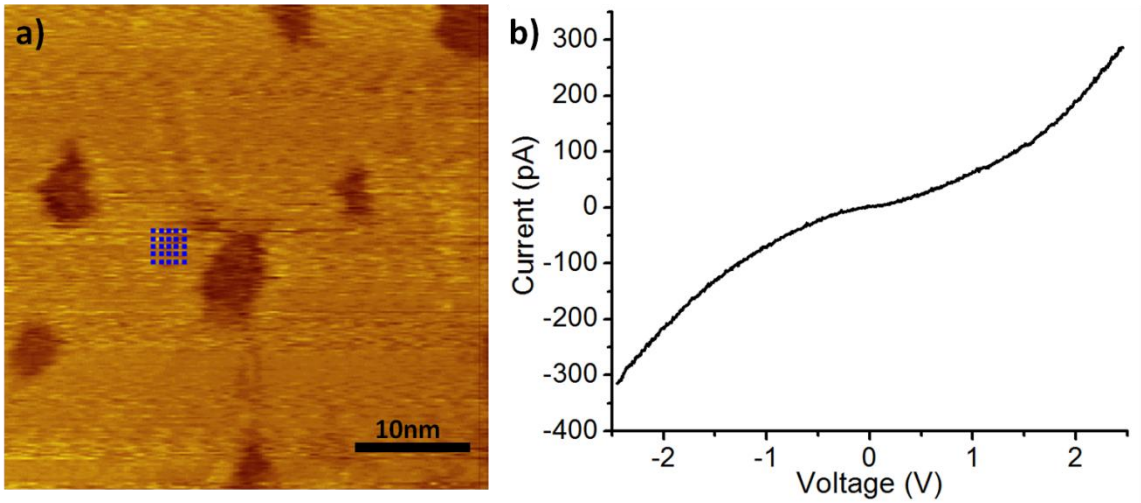

Figure 4.6 (a) Image of 1-octanethiol SAM matrix. Blue dots indicate the spots where I-V spectra were collected, Z scale: 0.4 nm. (b) I-V spectrum measured with a good tip, of 1-octanethiol molecule under dark condition averaged from 50 I-V curve measurements. Scanning condition was 2.5V, 300pA

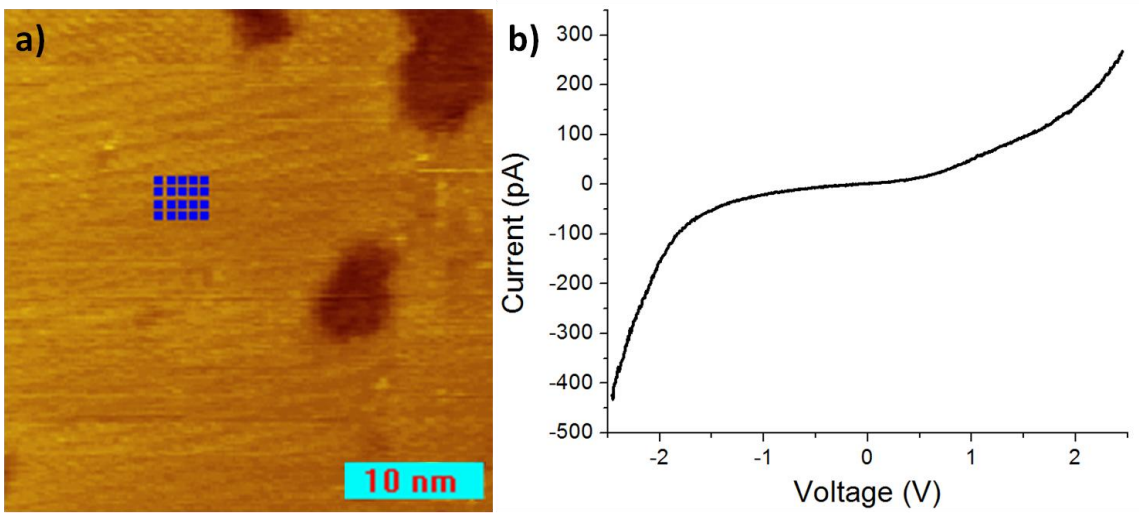

Figure 4.7 (a) Image of 1-octanethiol SAM matrix. Blue dots indicate the spots where I-V spectra were collected. Z scale: 0.4 nm. (b) I-V spectrum with a contaminated tip, of 1-octanethiol molecule under dark condition averaged from 40 I-V curve measurements. Scanning condition was 2.5V, 300pA.

A direct comparison of I-V curves of 1-octanethiol molecule between dark and illumination under light of different wavelengths (Figure 4.8) shows that within the

applied voltage range, only mild slope changes are observed in 1-octanethiol molecule, wavelength. Considering the HOMO-LUMO gap of about 8 eV in 1-octanethiol molecules [104, 105], the applied voltage range is simply too small to reach resonant tunneling with either electronic orbital of the 1-octanethiol molecule. Therefore minimal slope change was observed, and the spectra exhibit similar LDOS.

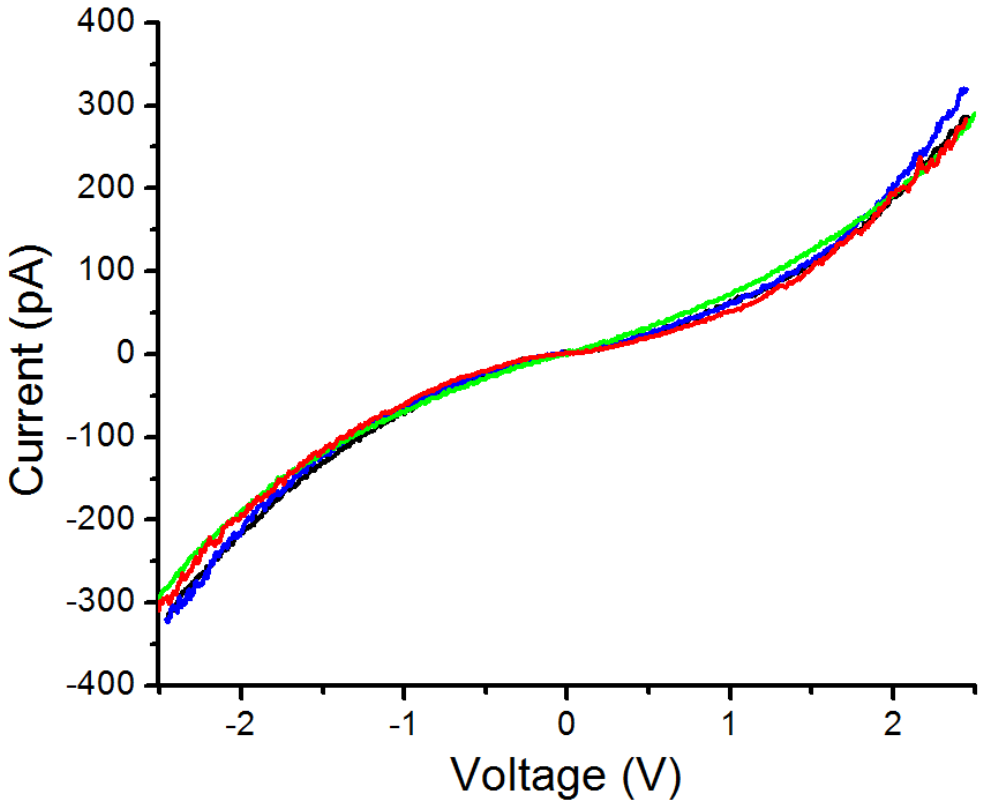

Figure 4.8 I-V spectra of 1-octanethiol molecule under dark and illuminations with light of different wavelengths. The color matches the light used (blue 405nm, green 533nm and red 655nm), and black curve corresponds to the dark conditions. I-V spectra were averaged over 50 (dark), 24 (blue), 68 (green), 14 (red) I-V curves over 1-octanethiol SAMs. Scanning condition was 2.5V, 300pA.

4.3.2 PZn_1 Molecule

STM images in Figure 4.9 show a typical PZn_1 single molecule inserted in 1-octanethiol SAMs and I-V spectra were acquired at defined spots as indicated. The

defined regions or lines usually cover both PZn_1 molecule as well as 1-octanethiol molecule, and two I-V spectra were acquired at each spot. Representative curves corresponding to each type of molecules are also shown.

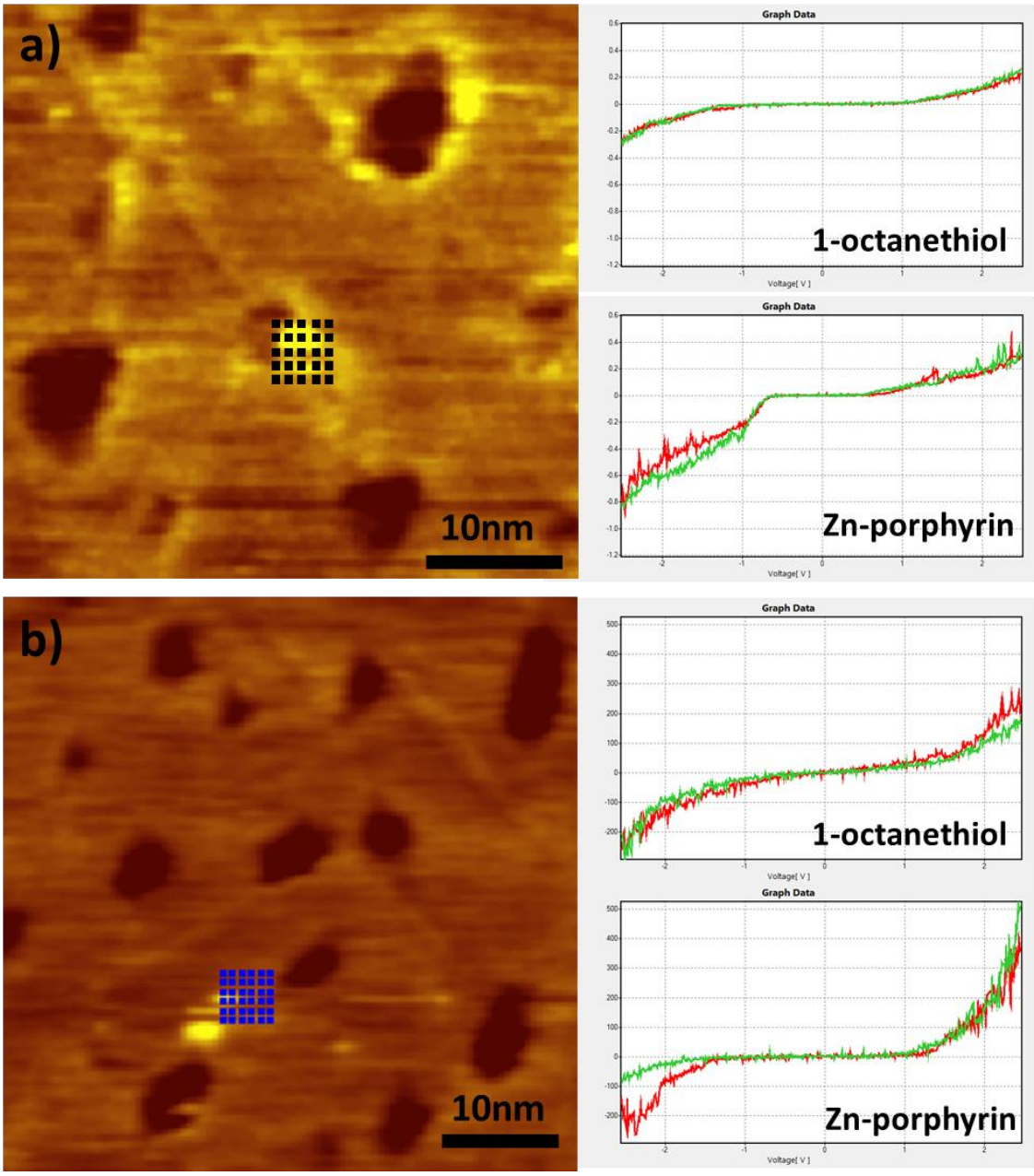

Figure 4.9 STM image of zinc-porphyrin single molecule embedded in 1-octanethiol SAM matrices. I-V spectra were collected at the black or blue spots while scanning. Scanning condition: 2.5V, 300pA. (a) Z scale: 1.4 nm. X axis: voltage, range: -2.5V to 2.5V; Y axis: current, range -1.2 nA to 0.6 nA. (b) Z scale: 1.5 nm. X axis: voltage, range: -2.5V to 2.5V; Y axis: current, range -0.3 nA to 0.6 nA.

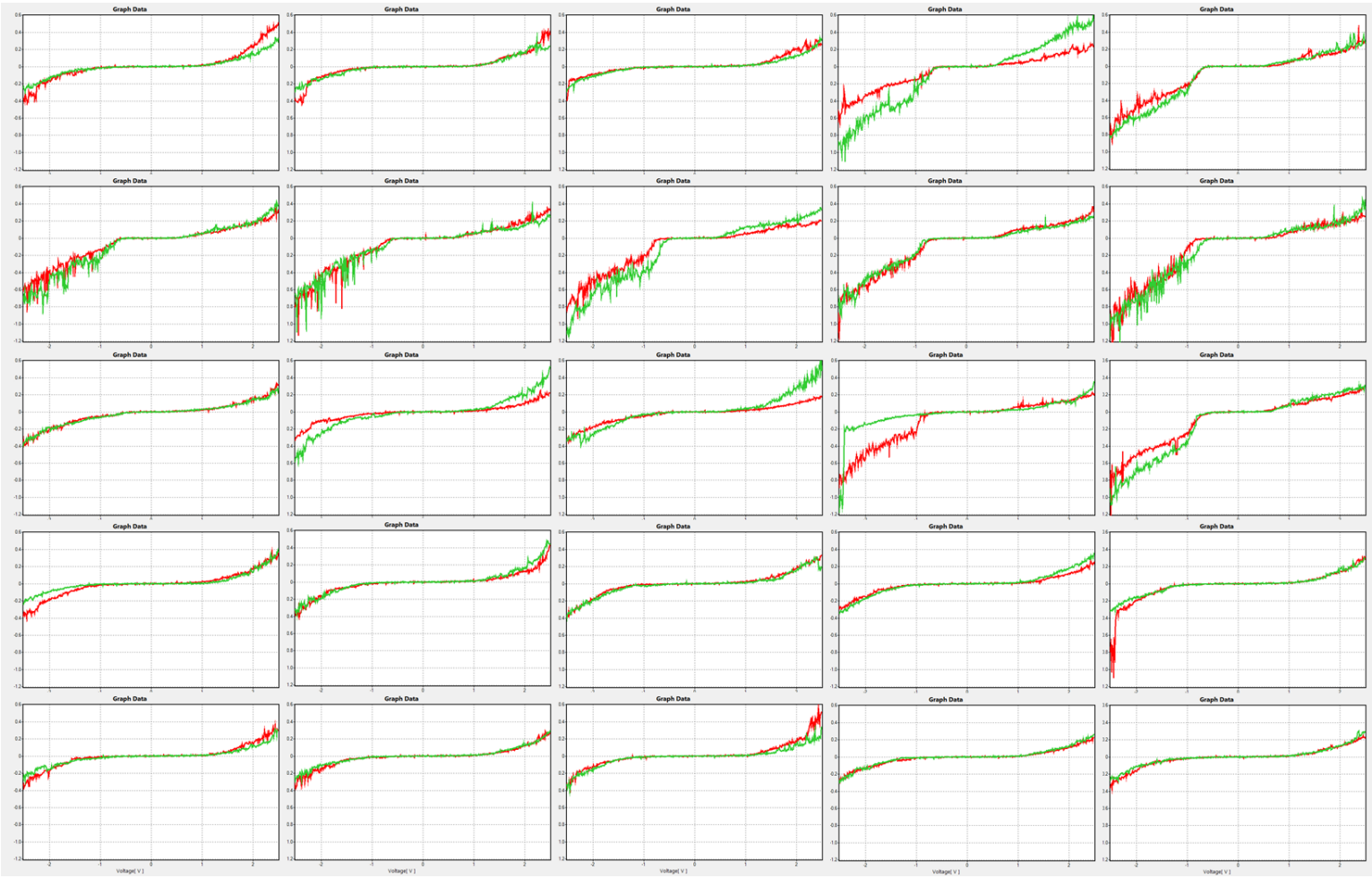

Figure 4.10 I-V spectra of the PZn_1 single molecule shown in Figure 4.9a. The position of the I-V curve corresponds to the spot it was acquired in Figure 4.9a. I-V spectra exhibit two distinct behaviors. X axis: voltage, range: -2.5V to 2.5V; Y axis: current, range -1.2 nA to 0.6 nA.

I-V spectra collected over each spot in Figure 4.9 were shown in Figure 4.10. Based on the features, I-V curves can be separated into two distinct groups. In I-V curves on the top right section and in the second row, there are sudden current increments at both 0.7V and -0.7V, while the rest of the I-V curves manifest a smooth and slow current increase with the voltage. Since there are only two different molecules on the surface, one group must be associated with zinc-porphyrin molecules, while the other group of I-V curves was acquired from 1-octanethiol. With knowledge of I-V curves of 1-octanethiol molecules, it can be concluded that the I-V curves from top right section and in the second row were collected from the zinc-porphyrin molecule. Note that the location of the two groups doesn't necessarily correspond to the location of the molecules according to the topography image. Also, data sets with I-V curves of 1-octanethiol that are not consistent (as shown in Figure 4.10) with previous studies are not included in subsequent analysis, according to the criterion described in Section 4.3.1. I-V curves that satisfy the criterion are considered successful measurements, and thus are selected and averaged for analysis.

4.3.2.1 Under Dark Condition

Figure 4.11 shows an I-V spectrum averaged from 26 I-V spectra collected from different PZn_1 molecules under dark conditions. Although in general the curve appears similar to that of the 1-octanethiol, differences exist that yield information about electronic density of states of the PZn_1 molecule. As Figure 4.11b shows, at around +2V and -2V, there are sudden increases in the slope of the I-V curve, indicating a larger local density of states at the corresponding energy level that potentially originates from molecular orbitals. In principle, we would interpret the increased slope as an indication

that the Fermi energy of the tip is of the same energy as the LUMO or the HOMO, and electrons transport into the LUMO or from the HOMO via resonant tunneling.

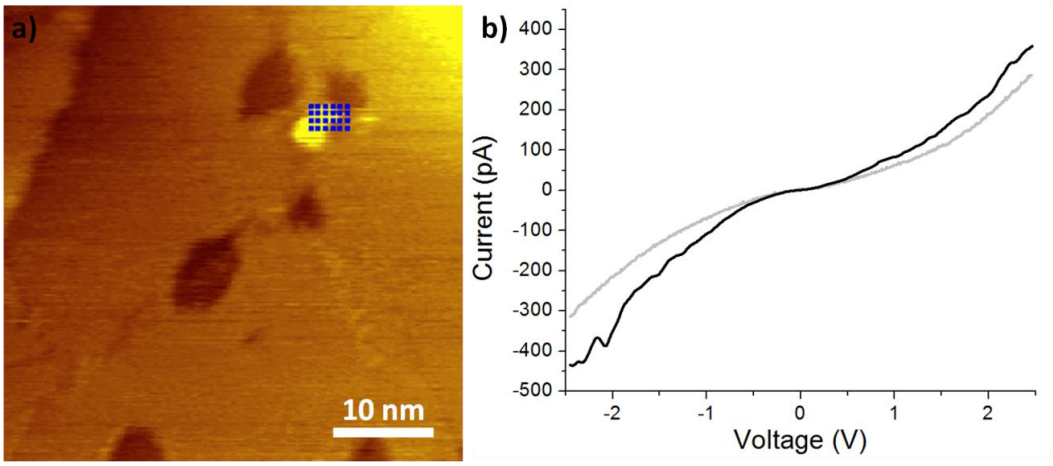

Figure 4.11 (a) Image of 1-octanethiol SAM matrix with PZn_1 molecules. Blue dots indicate the spots where I-V spectra were collected. Z scale: 1.4 nm. (b) Dark condition I-V spectrum, of 1-octanethiol (light gray, averaged from 50 I-V spectra) and PZn_1 molecule (black, averaged from 26 I-V spectra). Note that the I-V curves are not necessarily measured from the molecule shown in (a). Scanning condition was 2.5V, 300pA.

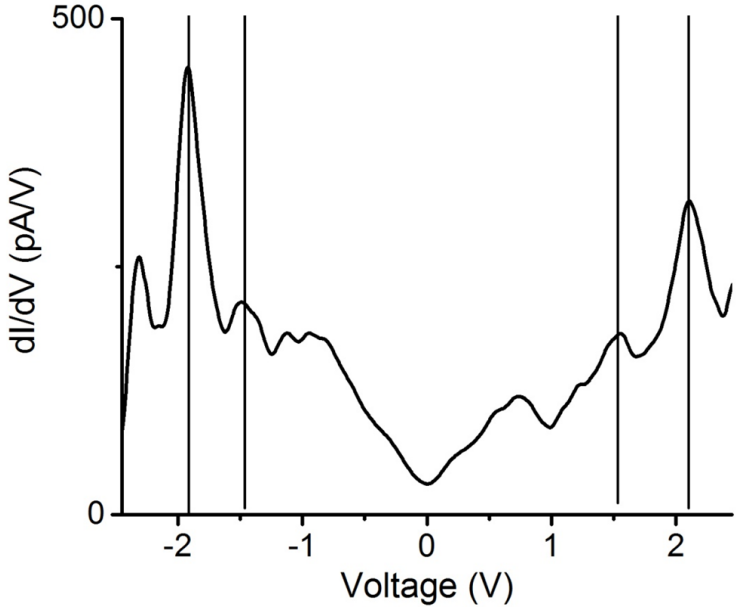

Figure 4.12 Differentiated I-V spectrum of PZn_1 molecule. As peaks at ~-1.0V and 0.75V are considered Au(111) substrate or the Au-thiol interface states [49, 62], and typical HOMO-LUMO gap of similar porphyrin molecules are from 2 to 3 eV, vertical

lines are positions where peaks associated with PZn_1 molecular orbital appear. Scanning condition was 2.5V, 300pA.

Differential analysis of the spectrum reveals details of the electronic structure (Figure 4.12). As outlined in Chapter 3, the differential analysis enables us to examine the electronic structure of the PZn_1 molecule. The dI/dV-V spectrum exhibits multiple peaks, indicative of the local density of states. Two broad peaks at ~-1.0V and 0.75V are believed to be the contribution of Au(111) substrate or the Au-thiol interface states, which lie within the HOMO-LUMO gap [49, 62]. Theoretical calculation as well as previous experiments on similar porphyrin molecules [40, 49, 62] show that the HOMO-LUMO energy gap varies from 2 to 3eV. Applying the knowledge of the HOMO-LUMO energy gap of porphyrin molecules and considering the peak positions in dI/dV spectra under different illumination conditions, the peaks at -1.5V and 1.5V are attributed to the contribution of HOMO and LUMO of PZn_1 molecule, and thus the HOMO-LUMO energy gap is about 3.0 eV. The peaks ~-1.9V and 2.1V are also attributed to PZn_1 molecular orbitals, and were labeled with vertical lines. Though no theoretical calculations of molecular orbital energy levels were directly performed for the molecule attached to substrate in our experiment, our measurements of HOMO-LUMO gap and other molecular orbital energies are similar to previous results [40, 49, 62] .

4.3.2.2 Wavelength (Energy) Dependence of Electronic Structure

STS spectra of PZn_1 molecules under different light illumination are shown in Figure 4.13. With illumination, the I-V curves differ from those acquired under dark conditions. The slopes of the spectra in the presence of light are small and stable within the range from -1.0V to 1.0V, indicating low conductance; while in the vicinity of -1.5V and 1.5V, the slopes show sudden increases, indicating the energies of the HOMO and LUMO of the molecule.

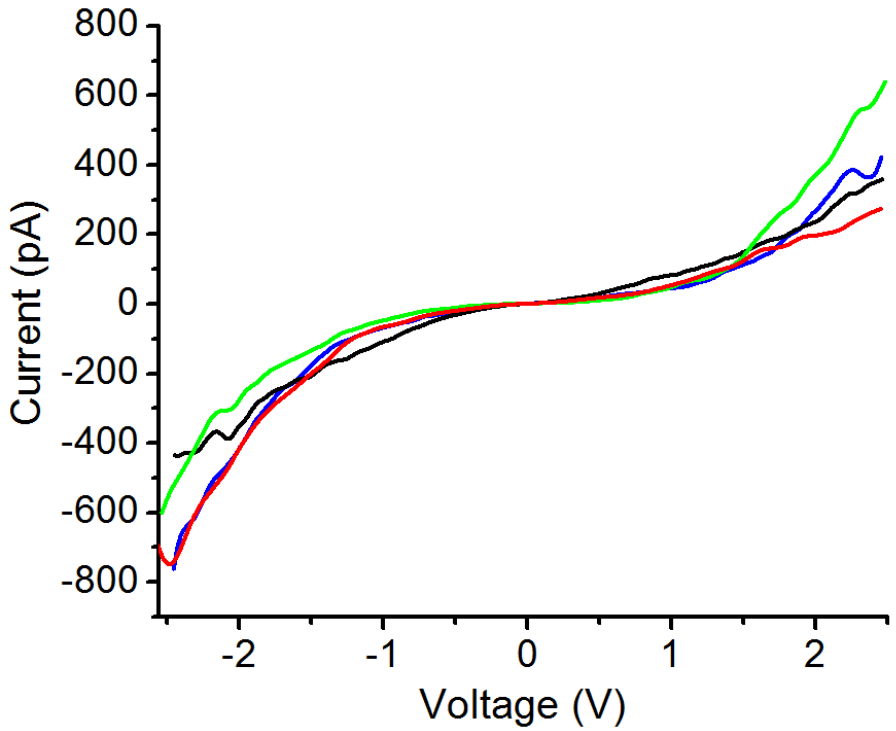

Figure 4.13 I-V spectra of PZn_1 molecule under dark and illuminations with light of different wavelengths. The color matches the light used (blue 405nm, green 533nm and red 655nm), and black curve corresponds to the dark conditions. I-V spectra were averaged over 26 (dark), 12 (blue), 10 (green), 18 (red) I-V curves over PZn_1 molecules. Scanning condition was 2.5V, 300pA.

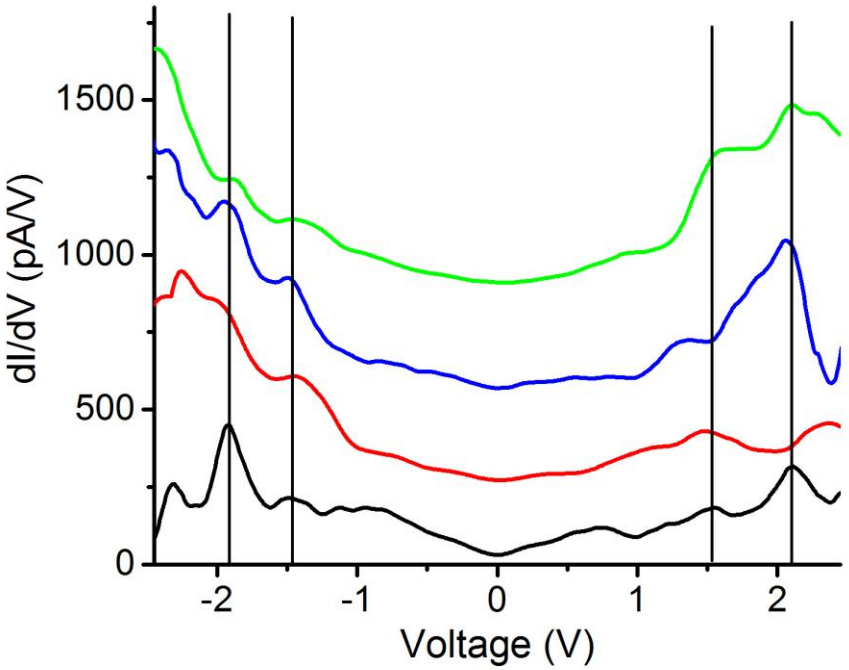

Figure 4.14 Differentiated I-V spectra of PZn_1 molecule under different illumination conditions. Vertical lines are positions where peaks associated with PZn_1 molecular orbital appear under dark condition. The color matches the light used, and black curve corresponds to the dark condition. Curves were vertically shifted to avoid overlapping. Scanning condition was 2.5V, 300pA

Differentiated STS spectra reveal further details, as shown in Figure 4.14. With blue light (405 nm) illuminating the tip-sample junction, the LUMO peak at +1.5V in dark condition shifts to +1.2V, suggesting a slight decrease in the HOMO-LUMO gap. With red light (655 nm), while HOMO-LUMO gap remained constant, the peak at 2.1V in dark conditions shifts ~ 0.3V. With green light (533 nm) illumination, the peak positions do not change. This is consistent with the UV-Vis spectrum of PZn_1 (Figure 4.1), the molecule does not absorb photons at 533 nm. However, with green light, it seems that the intensity of the LUMO peaks increased, showing larger density of states.

4.3.3 PZn_2 Molecule

Similar to the results shown in Section 4.3.2, STS measurements were performed on PZn_2 molecule. The I-V curves at defined regions were acquired, and those associated with PZn_2 molecule were averaged, and differentiated to obtain the dI/dV spectra.

4.3.3.1 Under Dark Condition

Figure 4.15 shows an I-V spectrum collected from PZn_2 molecules under dark conditions. It can be seen from the spectrum that compared to the PZn_1 molecule, the slope variation of the I-V spectrum of PZn_2 is more apparent. As Figure 4.15 shows, the current remains small from 0V to approximately 1.0V. Moreover, at around +2.0V and -1.5V, there are sudden increases in the slope of the I-V curve, indicating a larger local density of state at the corresponding energy level.

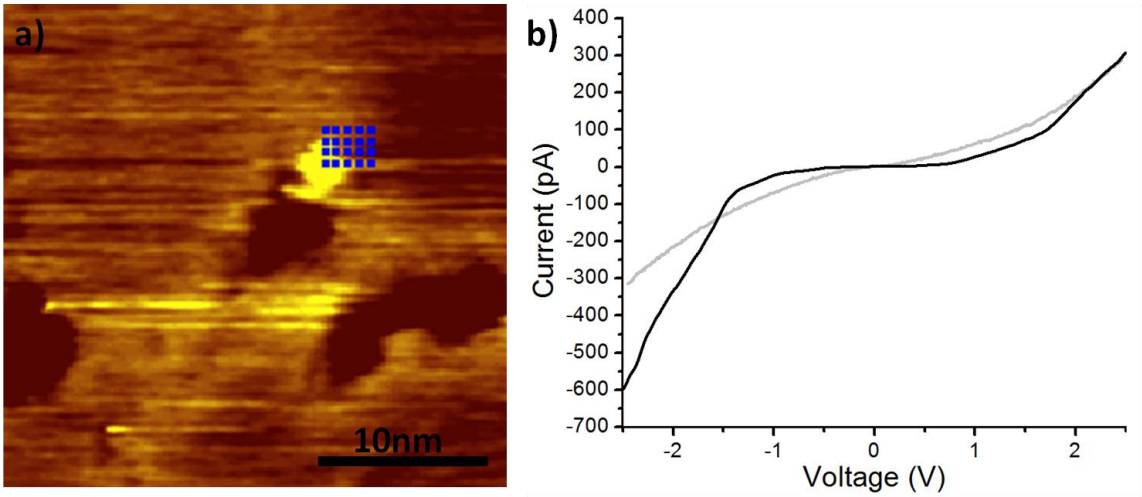

Figure 4.15 (a) Image of 1-octanethiol SAM matrix with PZn_2 molecules. Blue dots indicate the spots where I-V spectra were collected. Z scale: 1.6 nm. (b) I-V spectrum of 1-octanethiol (light gray, averaged from 50 I-V spectra) and PZn_1 molecule (black, averaged from 12 I-V spectra) under dark condition. Note that the I-V curves are not

necessarily measured from the molecule shown in (a). Scanning condition was 2.5V, 300pA.

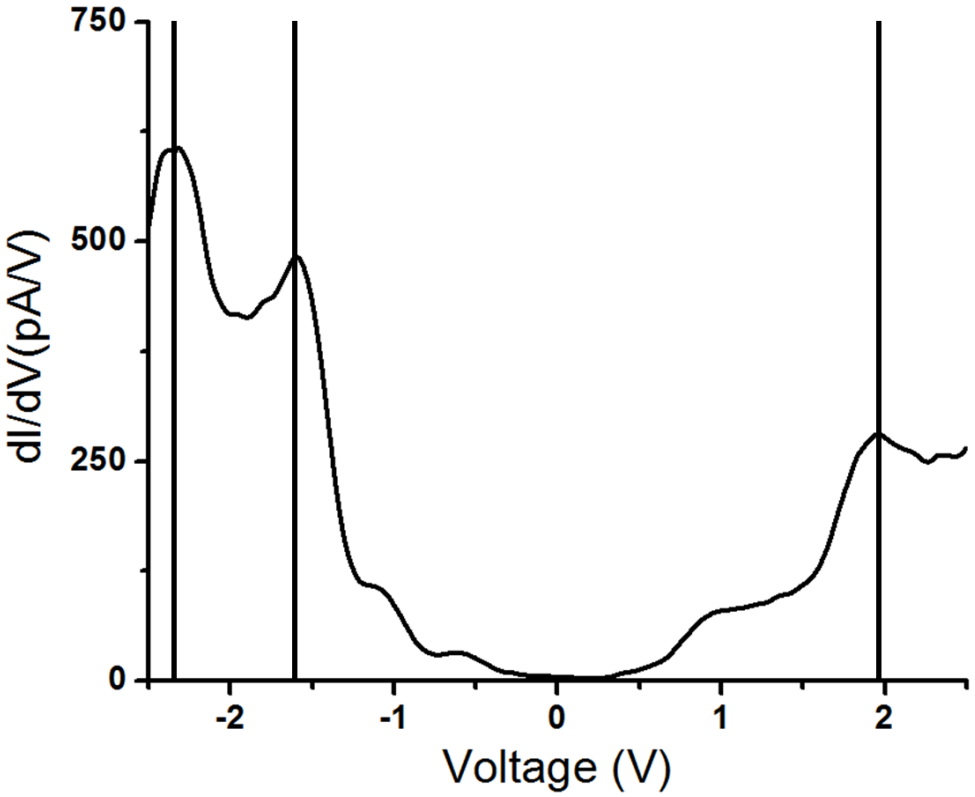

Figure 4.16 Differentiated I-V spectrum of PZn_2 molecule. Vertical lines are positions where peaks associated with PZn_2 molecular orbital appear. Scanning condition was 2.5V, 300pA.

More details are evident in the differential analysis of the I-V curves as shown in Figure 4.16. Multiple peaks are present in the dI/dV-V spectra, with each peak indicating an increase of local density of states. Applying knowledge of HOMO-LUMO energy gap of porphyrin molecules and considering the peak positions in dI/dV spectra under different illumination conditions, the peaks at -1.6V and 1.9V are attributed to HOMO and LUMO of PZn_2 molecular orbitals, and another peak at -2.3V also correspond to a PZn_2 molecular orbital, as indicated with the vertical lines. Therefore, STS shows a HOMO-LUMO gap of about 3.5eV, 0.5eV larger than its monomer counterpart. The

broad shoulder around 1.0V could indicate electronic states due to interaction between the Au(111) surface and thiolate bond of the PZn_2 molecule [49, 62]. The higher HOMO-LUMO gap in the dimer compared to the monomer is counterintuitive since the bonding between the two PZn macrocycles in the dimer molecule should bring the HOMO and LUMO energies closer, according to previous DFT calculation [43, 64, 99]. Such behavior will be discussed in the next chapter.

4.3.3.2 Wavelength (Energy) Dependence of Electronic Structure

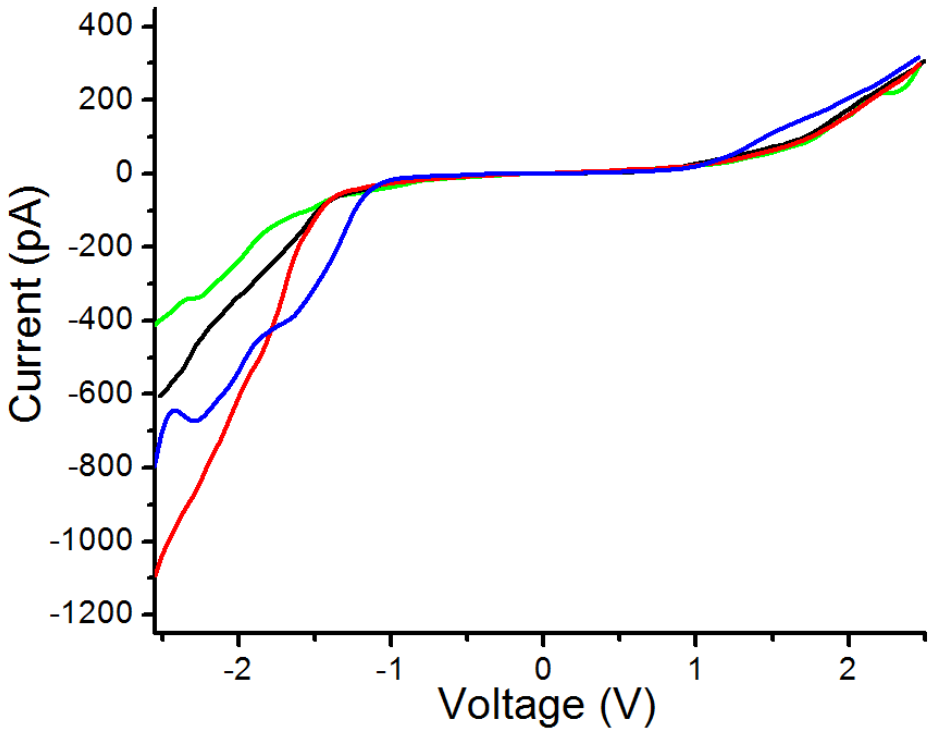

Figure 4.17 I-V spectra of PZn_2 molecule under dark and illuminations with light of different wavelengths. The color matches the light used (blue 405nm, green 533nm and red 655nm), and black curve corresponds to the dark conditions. I-V spectra were averaged over 12 (dark), 14 (blue), 13 (green), 15 (red) I-V curves over PZn_2 molecules Scanning condition was 2.5V, 300pA.

STS spectra of PZn_2 molecules under different light illumination are shown in Figure 4.17. With illumination, I-V curves differ from those acquired under dark conditions. The slopes of the spectra with light are less and stable within the range from -1.0V to 1.0V, while in the vicinity of -1.5V (except for the blue light case) and 1.5V, the slopes show sudden increases, indicating the energies of the HOMO and LUMO of the molecule. Differentiated STS spectra are shown in Figure 4.18. With blue light (405 nm) illuminating the tip-sample junction, the LUMO peak at +1.9V in dark condition shifts to +1.3V, and the HOMO peak at -1.6V shifts to -1.3V, indicating a decrease of 0.9 eV in HOMO-LUMO gap. With red light (655 nm), the HOMO and LUMO shift slightly farther apart from 3.5eV to 3.6eV, that is within our experimental error. With green light (533 nm) illumination, the peak positions around HOMO and LUMO levels do not change; however, the peak below the HOMO shifts toward the HOMO energy level by 0.3 eV.

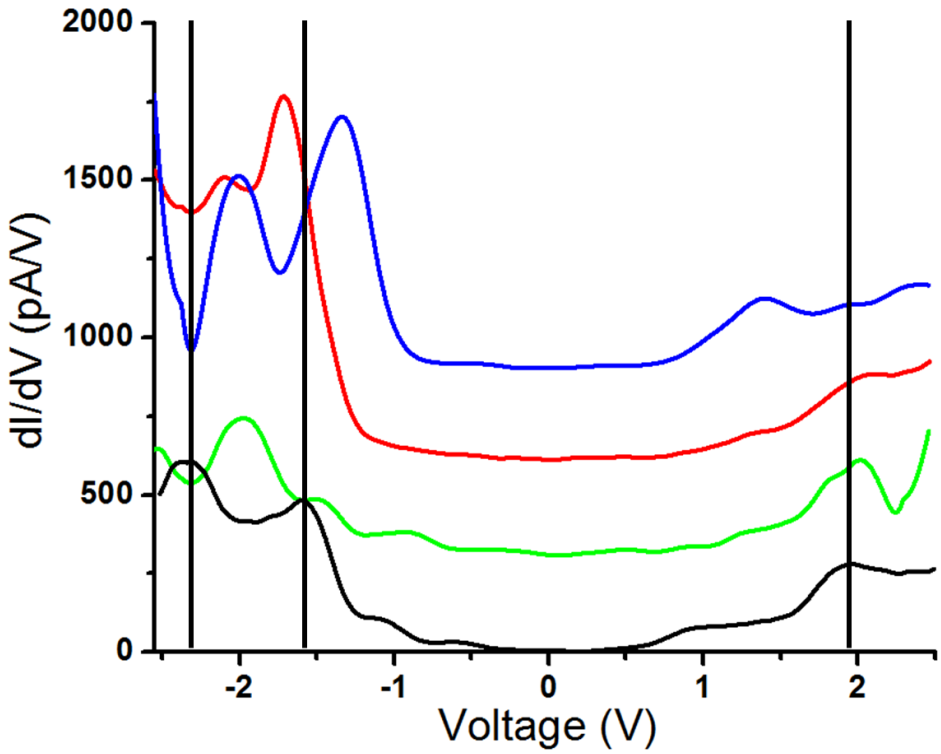

Figure 4.18 Differentiated I-V spectra of PZn_2 molecule under different illumination conditions. Vertical lines are positions where peaks associated with PZn_2 molecular orbital appear under dark condition. The color matches the light used, and black curve corresponds to the dark condition. Curves were vertically shifted to avoid overlapping. Scanning condition was 2.5V, 300pA

In summary, when adsorbed on SAM-Au(111) substrate, the HOMO-LUMO gap for PZn_1 molecule is 3.0eV under dark condition, while the PZn_2 molecule exhibits a larger 3.5 eV HOMO-LUMO gap. Under blue laser (405nm) illumination HOMO-LUMO gaps for both monomer and dimer zinc-porphyrin molecules is narrower than in dark conditions. Under other wavelength illumination results vary. With all experimental data at hand, the interpretation of all results will be discussed in the following chapter.

CHAPTER 5 Illumination effect and Macrocycle Coupling on Molecular Orbital Energy Levels

Scanning tunneling spectroscopy was performed on different zinc-porphyrin oligomers as a function of illumination conditions, and results were presented in Chapter 4. With these results we aim to determine the molecular orbital energy levels, and consequences of molecular structure to optoelectronic properties. Section 5.1 describes the different models adopted to obtain the molecular orbital energy levels from measured differentiated scanning tunneling spectra; section 5.2 and section 5.3 discuss the illumination effect on PZn_1 and PZn_2 molecular orbital levels respectively, using a charging molecule model; and section 5.4 discusses the macrocycle coupling effect on zinc-porphyrin molecular orbital levels.

5.1 Capacitive and Resistive Model

The peak positions in scanning tunneling spectra do not directly match the molecular orbital energy levels directly, due to the nature of the molecule, possible charging and the interface coupling between the molecule and the substrate. Therefore, to determine the energy levels of an organic molecule, the relationship of the peak positionsand the true orbital energy levels need to be understood. The issue is how the value of the bias applied in the measurement relates to the bias on the molecule. Two distinct models are examined in this section, in one model the zinc-porphyrin molecule is treated as a capacitor, while in the other model it is treated as a resistor.

5.1.1 Capacitive Model

With the Au(111) substrate-porphyrin-vacuum-tip tunneling junction, the voltage distribution across each component needs to be calculated to relate the peak positions to the electronic structure of the molecule. When the local density of states is negligible, for example, between the HOMO and LUMO, molecules can be treated as electrically insulating materials, and thus a capacitive equivalent circuit model can be applied [109].

Figure 5.1 shows the structure of the Au(111) substrate-porphyrin-vacuum-tip tunneling junction. The vacuum gap and the molecule are both treated as parallel plate capacitors. Therefore, the capacitance of the molecule and the vacuum gap can be calculated by the standard capacitor plate model with $C = \varepsilon A/d$, where the capacitance C is given by the permittivity ε between the plates, and the area and separation of the plates, A and d, respectively. We obtain the following equations:

$$C_{gap} = \frac{\varepsilon_0 A}{Z_{gap}} \tag{5.1}$$

$$C_{mol} = \frac{\varepsilon_{mol}\varepsilon_0 A}{Z_{mol}} \tag{5.2}$$

$$C_{total} = \frac{C_{mol}C_{gap}}{C_{mol}+C_{gap}} \tag{5.3}$$

where C_{gap} and C_{mol} are the capacitances of the vacuum gap and PZn_n molecule; A is the area of the PZn_n molecule; Z_{gap} and Z_{mol} are the length of the vacuum gap and PZn_n molecule; ε_0 and ε_{mol} are the vacuum permittivity and relative permittivity of the PZn_n molecule.

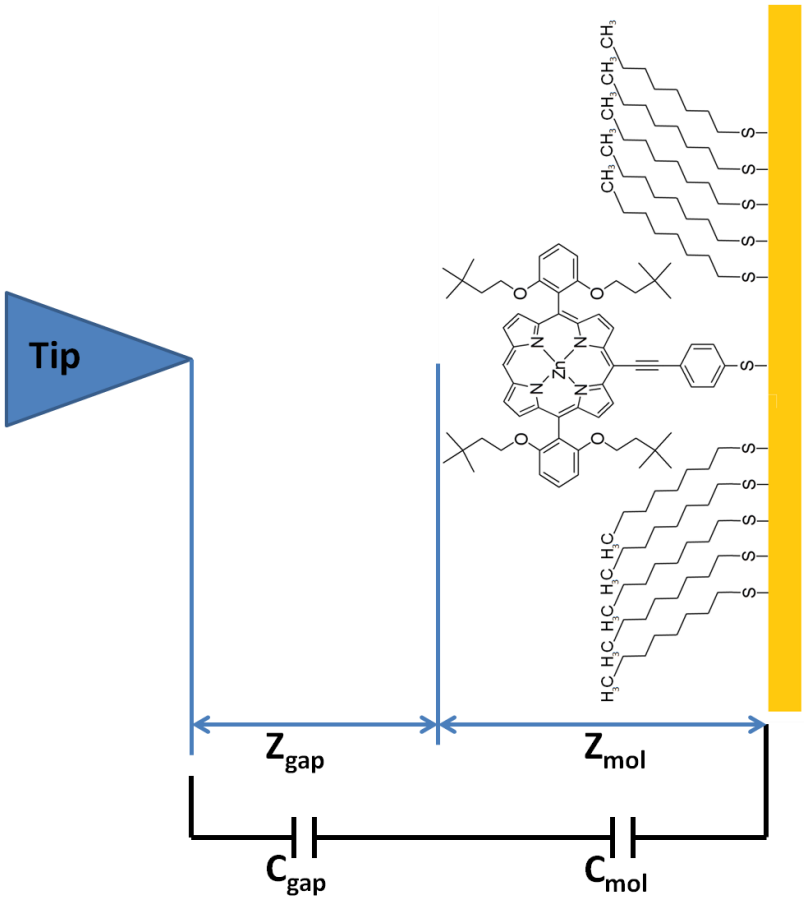

Figure 5.1 Schematic diagram of the Au(111) substrate-porphyrin-vacuum-tip tunneling junction, and the capacitive equivalent circuit model. Z_{gap} is the tip-molecule gap distance and Z_{mol} is the length of the molecule.

The capacitor model requires that the voltage between the tip and the substrate be distributed across the gap and the zinc-porphyrin molecule. When in series, the charge on each capacitor is the same, so the voltage distribution should follow equation 5.4:

$$C_{mol}V_{mol} = C_{gap}V_{gap} = C_{total}V_{total} \tag{5.4}$$

Using the Fermi energy level of the tip as a reference (since the sample is biased in the experiment), the energy for the LUMO and HOMO level (E_{LUMO} and E_{HOMO}) should be the value of the peak voltages in the STS, distributed on the vacuum gap [50].

The relations between the energy and the measured voltage peak are described by equations 5.5 and 5.6:

$$E_{LUMO} = eV_{gap} = eV_{LUMO}\frac{C_{total}}{C_{gap}} = eV_{LUMO}\frac{\frac{C_{mol}C_{gap}}{C_{mol}+C_{gap}}}{C_{gap}} = eV_{LUMO}\frac{C_{mol}}{C_{mol}+C_{gap}} \quad (5.5)$$

$$E_{HOMO} = eV_{HOMO}\frac{C_{mol}}{C_{mol}+C_{gap}} \quad (5.6)$$

Where V_{LUMO} and V_{HOMO} are the peak voltages measured in the STS, which is the V_{total} in Equation 5.4. Figure 5.2 illustrates the energy levels of the tip-sample structure. Note equations 5.5 and 5.6 apply to other molecular orbital levels as well.

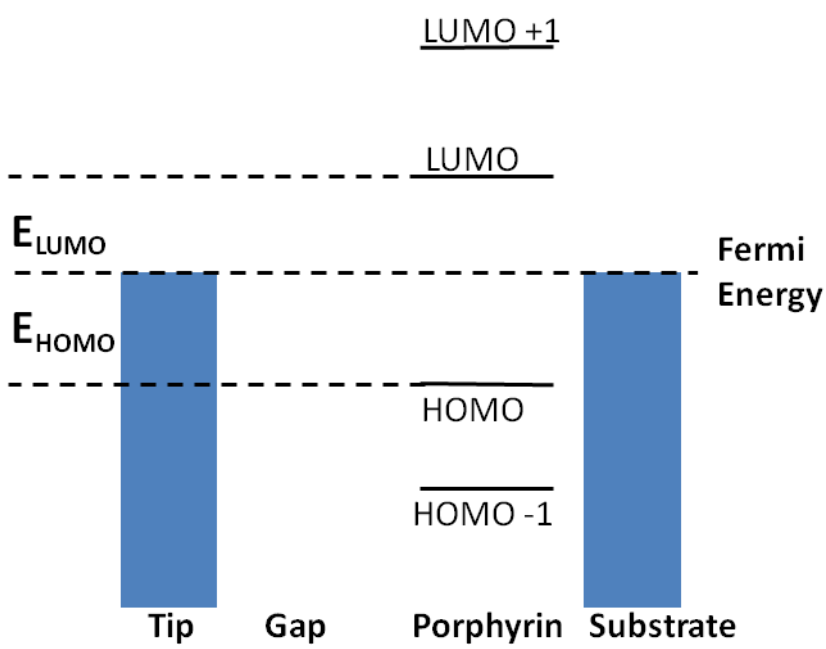

Figure 5.2 Schematic diagram of the energy levels of the Au(111) substrate-porphyrin-vacuum-tip structure.

Now we proceed with the molecular orbital energy level analysis by applying the capacitive model to the experimental data. To start we applied the model to PZn_1 molecules under dark condition and blue light (405 nm) illumination. The theoretical

value of the length of the PZn_1 molecule Z_{mol} is 1.56 nm [63]. We consider the cross-section area, A, as 2 nm^2 and the vacuum gap distance Z_{gap} as 1 nm. The dielectric constant for PZn_1, ε_{mol}, istaken as that of a similar zinc-porphyrin monomer molecule, about 4.2 [110]. Applying those parameters to equation 5.1 and 5.2, C_{mol} and C_{gap} are estimated to be 0.048 aF and 0.018 aF, respectively.

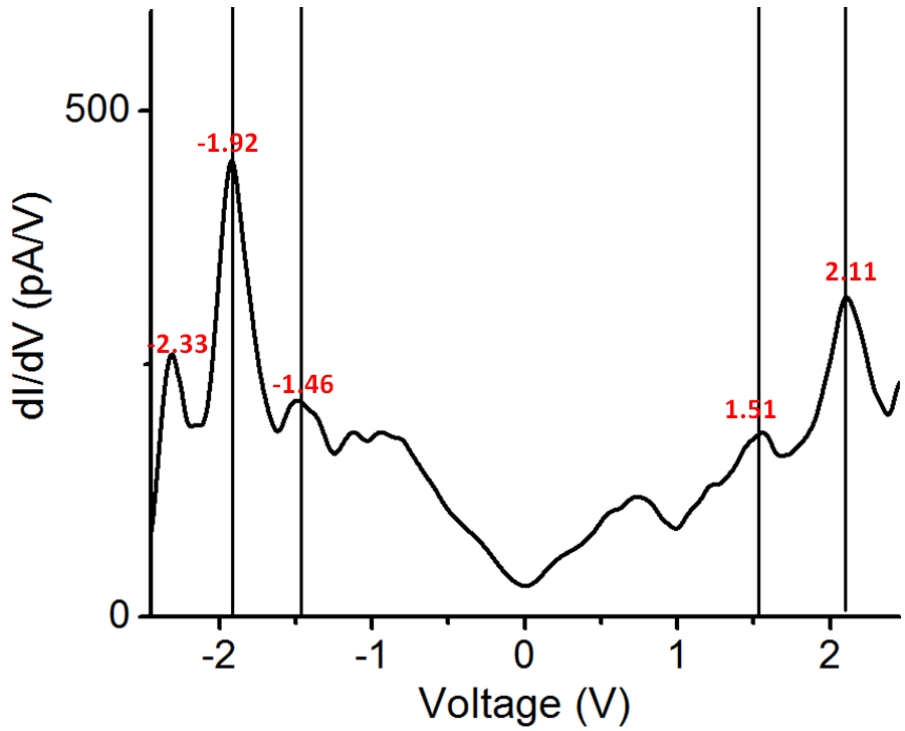

Figure 5.3 Differentiated I-V spectrum of PZn_1 molecule under dark conditions. Vertical lines are positions of the peaks associated with PZn_1 molecular orbitals. Peak values were picked using OriginPro 7.5.

To obtain the molecular energy levels, in addition to the estimation of the capacitance we need the precise peak positions in STS spectra. Figure 5.3 shows the differentiated I-V spectrum of PZn_1 molecule under dark conditions. The peak voltages at HOMO and LUMO levels as well as the ones beyond are labeled in the figure. Using

equation 5.5 and 5.6, applying the estimated values of the capacitance of the molecule and the vacuum gap, the molecular orbital energy levels in the table 5.1 result:

Table 5.1 Voltage peaks and molecular orbital energy levels according to capacitive model under dark condition.

Voltage peak positions (V)	-2.33	-1.92	-1.46	1.51	2.11
Molecular Energy Levels (eV)	-1.69	-1.40	-1.06	1.09	1.53

Similarly, we applied the model to PZn_1 molecules under blue light (405 nm) illumination. Here the length of PZn_1 molecule Z_{mol}, the cross-section area A, and vacuum gap distance Z_{gap} were all assumed unchanged. As for the dielectric constant for PZn_1, we note that previous results show that photoinduced polarizability of similar zinc-porphyrin molecules increases by 117–267% [111]. She et al showed that polarizability volume for a similar zinc-porphyrin monomer changes from 90 $Å^3$ in ground state to 150 $Å^3$ in excited state [112]. Assuming with the PZn_1 molecule in our experiment, that the polarizability α increases by the same ratio 150/90 = 5/3 when the molecule is excited, then ε_{mol} in the blue light illumination can be estimated to be 6.33. Applying all parameters to equation 5.1 and 5.2, we obtain that C_{gap} remains 0.018 aF, and that C_{mol} increases to 0.072 aF.

To obtain the energy levels we also need the precise peak position in STS spectra. Figure 5.4 shows the differentiated I-V spectrum of PZn_1 molecule under blue light illumination. Using equation 5.5 and 5.6, applying the new estimated values of the

capacitance of the molecule and the vacuum gap, we obtain the molecular orbital energy levels in table 5.2:

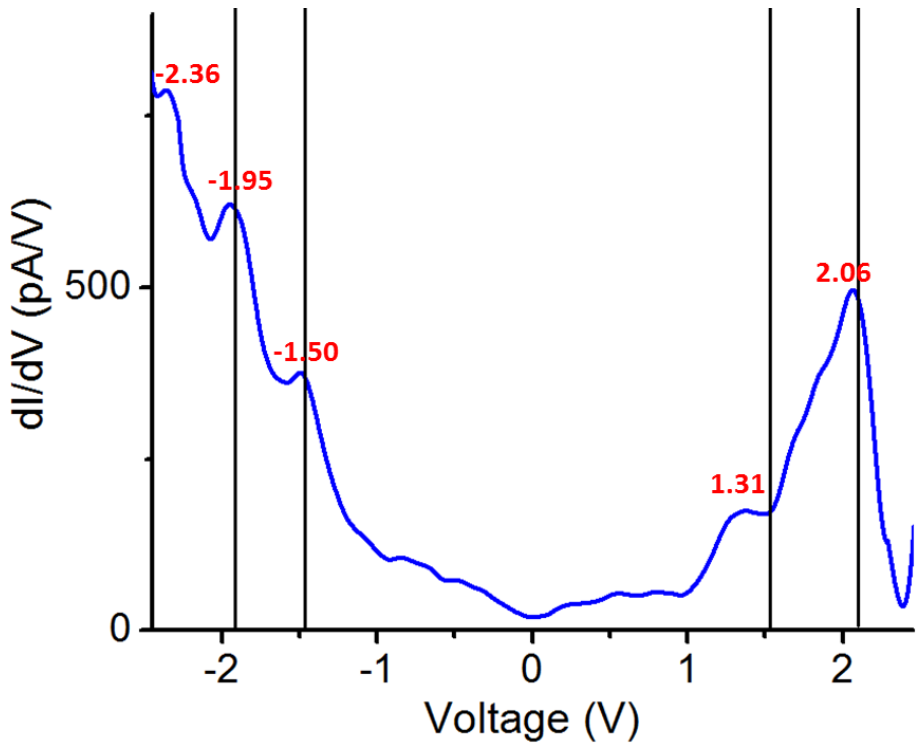

Figure 5.4 Differentiated I-V spectrum of PZn_1 molecule under blue light (405 nm) illumination. Vertical lines are positions where peaks associated with PZn_1 molecular orbital under dark conditions. Peak values were picked using OriginPro 7.5.

Table 5.2 Voltage peaks and molecular orbital energy levels according to capacitive model under blue light illumination.

Voltage peak positions (V)	-2.36	-1.95	-1.50	1.31	2.06
Molecular Energy Levels (eV)	-1.89	-1.56	-1.20	1.10	1.65

With values of adjusted energy levels in table 5.1 and table 5.2, we can reconstruct the molecular orbital energy levels under dark conditions and blue light

illumination, using the capacitive model. Figure 5.5 shows the molecular energy levels. It can be seen that under illumination, the HOMO-LUMO gap of the molecule increases.

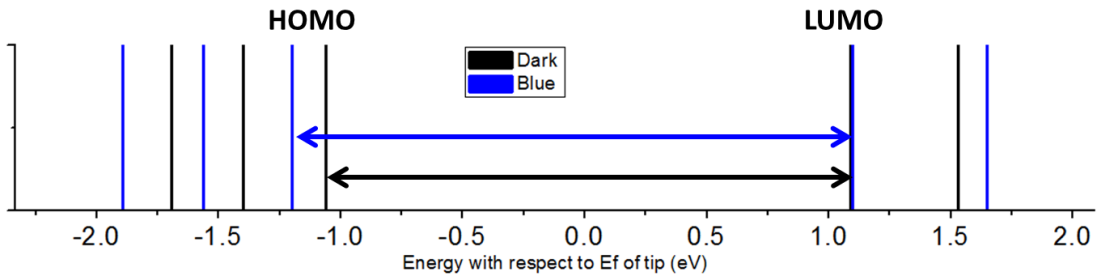

Figure 5.5 Adjusted energy levels of PZn_1 molecule under dark conditions and blue light illuminations. Vertical lines indicate the energy levels and the arrows indicate the HOMO-LUMO gaps.

5.1.2 Resistive Model

A alternative approach is to consider the Au(111) substrate-porphyrin-vacuum-tip tunneling junction, as a resistive equivalent circuit. This occurs when the local density of states is large (especially as in metal). Since PZn_1 is a conjugated molecule, the molecular conductivity is high compared to other insulating organic molecules, the resistive equivalent circuit model may apply. A voltage distribution among each component will be calculated to further analyze the peak position of the STS.

Figure 5.6 shows the structure of the Au(111) substrate-porphyrin-vacuum-tip tunneling junction with a resistive equivalent circuit model. Now the vacuum gap and the molecule are treated as two resistors in series. The voltage between the tip and the substrate is still distributed across the gap and the zinc-porphyrin molecule. Since the current flow through a series of resistors is the same, the voltage distribution can be described in equation 5.7:

$$\frac{V_{mol}}{R_{mol}} = \frac{V_{gap}}{R_{gap}} = \frac{V_{total}}{R_{total}} \tag{5.7}$$

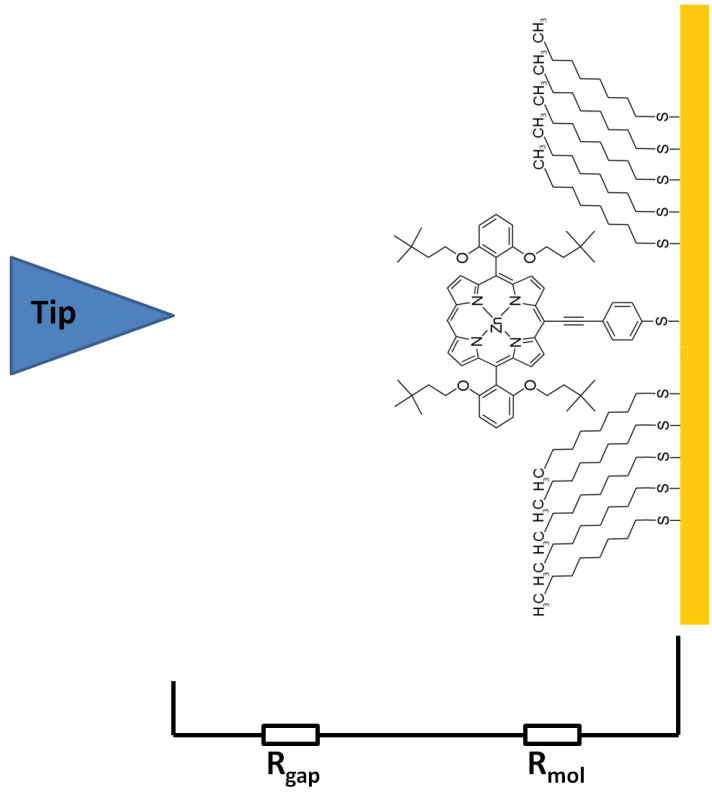

Figure 5.6 Schematic diagram of the Au(111) substrate-porphyrin-vacuum-tip tunneling junction, and the resisitive equivalent circuit model.

where R_{total} is the total resistance across the tip and substrate and is the sum of R_{gap} and R_{mol}. Using the Fermi energy level of the tip as a reference, the energy for the LUMO and HOMO level (E_{LUMO} and E_{HOMO}) should be the value of the peak voltages in the STS, distributed on the vacuum gap. The relations between the energy and the measured voltage peak are described by equations 5.8 and 5.9:

$$E_{LUMO} = eV_{gap} = eV_{LUMO}\frac{R_{gap}}{R_{total}} = eV_{LUMO}\frac{R_{gap}}{R_{mol}+R_{gap}} \tag{5.8}$$

$$E_{HOMO} = eV_{HOMO}\frac{R_{gap}}{R_{mol}+R_{gap}} \tag{5.9}$$

where V_{LUMO} and V_{HOMO} are the peak voltages measured in the differentiated STS, and R_{gap} and R_{mol} are resistances of the vacuum gap and PZn_n molecule.

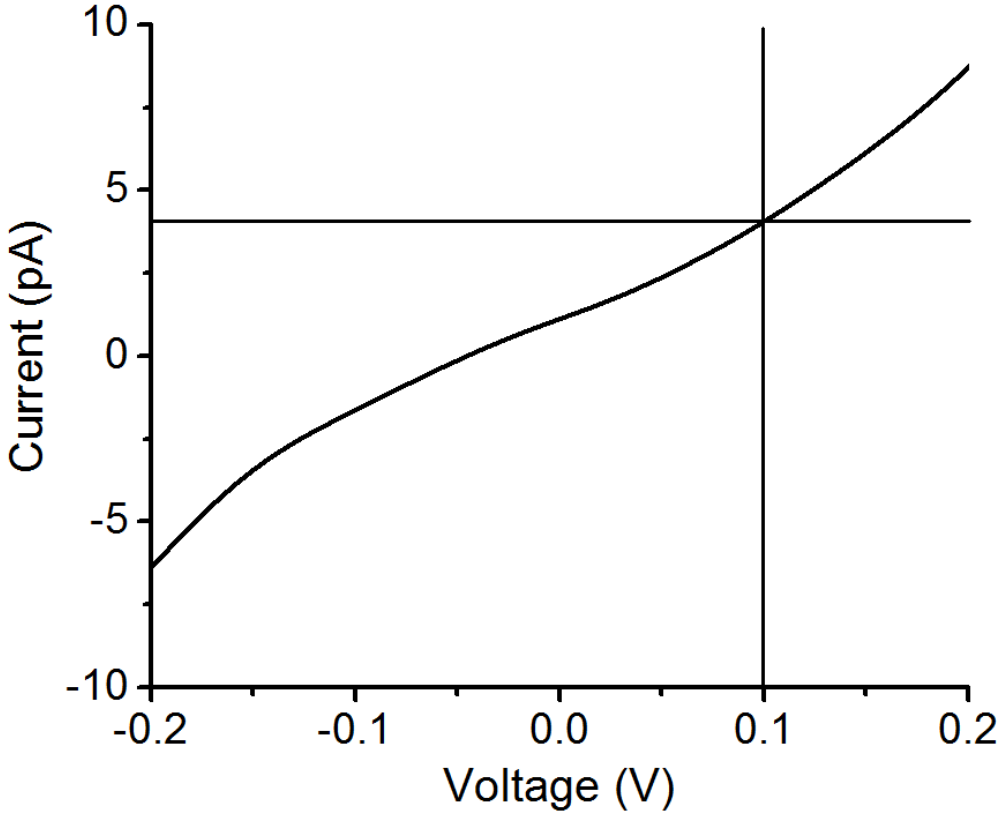

Figure 5.7 A narrower range view of the I-V spectra of PZn_1 molecule under dark conditions shown in Figure 4.13. At 100 mV the current is about 4 pA. Scanning condition was 2.5V, 300pA.

To apply this model we need the resistance of the molecule. We first consider PZn_1 molecule under dark conditions. For the resistance of the molecule we don't have the direct measurement; however, from previous research [61], the mechanical controllable break junction technique was applied to similar zinc-porphyrin single molecules, and under 100 mV applied voltage, the conductance of a single zinc-porphyrin molecule is about 10^{-4} G_0, where G_0 is the conductance quantum. Therefore, the R_{mol} is on the order of $10^8\Omega$. Figure 4.13 shows the I-V spectrum measured under dark conditions,

where the total resistance of the series of vacuum gap and PZn_1 single molecule can be extracted from. To compare at the same applied voltage, a detailed I-V curve from -0.2V to 0.2V was extracted from Figure 4.13, and shown in Figure 5.7. From the I-V spectrum the current at 100 mV applied voltage is about 4 pA, giving a resistance on the order of $10^{10}\Omega$, which is the sum of R_{mol} and R_{gap}. This means that the main contribution to R_{total} is from R_{gap} Since R_{mol} is 2 order of magnitude smaller than R_{total}, equation 5.8 and 5.9 became:

$$E_{LUMO} = eV_{LUMO}\frac{R_{gap}}{R_{total}} = eV_{LUMO}\frac{R_{total}-R_{mol}}{R_{total}} \approx eV_{LUMO} \tag{5.10}$$

$$E_{HOMO} \approx eV_{HOMO} \tag{5.11}$$

i.e. the positions of the voltage peaks can be directly considered as the energy displacements from the tip Fermi energy, or the molecular orbital energy levels. The energy levels, which are the peak positions in differentiated STS are shown here in Table 5.3 and 5.4:

Table 5.3 Voltage peaks and molecular orbital energy levels according to resistive model under dark conditions. Values are indicated for completeness only considering peak positions show no adjustment on this model.

Voltage peak positions (V)	-2.33	-1.92	-1.46	1.51	2.11
Molecular Energy Levels (eV)	-2.33	-1.92	-1.46	1.51	2.11

Table 5.4 Voltage peaks and molecular orbital energy levels according to resistive model under blue light illumination. Values are indicated for completeness only considering peak positions show no adjustment on this model.

Voltage peak positions (V)	-2.36	-1.95	-1.50	1.31	2.06
Molecular Energy Levels (eV)	-2.36	-1.95	-1.50	1.31	2.06

To summarize, two models were applied to differentiated STS spectra to obtain the molecular energy levels. Under the capacitive model, because the vacuum gap capacitance is comparable to the molecular capacitance, each molecular orbital energy level is adjusted with respect to the corresponding differentiated STS peak position. Applying the capacitive model to both dark and blue light illumination conditions, such adjustment was smaller under the blue illumination compared to dark conditions. Under the resistive model, since the molecular resistance is two orders of magnitude smaller than the vacuum gap, the adjustment is negligible, i.e. the differentiated STS peak position is the molecular orbital energy level. Correction to the HOMO-LUMO gap under capacitive model is lower than the gap under resistive model. Also, comparing dark and blue illumination, the HOMO-LUMO gap increases under the capacitive model, while decreases under resistive model.

It is not intuitive to choose between the two models based on the coupling at the interface or the intrinsic properties of the zinc-porphyrin molecules; however, the different consequences of illumination on HOMO-LUMO gap from two distinct models do provide information. It is widely accepted that the optical band gap of an organic semiconductor is narrower than the electronic band gap [113], and the difference of these

two band gaps is usually equal to the exciton binding energy. So with photon excitation, the resulted energy gap could be smaller than that in dark condition, and resistive model seems to fit in this scenario. Therefore, the resistive model is applied to the data, and the results fit well with the charged molecule model discussed in the next section.

5.2 Illumination Effect on PZn_1 Molecular orbital levels

The purpose of our measurements is to understand the illumination wavelength dependence of the PZn_1 molecular electronic structure. In section 4.3.2 we investigated the scanning tunneling spectroscopy measurements of the PZn_1 molecule under dark and different illumination conditions. We observe that through absorption of photons, molecules enter into excited states, which then become charged, exhibiting different molecular electronic structure.

5.2.1 Charging of Porphyrin Molecules

Studies of charged porphyrins and porphyrin derivatives were conducted previously with STM, with the organic molecules mostly within a sandwich structure, between two insulating layers; usually one being the vacuum between tip and the molecule, the other being an insulating thin film such as oxidized NiAl(110) [98] or NaCl [114, 115] . Here the charging and discharging of the molecule was achieved via electron tunneling through the double barrier junction: when the sample voltage is positive, electrons tunnel through the tip-sample vacuum junction and the molecule is negatively charged with one extra electron, when the sample voltage is negative electrons are pulled out from the molecule into the tip leaving the molecule neutral. Such charging leaves the molecule with a new occupied state.

In our research, the charging of PZn_1 molecule was not achieved by the injection or withdrawal of the electron via the tip. The thiolate-Au bond offers strong coupling between the molecule and the substrate, and thus there would be no double barrier junctions. However, the laser illumination at certain wavelengths can facilitate the charging process of the molecule.

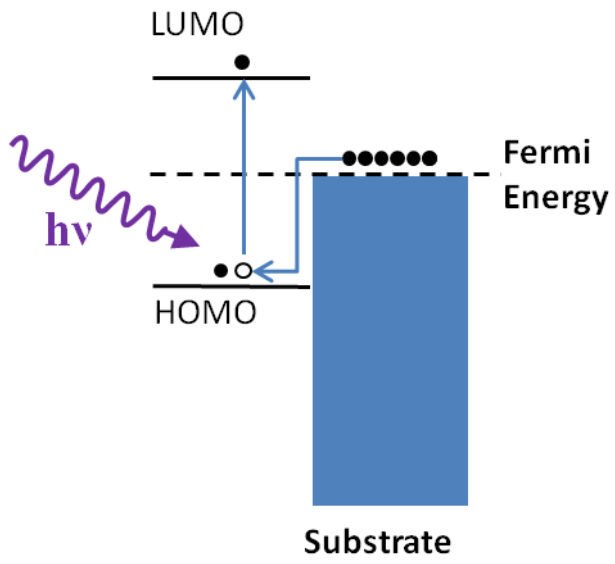

Figure 5.8 Schematic diagram of the charging process of the molecule facilitated by laser illumination.

Charging of the molecule is illustrated in Figure 5.8. With illumination at certain wavelengths, the impinged photon energy is larger than that of the HOMO-LUMO gap of the PZn_1 molecule (Refer to the optical absorption spectra of PZn_n molecules in Figure 4.1), and thus was absorbed by the molecule, forming an electron-hole pair (exciton). Now the molecule is in an excited state. However, with strong coupling between the molecule and the Au substrate, the molecule is connected to an electron reservoir; therefore, one electron transfers from the substrate to the HOMO level of the molecule, filling the hole created by the laser excitation. The PZn_1 molecule is left with an extra

electron on the LUMO level, and is therefore negatively charged as PZn_1^{-1}. Since the laser used for illuminating the tunneling gap was continuous wave, this charged state is considered to be a steady state under our experiment conditions.

In the charged state the molecular energy levels are arranged differently due to the extra electron.

5.2.2 Charging effect on HOMO-LUMO gaps

Molecular energy structures of PZn_1 molecule differ under different probing conditions, as described in Section 4.3.2. Among the differences the most prominent one is the HOMO-LUMO gap of the molecule.

, The HOMO-LUMO gap differences can be observed from the STS spectra, Figure 5.9. While under dark condition we conclude the HOMO-LUMO gap is 3.0 eV, under blue light (405 nm) illumination, the LUMO peak shifts 0.3 V towards zero, showing a slight decrease of the HOMO-LUMO gap, 2.7 eV. The difference can be explained via the charged molecule model.

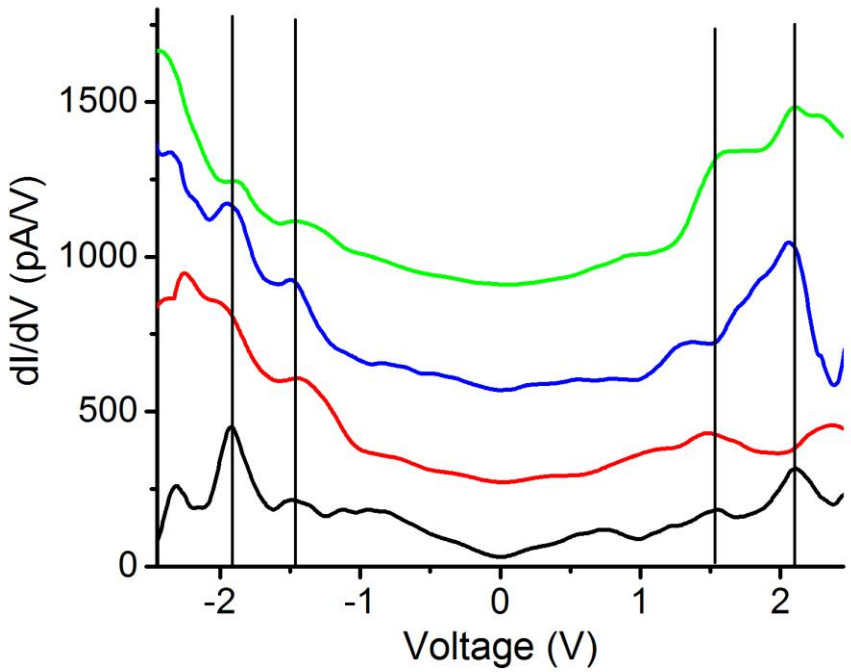

Figure 5.9 (Reproduced from Figure 4.14) Differentiated I-V spectra of PZn_1 molecule under different illumination conditions. Vertical lines are positions where peaks associated with PZn_1 molecular orbital appear under dark condition. The color matches the light used, and black curve corresponds to the dark condition. Curves were vertically shifted to avoid overlapping. Scanning condition was 2.5V, 300pA.

With blue light at 405 nm, the corresponding photon energy is about 3.06 eV, well above the measured HOMO-LUMO gap of the PZn_1 molecule. And from the optical absorption spectra of PZn_1 molecule we know that this wavelength falls in the vicinity of the Soret band of the absorption spectrum. Therefore, we can assume that the molecule can absorb photons, and become charged. According to previous theoretical research, the molecular orbitals of charged organic molecule will rearrange [116], causing a difference in the HOMO-LUMO gap. Similar Zn-porphyrin molecules (ZnTPP and ZnP) show a decrease of the HOMO-LUMO gap when negatively charged, compared to the neutral state, according to the theoretical calculation [40]. Let us consider the calculated energy

gaps in the case of one extra electron in the neutral molecule, i.e. singly negatively charged molecule. For ZnTPP the HOMO-LUMO gap decreases from 2.49 eV to 1.47 eV, while for ZnP (porphine) the gap decreases from 2.60 eV to 1.74 eV. The extra electron in both cases is accommodated in the porphine π* orbital. Calculation also shows evidence of little mixing between metal and macrocycle molecular orbitals. In our experiment, a decrease of the energy gap of 0.3 eV is consistent with the trend of HOMO-LUMO gap indicated by calculations on related charged molecules. By analogy we can postulate in our case: 1) there is little interaction between the metal and the porphine π orbitals, 2) the decrease in HOMO-LUMO gap is due to the negative charging of the macrocyle and electrostatic interaction therefrom, and 3) the extra electron goes into the porphine π* orbitals. The consideration that the extra electron goes into the porphine π* orbitals is consistent as well with full Zn 3d orbital in the neutral ZnTPP [40], in which the extra electron cannot occupy an already full 3d shell. Other ligands in the macrocycle are not expected to introduce substantial reorganization in the porphyrine electronic structure. In fact, a single metal porphine compared to a metal porphine with four phenyl ligands (ZnTPP) has similar results in terms of Zn 3d occupancy and interactions in macrocycle constituents [40]. Analogously, in our case the addition of larger ligands (bis[3,5-bis(3,3-dimethyl-1-butyloxy)phenyl) to porphine should not change the small interaction of Zn 3d low-lying orbitals and porphine and ligands. Thus, the postulate above seems a reasonable analogy.

With green light (533 nm) illumination, the shift of peak positions of STS spectra was absent. The HOMO-LUMO gap of the PZn_1 molecule therefore remains 3.0 eV. This could be explained by the lack of light absorption of the molecule at corresponding

photon energies. The HOMO-LUMO gap of 3.0 eV is much larger than the incident photon energy of 2.33 eV, and also, according to the UV-Vis spectrum of PZn_1 in Figure 4.1, no absorption peak was present around 533 nm.

With red light (655 nm, 1.89 eV) illumination, from the dI/dV spectra we can see that compared to the dark conditions, the HOMO has a slight peak shift of about 0.1 eV to higher energy, while the LUMO peak also shifted toward a lower energy of about 0.1 eV. Also, the peak at 2.1V in dark conditions shifts to positive direction by ~0.3eV. Referring back to the UV-Vis absorption spectrum (Figure 4.1), the PZn_1 molecule does exhibit an absorption peak around 650 nm, but the lower absorption peak indicates fewer photons are absorbed. While here the slight shift of HOMO and LUMO peak could be attributed to experimental error, an alternative explanation is that the observed energy shifts were an averaged effect between charged and uncharged molecules, therefore showing a decrease in HOMO-LUMO gap, but not as prominent as that of the case illuminated at 405 nm.

5.2.3 Other Effects

Another result is that under dark conditions, two broad peaks exist at ~-1.0V and 0.75V within the HOMO-LUMO gap, and are believed to be the contribution of Au(111) substrate or the Au-thiol interface states. When under illumination, such peaks seem to be absent. We believe the absence of these peaks comes from the STS measurement. When the light illumination is on, as shown in Figure 3.12, even after reaching the equilibrium, the tip-sample distance will increase slightly to keep the same scanning setpoint. As a result, in the STS spectra, the current in the voltage region within the HOMO-LUMO gap

decreases (Figure 4.13). Therefore, the peaks within the HOMO-LUMO gap cannot be observed under illumination, due to the low current due to the increased tip-sample distance.

5.3 Illumination Effect on PZn_2 Molecular orbital levels

We aim to explain the illumination effect on PZn_2 molecular orbital energy levels as well. Similar to the description in Section 5.3, laser illumination of certain wavelengths results in photon absorption of the molecules, the zinc-porphyrin molecules are excited and end up in charged states, which have different molecular energy levels than the neutral molecules.

5.3.1 Charging effect on HOMO-LUMO gap

We investigated the PZn_2 response under dark and laser illumination conditions to address optoelectronic properties in the dimer itself and to compare them to PZn_1 properties. Figure 5.10 shows the STS spectra for PZn_2 molecule under dark and different illumination conditions, and the HOMO-LUMO gap difference is readily observed. Under dark conditions the HOMO-LUMO gap is 3.5 eV; under blue light (405 nm) illumination, the LUMO peak shifts from +1.9V in dark condition to +1.3V, and the HOMO peak shifts in the positive direction for ~0.3V, from -1.6V to -1.3V, showing a decrease of 0.9 eV in HOMO-LUMO gap, which is now 2.6 eV. This phenomenon could be explained by the charged molecule model, as in the case of PZn_1 molecule.

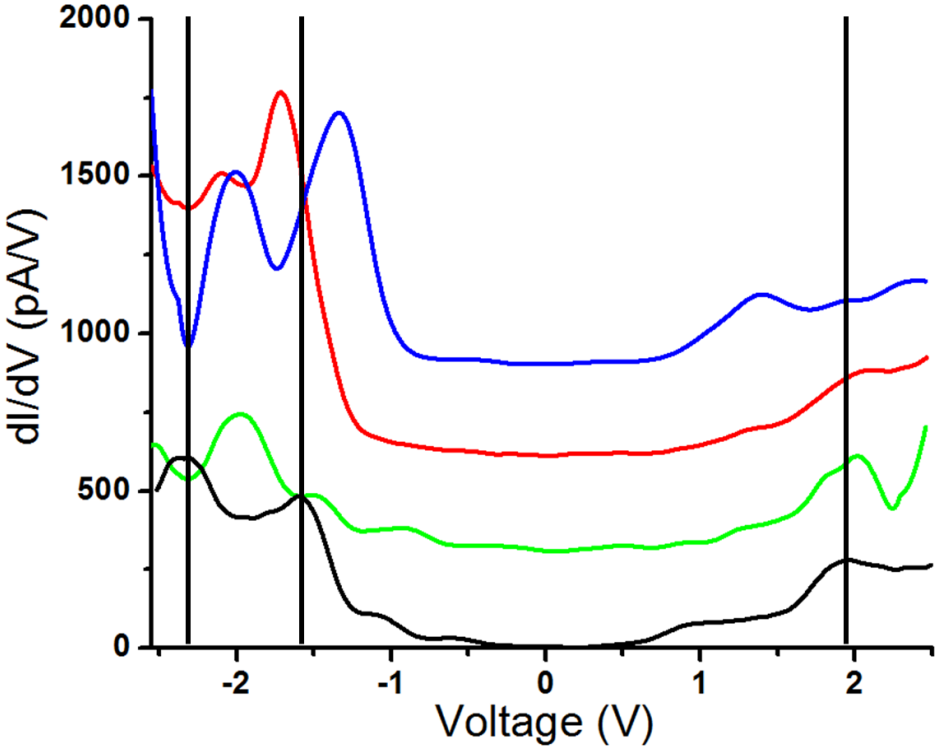

Figure 5.10 (Reproduced from Figure 4.18) Differentiated I-V spectra of PZn_2 molecule under different illumination conditions. Vertical lines are positions where peaks associated with PZn_2 molecular orbital appear under dark condition. The color matches the light used, and black curve corresponds to the dark condition. Curves were vertically shifted to avoid overlapping. Scanning condition was 2.5V, 300pA

The optical absorption spectrum of PZn_2 molecule (Figure 4.1) shows a broad Soret band peak around 405 nm region, therefore upon illumination the PZn_2 molecule absorb a photon and was excited. As described earlier in Section 5.3.1, the excited molecule would acquire an electron from the electron reservoir which is the Au(111) substrate so the HOMO is still filled. Molecular orbitals of the charged organic molecule will differ in energy [116] , yielding a different HOMO-LUMO gap. Although there was no theoretical calculation of HOMO-LUMO gap energies for charged dimer zinc-

porphyrin molecule, we believe the dimer zinc-porphyrin should have a similar trend as the monomer zinc-porphyrin, which is the case in our experimental observation.

With red light (655 nm), the HOMO and LUMO shift slightly farther apart from 3.5eV to 3.6eV, that is within our experimental error. With green light (533 nm) illumination, the peak positions around HOMO and LUMO level do not change. This behavior could be attributed to an absence of photon absorption, since neither 655 nm nor 533 nm were close to the peaks in the UV-Vis absorption spectra for PZn_2 molecules. However, in both illumination cases, the peak right below HOMO shifts toward the HOMO energy level by 0.2 (red) to 0.3 (green) eV.

5.4 Macrocycle coupling effect on Molecular orbital levels

In our experiments we used two different molecules: PZn_1 and PZn_2, monomer and dimer, respectively. The difference between the two molecules is that PZn_2 has an extra zinc-porphyrin macrocycle, coupled through the ethyl bridge. The coupling between the two porphyrin macrocycles will affect the molecular orbitals of the molecule, changing the energy levels of certain orbitals.

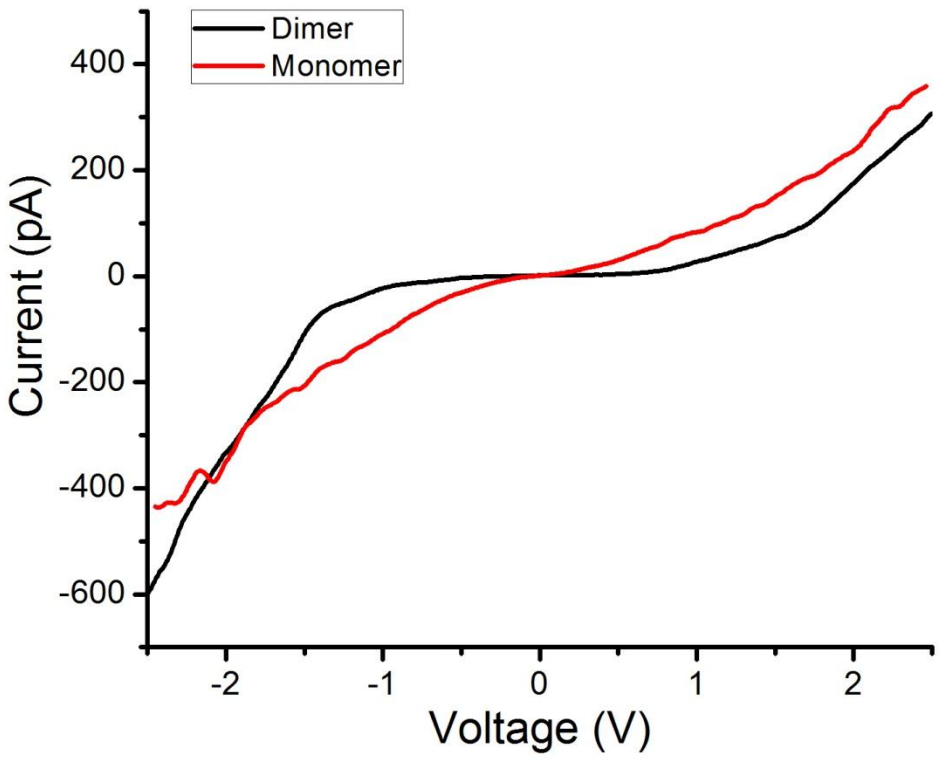

Figure 5.11 I-V spectra of PZn_1 (monomer, red) and PZn_2 (dimer, black) molecule under dark conditions. Scanning condition was 2.5V, 300pA.

Figure 5.11 shows the I-V spectra of PZn_1 and PZn_2 single molecule under dark conditions. For PZn_2 molecules, the absolute value of current does not increase until over 1V or -1.5V; however, for the PZn_1 molecule the current is larger around zero voltage. More details can be seen in the differentiated STS spectra, shown in Figure 5.12. Compared to the PZn_1 molecules, the LUMO and HOMO of PZn_2 molecule both shift further away from Fermi energy of the tip, showing an increase of 0.5 eV in the HOMO-LUMO gap. As stated in Chapter 4, the higher HOMO-LUMO gap in the dimer compared to the monomer is counterintuitive, since the bonding between the two PZn macrocycles in the dimer molecule should bring the HOMO and LUMO energies closer, according to previous DFT calculation [43, 64, 99] and experiment results [117]. We

propose several possible explanations of the differences and similarities between our measurement and previous results.

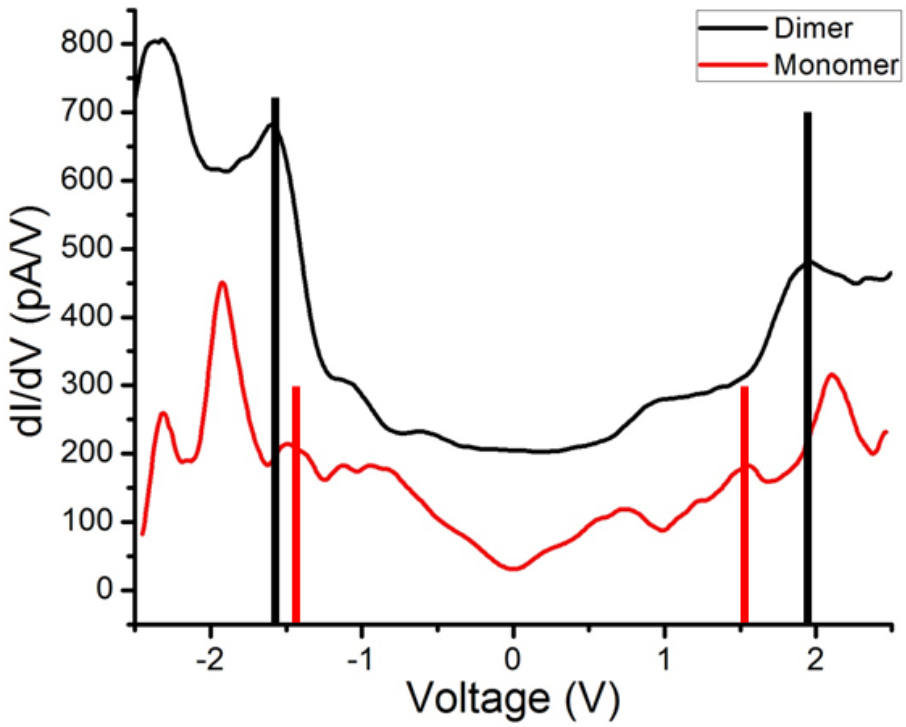

Figure 5.12 Differentiated I-V spectra of PZn_1 (monomer, red) and PZn_2 (dimer, black) molecule under dark conditions. Vertical lines indicate HOMO and LUMO orbitals. Scanning condition was 2.5V, 300pA.

One explanation is based on the consequence of PZn_2 molecules' bundling during sample preparation. In topography images the PZn_2 molecules appear to have larger lateral sizes than expected for single molecules, and this may arise from several PZn_2 molecules bundling together. According to previous experimental research [118], when porphyrin macrocycles bundle together face-to-face, as shown in Figure 5.13, the Soret band peak position in UV-Vis absorption spectrum differs among monomer, dimer, and trimer. In dichloroethane (DCE) solvent, with the monomer configured as in Figure 5.13a, the Soret band peak is at 420.0 nm (2.95 eV); while for the dimer configured as in

Figure 5.13b, the Soret band peak blue shifts to 414.9 nm (2.99 eV), and for the trimer configured as in Figure 5.13c, the Soret band peak blue shifts further to 408.4 nm (3.04 eV). Knowing that the Soret band is correlated to the HOMO-LUMO gap according to Gouterman four orbital theory [37], it can be conclude that with the face-to-face bundling, the HOMO-LUMO gap increases. Although the increase is small, the trend matches our results. In our experiment, it cannot be ruled that the STS spectra were taken with the PZn_2 molecules bundled with face-to-face configuration, resulting in an increase of HOMO-LUMO gap compared to the PZn_1 single molecules.

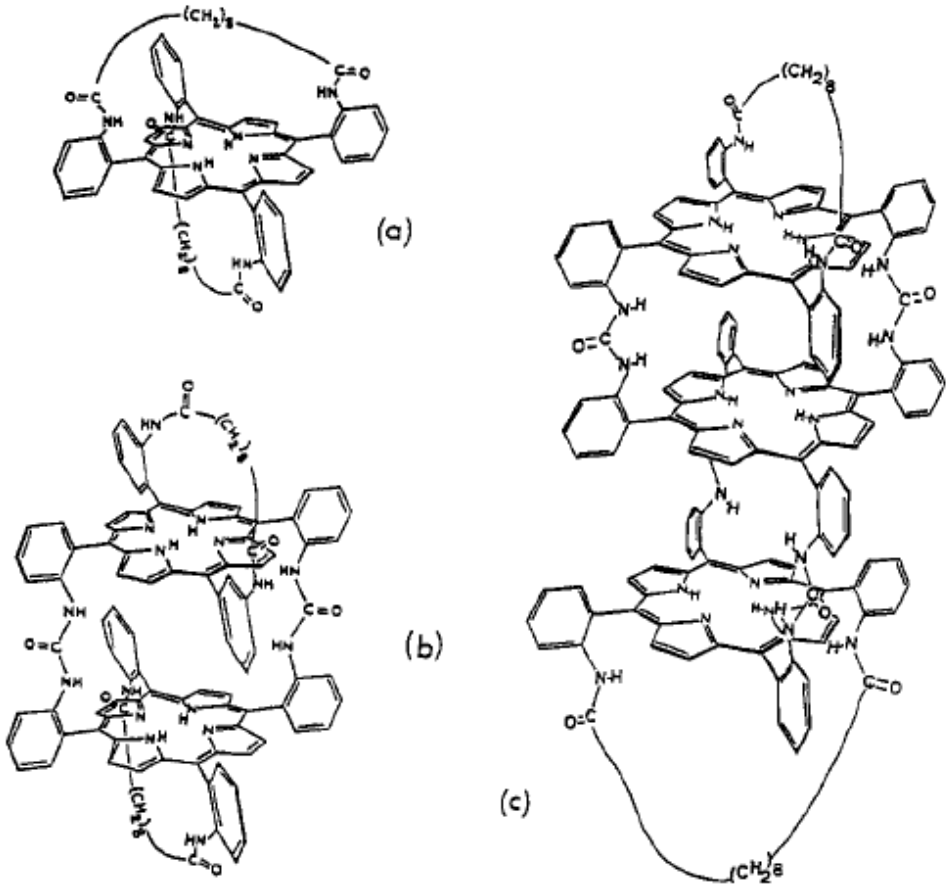

Figure 5.13 Structure of the face-to-face coupled porphyrins. Adapted from Ref. [118]

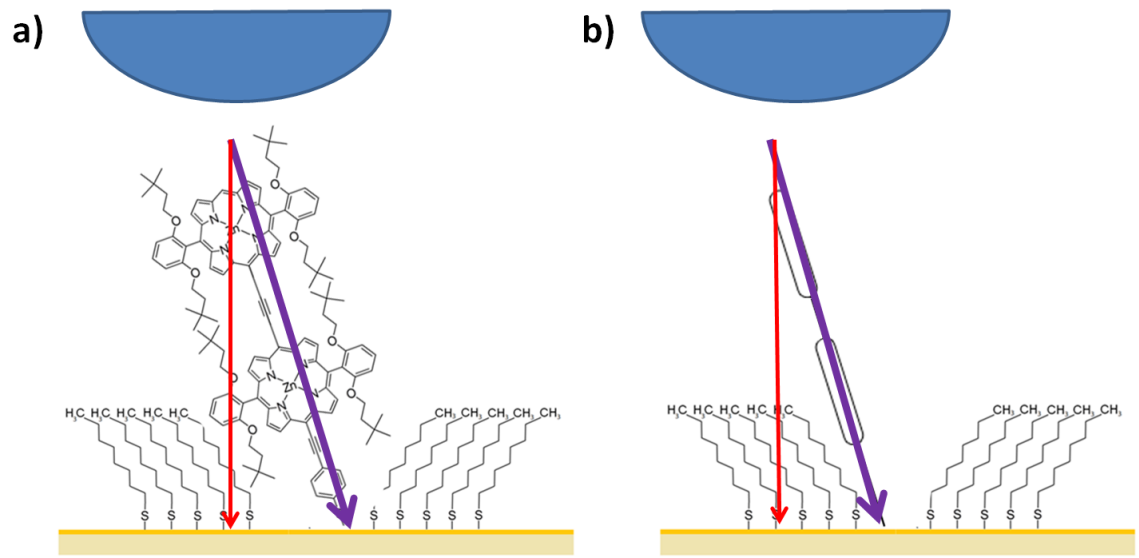

Figure 5.14 Schematic illustration of PZn_2 molecule tilting in the 1-octanethiol matrix. Two different possible tilting directions of the zinc-porphyrin molecule are shown in: a) tilting within the macrocycle plane, and b) tilting out of the macrocycle plane. Purple arrow (thicker line) shows the current pathway through the PZn_2 molecule while the red arrow (thinner line) shows the current pathway through the 1-octanethiol SAMs.

An alternative originates from the configuration of the inserted PZn_2 molecules. Compared to PZn_1, the PZn_2 molecule is 1.1 nm longer, theoretically. Thus, it is much higher than the surrounding 1-octanethiol molecule matrix. It is conceivable that the PZn_2 molecule is tilted at an angle from surface normal, and therefore the higher part of the PZn_2 molecule is on top of the 1-octanethiol SAM, as shown in Figure 5.14. When the I-V spectra are acquired, the current may follow two different pathways: 1) current flow through the PZn_2 molecule and electrons tunnel directly to the Au substrate (Purple arrows in Figure 5.14), 2) current flow into the PZn_2 molecule and electrons tunnel through the 1-octanethiol molecules right beneath the PZn_2 molecule to further continue into the Au substrate (Red arrows in Figure 5.14). Since the STS spectra are subsequently averaged, the measured curves are actually the I-V response of mixed PZn_2 molecules

and 1-octanethiol molecules. Since 1-octanethiol molecules have a much larger HOMO-LUMO gap, such mixing results in an enlarged HOMO-LUMO gap in the measurement.

The two possibilities mentioned above, bundling and tilting, are mechanisms that are potentially at play in our molecular configuration. In our experiments it is not possible to separate the contribution of bundling and tilting; however, considering both geometries produce the measured response we expect a combination of the two.

In this chapter we discussed the STS measurements from Chapter 4. Two different models were applied to relate the molecular orbital energy levels to the measured STS spectra and resistive model was chosen to further analyze the data, since the analysis with this model shows decreased HOMO-LUMO gap under light excitation, which fits the typical smaller optical band gap in organic semiconductors. To further explain the illumination effect on PZn_1 and PZn_2 molecular orbital energy levels, especially the decrease of the HOMO-LUMO gap, the charged molecule model was introduced: on absorption of photons, molecules reach excited states, which then become negatively charged molecules, exhibiting smaller HOMO-LUMO gaps. Under dark conditions, measurements showed that PZn_2 exhibits a larger HOMO-LUMO gap than PZn_1 molecules, which is counterintuitive. Two different hypotheses of face-to-face bundling of the molecule, or tilted molecule were introduced to explain the measurements.

CHAPTER 6 Conclusion and Future Directions

6.1 Conclusion

This research is a contribution to optoelectronics where there are few experimental efforts focused on understanding the effect of the interaction with light on porphyrin electronic structures, in the context of organic molecular electronic devices. This research experimentally determined the molecular orbital energy levels of zinc-porphyrin molecules attached to electrodes, as well as the illumination effect on the modulation of porphyrin electronic structures.

To achieve our research goal, several challenges have been met. The first is to prepare the sample with the porphyrin molecules in a device configuration, with the longitudinal axis of the porphyrin molecule perpendicular to the substrate. To achieve the configuration, 1-octanethiol molecule was used to form self-assembled monolayers, and zinc-porphyrin molecules were inserted in the defects of the 1-octanethiol SAMs. The second challenge is to adjust the laser to properly illuminate the zinc-porphyrin molecule below the scanning tip, and to maximize the effect of the light. We used control studies with an n-doped GaAs (100) sample to maximize the zero voltage offset, therefore ensuring the optimization of the illumination. The third challenge is to achieve a stable tunneling gap under light illumination. To overcome this challenge, the relaxation time of system was measured by monitoring the Z piezo position, and the spectra collection were all done after equilibrium was achieved, usually 10 minutes after turning on the illumination.

In our research, optoelectronically active porphyrin complexes were isolated, and individual molecules and clusters uprightly/vertically attached to electrodes. The density of states of the zinc-porphyrins were quantitatively determined from scanning tunneling probe techniques at room temperature, and were qualitatively consistent with calculations and experiments of similar porphyrin complexes.

Optical excitation at relevant energies resulted in differences in the local density of states. Under blue laser (405nm) illumination HOMO-LUMO gaps for both monomer and dimer zinc-porphyrin molecules is narrower than in dark conditions. Measurements were analyzed using a resistive model for voltage distribution, and charged molecule model was introduced to explain the decrease of HOMO-LUMO gap under light illumination: molecules achieved excited states after absorption of photons and then become negatively charged as electrons from the metal electron reservoir fills the hole left by the excited electron. The electronic structure of the charged molecule rearranges and thus yields the narrower HOMO-LUMO gap.

Also, we looked into the macrocycle coupling effect of the zinc-porphyrin on the molecular orbital energy levels. Measurements on PZn_1 and PZn_2 molecules were performed under dark conditions and showed a counterintuitive result that the HOMO-LUMO gap of PZn_2 molecules is larger than that of PZn_1 molecules. We explain these results with the mixing of two geometries for the molecules: face-to-face bundling and tilting.

6.2 Suggestion for Future works

Future work in this area could lie in several directions: 1) To improve the insertion mechanism and experimental conditions, 2) To better model the electronic structure of the zinc-porphyrin molecule in our research, 3) To further understand light interaction with the zinc-porphyrin molecules, and 4) To further exploit the zinc-porphyrin molecule to fabricate the electronic devices.

First, in our research, thiolate bond was used to achieve the chemisorption of the zinc-porphyrin molecules to the Au(111) substrate. We tried to optimize the output of the stably chemisorbed molecules, to make sure scanning tunneling spectroscopy measurement can be successfully conducted over the target molecules. However, the yield of good samples remains low. It would be possible use other groups to bond the molecule to the Au(111) substrate to improve the yield, thus improving the statistical validity of the electronic structure data. Also, our measurements were conducted under room temperature and high vacuum condition. To improve the measurement, the experiments could be conducted under low temperature and ultra-high vacuum conditions.

Second, theoretical calculation can be performed with the zinc-porphyrin molecules in our research. Calculation of electronic structures based on individual molecules were performed previously, however chemisorption onto Au(111) substrate via thiolated bond may change the molecular orbital energy levels. Also, how light interacts with the porphyrin molecule can also be theoretically modeled and calculated. Under the charged molecule model, the calculated electronic structures of negatively charged

molecule can show more information beyond the HOMO-LUMO gap, and therefore provide deeper insight on the molecular orbital energy levels.

Third, the light interaction with the zinc-porphyrin molecule could be further understood by designing new experiments. In our results, it can be expected that the zinc-porphyrin molecules under light illumination will stay under ground states most of the time, since the photon flux from the incident laser is not enough to keep the molecule at an excited state. However, we did observe differences under light illumination compare to under dark conditions. It could be possible that the adsorption to the Au(111) substrate will increase the lifetime of the excited states, or that tip field focusing effects or tip plasmonic enhancement become significant. Such hypothesis could be confirmed with future optical STM experiments.

Last but not the least, the goal to fabricate electronic/optoelectronic devices with zinc-porphyrin molecules remains to be accomplished. We could potentially try to fabricate single electron transistor (SET) with zinc-porphyrin molecules, and the properties of such SET devices could be understood from our experimental results of the molecular orbital energy levels. It is also possible to introduce optical modulation of the SET devices, to achieve possible optical gating SET devices.

In summary, more research could be performed to further explore the assemblies, the electronic properties, and the applications of the zinc-porphryin molecules. With improvement on the device fabrication technique, as well as deeper understanding of the electronics and optoelectronics of zinc-porphyrin molecules, we believe the porphyrin-based organic molecular devices have a bright outlook.

References

1. Waser, R., ed. *Nanoelectronics and Information Technology*. 3rd ed. 2012, Wiley-VCH.
2. Sze, S.M. and K.K. Ng, *Physics of Semiconductor Devices*. 2006: Wiley.
3. Moore, G.E., *Cramming more components onto integrated circuits (Reprinted from Electronics, pg 114-117, April 19, 1965).* Proceedings of the Ieee, 1998. **86**(1): p. 82-85.
4. Robertson, J., *High dielectric constant gate oxides for metal oxide Si transistors.* Reports on Progress in Physics, 2006. **69**(2): p. 327-396.
5. Huang, X., et al. *Sub 50-nm FinFET: PMOS*. in *Technical Digest - International Electron Devices Meeting*. 1999.
6. Aviram, A. and M.A. Ratner, *Molecular Rectifiers.* Chemical Physics Letters, 1974. **29**(2): p. 277-283.
7. Son, J.Y. and H. Song, *Molecular scale electronic devices using single molecules and molecular monolayers.* Current Applied Physics, 2013. **13**(7): p. 1157-1171.
8. Bernasek, S.L., *Molecular electronics: Van der Waals rectifiers.* Nature Nanotechnology, 2013. **8**(2): p. 80-81.
9. Nerngchamnong, N., et al., *The role of van der Waals forces in the performance of molecular diodes.* Nature Nanotechnology, 2013. **8**(2): p. 113-118.
10. Yee, S.K., et al., *Inverse Rectification in Donor-Acceptor Molecular Heterojunctions.* ACS Nano, 2011. **5**(11): p. 9256-9263.

11. Park, H., et al., *Nanomechanical oscillations in a single-C60 transistor.* Nature, 2000. **407**(6800): p. 57-60.

12. Park, J., et al., *Coulomb blockade and the Kondo effect in single-atom transistors.* Nature, 2002. **417**(6890): p. 722-725.

13. Pasupathy, A.N., et al., *Vibration-assisted electron tunneling in C 140 transistors.* Nano Letters, 2005. **5**(2): p. 203-207.

14. Champagne, A.R., A.N. Pasupathy, and D.C. Ralph, *Mechanically adjustable and electrically gated single-molecule transistors.* Nano Letters, 2005. **5**(2): p. 305-308.

15. Kushmerick, J., *Molecular transistors scrutinized.* Nature, 2009. **462**(7276): p. 994-995.

16. Song, H., et al., *Observation of molecular orbital gating.* Nature, 2009. **462**(7276): p. 1039-1043.

17. Liu, Z., et al., *Molecular Memories That Survive Silicon Device Processing and Real-World Operation.* Science, 2003. **302**(5650): p. 1543-1545.

18. Roth, K.M., et al., *Measurements of electron-transfer rates of charge-storage molecular monolayers on Si(100). Toward hybrid molecular/semiconductor information storage devices.* Journal of the American Chemical Society, 2003. **125**(2): p. 505-517.

19. Tao, N.J., *Electron transport in molecular junctions.* Nature Nanotechnology, 2006. **1**(3): p. 173-181.

20. Blum, A.S., et al., *Molecularly inherent voltage-controlled conductance switching.* Nature Materials, 2005. **4**(2): p. 167-172.

21. Lee, J., et al., *Molecular monolayer nonvolatile memory with tunable molecules.* Angewandte Chemie - International Edition, 2009. **48**(45): p. 8501-8504.

22. Raman, K.V., et al., *Interface-engineered templates for molecular spin memory devices.* Nature, 2013. **493**(7433): p. 509-513.

23. Heath, J.R. and M.A. Ratner, *Molecular electronics.* Physics Today, 2003. **56**(5): p. 43-49.

24. Galperin, M. and A. Nitzan, *Molecular optoelectronics: The interaction of molecular conduction junctions with light.* Physical Chemistry Chemical Physics, 2012. **14**(26): p. 9421-9438.

25. Arramel, et al., *Reversible light induced conductance switching of asymmetric diarylethenes on gold: Surface and electronic studies.* Nanoscale, 2013. **5**(19): p. 9277-9282.

26. Battacharyya, S., et al., *Optical Modulation of Molecular Conductance.* Nano Letters, 2011. **11**(7): p. 2709-2714.

27. Lutz, T., et al., *Molecular Orbital Gates for Plasmon Excitation.* Nano Letters, 2013. **13**(6): p. 2846-2850.

28. Banerjee, P., et al., *Plasmon-induced electrical conduction in molecular devices.* ACS Nano, 2010. **4**(2): p. 1019-1025.

29. Conklin, D., et al., *Exploiting plasmon-induced hot electrons in molecular electronic devices.* ACS Nano, 2013. **7**(5): p. 4479-4486.

30. Conklin, D., et al., *Electronic transport in porphyrin supermolecule-gold nanoparticle assemblies.* Nano Letters, 2012. **12**(5): p. 2414-2419.

31. Conklin, D., et al., *Controlling polarization dependent reactions to fabricate multi-component functional nanostructures.* Advanced Functional Materials, 2011. **21**(24): p. 4712-4718.

32. Fleischer, E.B., *The structure of porphyrins and metalloporphyrins.* Accounts of Chemical Research, 1970. **3**(3): p. 105-112.

33. Marsh, D.F. and L.M. Mink, *Microscale synthesis and electronic absorption spectroscopy of tetraphenylporphyrin H2(TPP) and metalloporphyrins ZnII(TPP) and NiII(TPP).* Journal of Chemical Education, 1996. **73**(12): p. 1188-1190.

34. Milgrom, L.R., *The Colours of Life: An Introduction to the Chemistry of Porphyrins and Related Compounds*. 1997, Oxford: Oxford University Press.

35. Ghosh, M., et al., *Photophysics of Soret-excited free base tetraphenylporphyrin and its zinc analog in solution.* Spectrochimica Acta - Part A: Molecular and Biomolecular Spectroscopy, 2013. **116**: p. 466-472.

36. Weaver, J.J., *Corroles*, in *Chemistry and Chemical Engineering*. 2005, California Institute of Technology: Pasadena, CA.

37. Gouterman, M., *Spectra of Porphyrins.* Journal of Molecular Spectroscopy, 1961. **6**(1): p. 138-&.

38. Otsuki, J., *STM studies on porphyrins.* Coordination Chemistry Reviews, 2010. **254**(19-20): p. 2311-2341.

39. Venkataramanan, N.S., et al., *Electronic structures and spectra of symmetric meso-substituted porphyrin: DFT and TDDFT—PCM investigations.* International Journal of Quantum Chemistry, 2011. **111**(10): p. 2340-2351.

40. Liao, M.S. and S. Scheiner, *Electronic structure and bonding in metal porphyrins, metal=Fe, Co, Ni, Cu, Zn.* Journal of Chemical Physics, 2002. **117**(1): p. 205-219.

41. Cho, S., et al., *Electron delocalization in various triply linked zinc(II) porphyrin arrays: role of antiaromatic junctions between aromatic porphyrins.* Physical Chemistry Chemical Physics, 2011. **13**(36): p. 16175-16181.

42. Yamaguchi, Y., *Theoretical prediction of electronic structures of fully pi-conjugated zinc oligoporphyrins with curved surface structures.* Journal of Chemical Physics, 2004. **120**(17): p. 7963-7970.

43. Miyahara, T., et al., *Ground and excited states of linked and fused zinc porphyrin dimers: Symmetry adapted cluster (SAC)-configuration interaction (CI) study.* Journal of Chemical Physics, 2002. **117**(24): p. 11196-11207.

44. Scudiero, L., D.E. Barlow, and K.W. Hipps, *Physical properties and metal ion specific scanning tunneling microscopy images of metal(II) tetraphenylporphyrins deposited from vapor onto gold (111).* Journal of Physical Chemistry B, 2000. **104**(50): p. 11899-11905.

45. Scudiero, L., et al., *Scanning tunneling microscopy, orbital-mediated tunneling spectroscopy, and ultraviolet photoelectron spectroscopy of metal(II) tetraphenylporphyrins deposited from vapor.* Journal of the American Chemical Society, 2001. **123**(17): p. 4073-4080.

46. Scudiero, L., D.E. Barlow, and K.W. Hipps, *Scanning tunneling microscopy, orbital-mediated tunneling spectroscopy, and ultraviolet photoelectron spectroscopy of nickel(II) octaethylporphyrin deposited from vapor.* Journal of Physical Chemistry B, 2002. **106**(5): p. 996-1003.

47. Deng, W.L. and K.W. Hipps, *Tip-sample distance dependence in the STM-based orbital-mediated tunneling spectrum of nickel(II) tetraphenylporphyrin deposited on Au(111).* Journal of Physical Chemistry B, 2003. **107**(39): p. 10736-10740.

48. Muellegger, S., et al., *Spectroscopic STM Studies of Single Gold(III) Porphyrin Molecules.* Journal of the American Chemical Society, 2009. **131**(49): p. 17740-17741.

49. Müllegger, S., et al., *Preserving charge and oxidation state of Au(III) ions in an agent-functionalized nanocrystal model system.* ACS Nano, 2011. **5**(8): p. 6480-6486.

50. Majima, Y., et al., *Negative differential resistance by molecular resonant tunneling between neutral tribenzosubporphine anchored to a Au(111) surface and tribenzosubporphine cation adsorbed on to a tungsten tip.* Journal of the American Chemical Society, 2013. **135**(38): p. 14159-14166.

51. Chan, Y.-H., et al., *Synthesis and characterization of a thiol-tethered tripyridyl porphyrin on Au(111).* Journal of Physical Chemistry C, 2008. **112**(15): p. 6110-6118.

52. Xi, W., et al., *Tunnelling conductance of vectorial porphyrin monolayers.* Journal of Materials Chemistry, 2008. **18**(26): p. 3109-3120.

53. Friesen, B.A., et al., *Differing HOMO and LUMO Mediated Conduction in a Porphyrin Nanorod.* Journal of the American Chemical Society, 2010. **132**(25): p. 8554-+.

54. Kim, S.H., et al., *Geometric and electronic properties of porphyrin molecules on Au(111) and NaCl surfaces.* Surface Science, 2013. **613**: p. 54-57.

55. Kim, H., et al., *Switching and sensing spin states of Co-porphyrin in bimolecular reactions on Au(111) using scanning tunneling microscopy.* ACS Nano, 2013. **7**(10): p. 9312-9317.

56. Yokoyama, T. and F. Nishiyama, *Direct Visualization of Electronic Asymmetry within a Phenyl-Linked Porphyrin Dimer.* Journal of Physical Chemistry Letters, 2014. **5**(8): p. 1324-1328.

57. Noguchi, Y., et al., *Fowler-nordheim tunneling in electromigrated break junctions with porphyrin molecules.* Japanese Journal of Applied Physics, Part 1: Regular Papers and Short Notes and Review Papers, 2007. **46**(4 B): p. 2683-2686.

58. Li, Z. and E. Borguet, *Determining Charge Transport Pathways through Single Porphyrin Molecules Using Scanning Tunneling Microscopy Break Junctions.* Journal of the American Chemical Society, 2012. **134**(1): p. 63-66.

59. Li, Z., et al., *Quasi-Ohmic Single Molecule Charge Transport through Highly Conjugated meso-to-meso Ethyne-Bridged Porphyrin Wires.* Nano Letters, 2012. **12**(6): p. 2722-2727.

60. Sedghi, G., et al., *Long-range electron tunnelling in oligo-porphyrin molecular wires.* Nature Nanotechnology, 2011. **6**(8): p. 517-523.

61. Perrin, M.L., et al., *Charge transport in a zinc-porphyrin single-molecule junction.* Beilstein Journal of Nanotechnology, 2011. **2**(1): p. 714-719.

62. Perrin, M.L., et al., *Large tunable image-charge effects in single-molecule junctions.* Nature Nanotechnology, 2013. **8**(4): p. 282-287.

63. Park, T.-H., *Synthesis and application of carbodithioate-terminated aryleneethynylenes* in *Department of Chemistry*. 2008, University of Pennsylvania: Philadelphia.

64. Lin, V.S.Y., S.G. Dimagno, and M.J. Therien, *Highly Conjugated, Acetylenyl Bridged Porphyrins - New Models for Light-Harvesting Antenna Systems.* Science, 1994. **264**(5162): p. 1105-1111.

65. Duncan, T.V., et al., *Exceptional near-infrared fluorescence quantum yields and excited-state absorptivity of highly conjugated porphyrin arrays.* Journal of the American Chemical Society, 2006. **128**(28): p. 9000-9001.

66. Susumu, K., et al., *Conjugated chromophore arrays with unusually large hole polaron delocalization lengths.* Journal of the American Chemical Society, 2006. **128**(26): p. 8380-8381.

67. Poirier, G.E. and E.D. Pylant, *The self-assembly mechanism of alkanethiols on Au(111).* Science, 1996. **272**(5265): p. 1145-1148.

68. Schreiber, F., *Structure and growth of self-assembling monolayers.* Progress in Surface Science, 2000. **65**(5-8): p. 151-256.

69. Love, J.C., et al., *Self-assembled monolayers of thiolates on metals as a form of nanotechnology.* Chemical Reviews, 2005. **105**(4): p. 1103-1169.

70. Smith, R.K., P.A. Lewis, and P.S. Weiss, *Patterning self-assembled monolayers.* Progress in Surface Science, 2004. **75**(1-2).

71. Chidsey, C.E.D., et al., *Molecular order at the surface of an organic monolayer studied by low energy helium diffraction [7].* The Journal of Chemical Physics, 1989. **91**(7): p. 4421-4423.

72. Chidsey, C.E.D. and D.N. Loiacono, *Chemical functionality in self-assembled monolayers: Structural and electrochemical properties.* Langmuir, 1990. **6**(3): p. 682-691.

73. Strong, L. and G.M. Whitesides, *Structures of self-assembled monolayer films of organosulfur compounds adsorbed on gold single crystals: Electron diffraction studies.* Langmuir, 1988. **4**(3): p. 546-558.

74. Alves, C.A., E.L. Smith, and M.D. Porter, *Atomic scale imaging of alkanethiolate monolayers at gold surfaces with atomic force microscopy.* Journal of the American Chemical Society, 1992. **114**(4): p. 1222-1227.

75. Bucher, J.P., L. Santesson, and K. Kern, *Selective imaging of self-assembled monolayers by tunneling microscopy.* Applied Physics A: Solids and Surfaces, 1994. **59**(2): p. 135-138.

76. Poirier, G.E. and M.J. Tarlov, *The c(4×2) superlattice of n-alkanethiol monolayers self-assembled on Au(111).* Langmuir, 1994. **10**(9): p. 2853-2856.

77. Nuzzo, R.G., E.M. Korenic, and L.H. Dubois, *Studies of the temperature-dependent phase behavior of long chain n-alkyl thiol monolayers on gold.* The Journal of Chemical Physics, 1990. **93**(1): p. 767-773.

78. Camillone Iii, N., et al., *Substrate dependence of the surface structure and chain packing of docosyl mercaptan self-assembled on the (111), (110), and (100) faces*

of single crystal gold. The Journal of Chemical Physics, 1993. **98**(5): p. 4234-4245.

79. Yeganeh, M.S., et al., *Interfacial atomic structure of a self-assembled alkyl thiol monolayer/Au(111): A sum-frequency generation study.* Physical Review Letters, 1995. **74**(10): p. 1811-1814.

80. Schlenoff, J.B., M. Li, and H. Ly, *Stability and self-exchange in alkanethiol monolayers.* Journal of the American Chemical Society, 1995. **117**(50): p. 12528-12536.

81. Donhauser, Z.J., et al., *Conductance switching in single molecules through conformational changes.* Science, 2001. **292**(5525): p. 2303-2307.

82. Mullen, T.J., et al., *Microcontact insertion printing.* Applied Physics Letters, 2007. **90**(6).

83. Binnig, G. and H. Rohrer, *Scanning tunneling microscopy.* Surface Science, 1983. **126**(1-3): p. 236-244.

84. Kolpak, A.M., et al., *Evolution of the structure and thermodynamic stability of the BaTiO3(001) surface.* Physical Review Letters, 2008. **101**(3).

85. Martirez, J.M.P., et al., *Atomic and electronic structure of the BaTiO3(001) (√5×√5)R26.6 surface reconstruction.* Physical Review Letters, 2012. **109**(25).

86. Eigler, D.M. and E.K. Schweizer, *Positioning single atoms with a scanning tunnelling microscope.* Nature, 1990. **344**(6266): p. 524-526.

87. Iwasaki, H., T. Yoshinobu, and K. Sudoh, *Nanolithography on SiO2/Si with a scanning tunnelling microscope.* Nanotechnology, 2003. **14**(11): p. R55-R62.

88. Bonnell, D., *Scanning Probe Microscopy and Spectroscopy: Theory, Techniques, and Applications*. 2 ed. 2000: Wiley-VCH. 493.

89. Yamashita, M., H. Shigekawa, and R. Morita, eds. *Mono-Cycle Photonics and Optical Scanning Tunneling Microscopy*. Springer Series in Optical Sciences. 2005, Springer Berlin Heidelberg. 389.

90. Grafström, S., *Photoassisted scanning tunneling microscopy*. Journal of Applied Physics, 2002. **91**(3): p. 1717-1753.

91. Van De Walle, G.F.A., et al., *Scanning tunneling microscopy on photoconductive semi-insulating GaAs.* Applied Physics Letters, 1987. **50**(1): p. 22-24.

92. Lukins, P.B. and T. Oates, *Single-molecule high-resolution structure and electron conduction of Photosystem II from scanning tunneling microscopy and spectroscopy*. Biochimica et Biophysica Acta - Bioenergetics, 1998. **1409**(1): p. 1-11.

93. Lukins, P.B., *Single-molecule electron tunneling spectroscopy of the higher plant light-harvesting complex LHC II.* Biochemical and Biophysical Research Communications, 1999. **256**(2): p. 288-292.

94. Van Der Molen, S.J., et al., *Stochastic and photochromic switching of diarylethenes studied by scanning tunnelling microscopy.* Nanotechnology, 2006. **17**(1): p. 310-314.

95. Baldacchini, C., A.R. Bizzarri, and S. Cannistraro, *Excitation of the ligand-to-metal charge transfer band induces electron tunnelling in azurin.* Applied Physics Letters, 2014. **104**(9).

96. Kumar, A.S., et al., *Reversible photo-switching of single azobenzene molecules in controlled nanoscale environments.* Nano Letters, 2008. **8**(6): p. 1644-1648.

97. Comstock, M.J., et al., *Reversible photomechanical switching of individual engineered molecules at a metallic surface.* Physical Review Letters, 2007. **99**(3).

98. Wu, S.W., N. Ogawa, and W. Ho, *Atomic-scale coupling of photons to single-molecule junctions.* Science, 2006. **312**(5778): p. 1362-1365.

99. Shediac, R., et al., *Singlet and triplet excited states of emissive, conjugated bis(porphyrin) compounds probed by optical and EPR spectroscopic methods.* Journal of the American Chemical Society, 2000. **122**(29): p. 7017-7033.

100. Rubtsov, I.V., et al., *Ultrafast singlet excited-state polarization in electronically asymmetric ethyne-bridged bis[(porphinato)zinc(II)] complexes.* Journal of the American Chemical Society, 2003. **125**(9): p. 2687-2696.

101. Vericat, C., M.E. Vela, and R.C. Salvarezza, *Self-assembled monolayers of alkanethiols on Au(111): surface structures, defects and dynamics.* Physical Chemistry Chemical Physics, 2005. **7**(18): p. 3258-3268.

102. Nikiforov, M.P., et al., *The effect of molecular orientation on the potential of porphyrin-metal contacts.* Nano Letters, 2008. **8**(1): p. 110-113.

103. Yoo, H., et al., *Statistical Analysis of Metal-Molecule Contacts in Alkyl Molecular Junctions: Sulfur versus Selenium End-Group.* Journal of Nanoscience and Nanotechnology, 2009. **9**(12): p. 7012-7015.

104. Wang, W., T. Lee, and M.A. Reed, *Mechanism of electron conduction in self-assembled alkanethiol monolayer devices.* Physical Review B - Condensed Matter and Materials Physics, 2003. **68**(3): p. 354161-354167.

105. Wang, W., T. Lee, and M.A. Reed, *Electronic transport in self-assembled alkanethiol monolayers.* Physica E: Low-Dimensional Systems and Nanostructures, 2003. **19**(1-2): p. 117-125.

106. Cui, X.D., et al., *Reproducible measurement of single-molecule conductivity.* Science, 2001. **294**(5542): p. 571-574.

107. Okabayashi, N., M. Paulsson, and T. Komeda, *Inelastic electron tunneling process for alkanethiol self-assembled monolayers.* Progress in Surface Science, 2013. **88**(1): p. 1-38.

108. Simmons, J.G., *Generalized Formula for the Electric Tunnel Effect between Similar Electrodes Separated by a Thin Insulating Film.* Journal of Applied Physics, 1963. **34**(6): p. 1793-1803.

109. Guisinger, N.P., N.L. Yoder, and M.C. Hersam, *Probing charge transport at the single-molecule level on silicon by using cryogenic ultra-high vacuum scanning tunneling microscopy.* Proceedings of the National Academy of Sciences of the United States of America, 2005. **102**(25): p. 8838-8843.

110. Savenije, T.J., et al., *Photogeneration and transport of charge carriers in a porphyrin p/n heterojunction.* Physical Review B - Condensed Matter and Materials Physics, 1997. **55**(15): p. 9685-9692.

111. Kathan-Galipeau, K., et al., *Direct probe of molecular polarization in de novo protein-electrode interfaces.* ACS Nano, 2011. **5**(6): p. 4835-4842.

112. She, C., et al., *Probing exciton localization/delocalization: Transient dc photoconductivity studies of excited states of symmetrical porphyrin monomers,*

oligomers, and supramolecular assemblies. Journal of Physical Chemistry A, 2009. **113**(29): p. 8182-8186.

113. Zahn, D.R.T., G.N. Gavrila, and M. Gorgoi, *The transport gap of organic semiconductors studied using the combination of direct and inverse photoemission.* Chemical Physics, 2006. **325**(1): p. 99-112.

114. Swart, I., T. Sonnleitner, and J. Repp, *Charge state control of molecules reveals modification of the tunneling barrier with intramolecular contrast.* Nano Letters, 2011. **11**(4): p. 1580-1584.

115. Yan, S., et al., *Turning on and off the rotational oscillation of a single porphine molecule by molecular charge state.* ACS Nano, 2012. **6**(5): p. 4132-4136.

116. Gohda, Y. and S.T. Pantelides, *Charging of molecules during transport.* Nano Letters, 2005. **5**(7): p. 1217-1220.

117. Wiengarten, A., et al., *Surface-assisted dehydrogenative homocoupling of porphine molecules.* Journal of the American Chemical Society, 2014. **136**(26): p. 9346-9354.

118. Tran-Thi, T.H., et al., *Effect of the exciton coupling on the optical and photophysical properties of face-to-face porphyrin dimer and trimer. A treatment including the solvent stabilization effect.* Journal of Physical Chemistry, 1992. **96**(3): p. 1073-1082.